Studies of Polymer Field-Effect Transistors

Felix Sunjoo Kim

A dissertation
submitted in partial fulfillment of the
requirements for the degree of

Doctor of Philosophy

University of Washington
2012

Reading Committee:
Samson A. Jenekhe, Chair
Danilo C. Pozzo
Denise M. Wilson

Program Authorized to Offer Degree:
Department of Chemical Engineering.

University of Washington

Abstract

Studies of Polymer Field-Effect Transistors

Felix Sunjoo Kim

Chair of the Supervisory Committee:
Professor Samson A. Jenekhe
Department of Chemical Engineering

The era of plastic electronics is rapidly emerging due to the increasing development and application of low-cost, printable, shape-conforming, and large-area devices, such as organic field-effect transistors (OFETs) and circuits, organic solar cells, and organic light-emitting devices. Deepening our understanding of charge-carrier dynamics in polymer semiconductors is critical to the future advances in organic electronics. This dissertation focuses on studies of OFETs and aims to better understand the charge transport properties of polymer semiconductors and factors that influence the performance of OFETs.

Case studies of structure–morphology–property relationships in unipolar p- and n-channel polymer OFETs as well as ambipolar OFETs reveal that variations in molecular structure and processing affect electronic energy levels, solid-state morphology and crystallinity, and thus the magnitude and polarity of charge carriers. The studies resulted in achievement of high-performance OFETs with high charge-carrier mobility of up to 0.3 cm^2/Vs. The morphology and electronic energy levels are also related to ambient stability and durability of polymer OFETs through kinetics and thermodynamics of interaction between the semiconductor and extrinsic molecules in ambient air. Air-stable ambipolar OFETs were realized by utilizing unipolar p- and n-type polymer semiconductors as the active channel elements. Complementary

digital logic circuits such as inverters and NAND- and NOR-gates, were also demonstrated using the unipolar and ambipolar OFETs.

Device engineering studies show that electron mobility and electrical stability of n-channel polymer OFETs can be significantly enhanced by inserting a low-dielectric-constant polymer dielectric buffer layer at the semiconductor/dielectric interface. Electron mobility was found to increase exponentially with decreasing dielectric constant of the buffer layer. Finally, poly(3-butylthiophene)-nanowire/polystyrene nanocomposites were also investigated as a means of controlling the solid-state morphology of active thin films in OFETs. High dc conductivity and high hole mobility were obtained throughout a wide range of the nanowire compositions (2–100 wt%) due in part to the very low percolation threshold (0.5 wt%).

Table of Contents

List of Figures

List of Tables

List of Abbreviations

AFM	atomic force microscopy
BBB	non-ladder-type poly(benzobisimidazobenzophenanthroline)
BBL	ladder-type poly(benzobisimidazobenzophenanthroline)
BC	bottom-contact
BCB	divinyltetramethylsiloxane-bis(benzocyclobutene)
BG	bottom-gate
BTI	bithiophene imide
CMOS	complementary metal-oxide-semiconductor
COC	cyclic olefin copolymer
CV	cyclic voltammetry
DPP	diketopyrrolopyrrole
DSC	differential scanning calorimetry
FET	field-effect transistor
HOMO	highest occupied molecular orbitals
LUMO	lowest unoccupied molecular orbitals
MOSFET	metal-oxide-semiconductor field-effect transistor
MSA	methanesulfonic acid
NDI	naphthalenetetracarboxylic diimide
NW	nanowire
ODCB	1,2-dichlorobenzene
OFET	organic field-effect transistor
OLED	organic light-emitting diode
OPV	organic photovoltaic cells
OTFT	organic thin film transistor
OTS8	octyltrichlorosilane, or octyltriethoxysilane
P2VN	poly(2-vinylnaphthalene)
P3AT	poly(3-alkylthiophene)
P3BT	poly(3-butylthiophene)
P3HT	poly(3-hexylthiophene)
PαMS	poly(α-methylstyrene)
PBT	poly(benzobisthiazole)

PDI	polydispersity index, or perylenetetracarboxylic diimide
PDP	power-delay product
PhBT	phthalimide-bithiophene copolymer
PNDI	poly(naphthalenetetracarboxylic diimide)
PPV	poly(*p*-phenylene vinylene)
PS	polystyrene
PTT	poly(thiazolothiazole)
PVBC	poly(vinylbenzyl chloride)
PVC	poly(vinylchloride)
PVK	poly(vinylcarbazole)
RFID	radio-frequency identification
SEM	scanning electron microscopy
TC	top-contact
TCB	1,2,4-trichlorobenzene
TEM	transmission electron microscopy
TFT	thin film transistor
TG	top-gate
UV/Vis/NIR	ultraviolet/visible/near-infrared
WAXD	wide-angle X-ray diffraction
XRD	X-ray diffraction

Acknowledgements

I wish to express my sincere appreciation to my dissertation advisor, Professor Samson A. Jenekhe, for his guidance and support. His insightful comments and valuable suggestions have been indispensable to the successful completion of my work. His support has also provided me the opportunity to interact with the scientific community at professional meetings and through collaborative efforts. I also thank Professors Rene Overney, Danilo Pozzo, Denise Wilson, and Xiaodong Xu for their time serving on my committee and for providing valuable comments.

During my graduate education I have enjoyed the opportunity of interacting with fellow students and researchers. I thank past and present members of the Jenekhe group – Dr. Alex Briseno, Taeshik Earmme, Dr. Hao Xin, Dr. Pei-Tzu Wu, Dr. Eilaf Ahmed, Guoqiang Ren, Ye-Jin Hwang, Dr. Selvam Subramaniyan, Dr. Haiyan Li, Dr. Nishit Murari, Dr. Soon-Ok Jeon, Brandon Stickelmeyer, Karl Kerr, Matthew Crane, Dr. Jessica Hancock, Dr. Abhishek Kulkarni, Dr. Takahiro Kojima, Dr. Masashi Mamada, Dr. Kazuhiro Nakabayashi, Prof. Taewoo Kwon, Prof. Unyong Jeong, Dr. Tricia Young-Bull, Nathan Morris, Emily Hollenbeck, and Berlin Sudduth. They have influenced my graduate work and life through intellectually stimulating discussion, fruitful collaborations, and sharing of exciting experience and moments.

I thank all of my collaborators, including Dr. Xugang Guo and Prof. Mark Watson at the University of Kentucky who have provided me an opportunity to study properties of their interesting new materials, Dr. Do-Kyung Hwang, Dr. Canek Fuentes Hernandez, and Prof. Bernard Kippelen at the Georgia Institute of Technology who have provided me a chance to learn more of device engineering, and others who are not listed here in the limited space, for inspiring me with critical comments and fresh ideas.

I would like to acknowledge the Department of Chemical Engineering, Ford motor company fellowship, the National Science Foundation, the US Department of Energy, and Solvay S. A. for financial support.

Finally, I would like to take this opportunity to express my gratitude to my parents, my brother, and my entire family and friends for their support and encouragement. Without them, this work would not have been possible.

Chapter 1. Introduction to Polymer Field-Effect Transistors

1.1. Background

Organic and plastic electronics have been of great interest for development of flexible, light-weight, large-area, and low-cost electronic devices, including organic field-effect transistors (OFETs) for flexible circuits, chemical and biological sensors, organic light-emitting diodes (OLEDs) for displays and lighting, and organic photovoltaic cells (OPVs) for solar energy conversion.[1-3] Among these devices, OFETs have been drawing great attention because, with advantages of unique mechanical properties and inexpensive processability that polymers can offer, the active electronic components realized from polymer semiconductors can be ultimately printed onto unconventional substrates to realize next-generation consumer electronic devices. Polymer-based OFETs are not only for developing flexible and shape-conforming circuits but also for understanding of fundamental charge transport properties of polymer semiconductors. Charge transport properties of various polymer semiconductors designed by creative chemists and materialized through their synthetic tools can be studied by using OFETs to elucidate the correlations between structure, processing, morphology, and properties. In this work, I present studies of OFETs based on π-conjugated polymer semiconductors, in order to improve our understanding of charge transport properties of polymer semiconductors and to develop high-performance OFETs with device/interface engineering.

1.2. π-Conjugated Polymer Semiconductors

π-Conjugated polymer semiconductors are a class of polymers with unique optoelectronic properties. The optoelectronic properties of polymer semiconductors come from the presence of energy bandgap (E_g) between valence band (electron-filled energy states) and conduction band (empty electronic energy states), similar to the physical phenomena discussed in the area of inorganic semiconductors and the band

theory.[4-5] Quantitatively, the bandgap of a polymer semiconductor is the minimum energy required to electronically excite the material from its ground state, and to create an exciton which is a pair of an additional electron in the conduction band and a hole (a missing electron) in the valence band. Although somewhat arbitrary, typical semiconductors have a bandgap less than 4 eV. Ultraviolet/visible/near-infrared (UV/Vis/NIR) light with the photon energy that is equivalent to or larger than the bandgap can be absorbed by the semiconductor as a result of electronic excitation. Materials with a bandgap far larger than 4 eV can be classified as an insulator at room temperature, because thermal excitation of electrons from the valence band (or occupied molecular orbitals in molecular solids) to the conduction band (unoccupied molecular orbitals), which is essential for charge transport in the material, is generally limited, resulting in dc conductivity (σ) less than 10^{-10} S/cm. Materials without a bandgap can be classified as a conductor because electrons can freely move along the partially filled energy band.

π-Conjugated polymer semiconductors have alternating single- and double bonds in the backbone (Figure 1-1).[6-8] According to a molecular orbital theory, electrons in the π-orbitals delocalize across many atomic sites in the polymer chain. The interaction of a large number of π-orbitals results in the formation of continuous energy bands instead of discrete energetic states. However, there is a finite bandgap with no energetic state available (*i.e.*, density of states is 0 at the given energy within the gap) between an electron-filled band and empty band, making the π-conjugated polymer an intrinsic semiconductor with a typical dc conductivity in the range of 10^{-9} to 10^{-2} S/cm. Theoretical and experimental investigations suggest that the bandgap of a polymer semiconductor is mainly determined by: (i) bond length alternation caused by the Peierls instability, (ii) backbone planarity distortion that reduces π-orbital overlaps, (iii) resonance energy of aromatic and quinoidal forms, (iv) electron-donating/electron-accepting strengths, substitution, and distribution of the constituent monomers, and (v) intermolecular orbital interactions.[9] Due to the molecular structure, π-conjugated polymer semiconductors are rigid in molecular scale and thermally rugged (T_m, T_d > 300 °C) compared to non-conjugated polymers. However, they are still

flexible in macroscale and processable from a solution, because their intermolecular interactions (van der Waals force and/or π-π interaction) are relatively weak compared to the covalent or ionic bonding. Studies have showed that chemical doping can result in very high conductivity (>> 1 S/cm) in the π-conjugated polymers.[10-12]

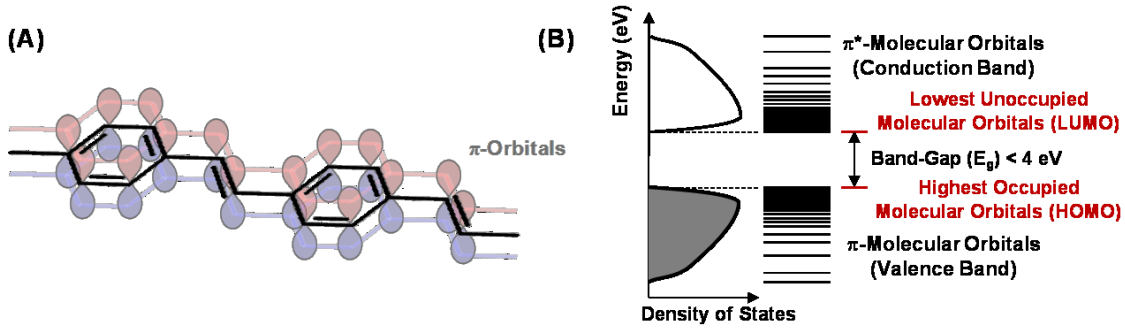

Figure 1-1. Energy band and bandgap formation in a π-conjugated polymer. (A) Schematic of π-conjugation in a representative example of a polymer semiconductor, poly(*p*-phenylene vinylene) (PPV). Note that alternating single- and double bonds present in the molecular backbone. (B) Schematic of electronic energy–density of state diagram of a π-conjugated polymer semiconductor.

Polymer semiconductors are mechanically flexible and have very low specific weight.[13-16] Similar to many of conventional non-conjugated polymers, polymer semiconductors can be processed in a solution-based roll-to-roll processing,[17-25] enabling continuous production of large-area devices and electronic components with very low capital investments. This advantage is important for production of disposable consumer electronics that requires extremely low manufacturing cost.[26] Another very important advantage of polymer semiconductors is that their properties can be controlled by molecular design and synthesis. For example, many efforts in the area have been focusing on the so-called bandgap engineering, where the electronic energy levels of a polymer semiconductor are tuned by designing molecules with a donor–acceptor architecture, a quinoidal structure, and a controlled conjugation length.[9,27-34] Mechanical properties and solution-based processability can also be controlled by introducing side-chains and functional groups.

Semiconductors can be classified as either *n*-type or *p*-type depending on the type of majority charge-carriers. Crystalline inorganic semiconductors, such as Si, Ge, and GaAs, are intrinsically ambipolar with high carrier mobilities for both holes and electrons.[5] Dopants, intentionally introduced impurities, can define the majority charge-carriers of an inorganic semiconductor. On the other hand, polymer semiconductors are generally unipolar, meaning that transport of one type of charge-carriers is dominant. For example, hole transport with a mobility of 0.001–0.1 cm^2/Vs in poly(3-hexylthiophene) (P3HT) have been routinely observed, whereas electron mobility have not been reported from transistors with a typical device structure. Although dopants may be introduced to improve the conductivity, intrinsic unipolarity of polymer semiconductor is hardly controllable. With some exceptions of ambipolar semiconductors reported recently,[35-42] ambipolarity can only be observed from polymer semiconductors under extremely controlled conditions.[43]

1.3. Polymer Field-Effect Transistors

1.3.a. Basics and Operation Mechanism

Transistor is a switching device with three electrical terminals. Specifically, field-effect transistor (FET), one of the most important devices that enable modern digital technology, consists of source, drain, and gate electrodes, a semiconductor bridging the source and drain electrodes, and a dielectric layer insulating a gate electrode from the semiconductor.[5,44] The area of the semiconductor placed between the source and drain electrodes is called the transistor channel. FETs are sometimes called as metal-oxide-semiconductor field-effect transistors (MOSFETs) because the gate insulator is frequently made of silicon dioxide or other metal oxides. Current flowing from source to drain under the potential difference of the electrodes is modulated by voltage applied at the gate. Due to the switching characteristics, FETs are basic active building blocks for making nearly all electronic systems that require signal processing. OFETs use thin films of organic semiconductors as active layer. OFETs are also called as organic thin

film transistors (OTFTs), implying that the operation mechanism is similar to amorphous inorganic thin film transistors (TFTs).

Figure 1-2 illustrates operational mechanism of OFETs.[45] No current (or very low current) flows across the channel without gate voltage applied (V_{GS} = 0; off-state), because the intrinsic conductivity of the polymer semiconductor is low and the charge-carriers are not induced. For an *n*-channel OFET, electrons can be induced in the semiconductor, within a few nanometers at most from the interface between the semiconductor and a dielectric layer, by applying positive gate voltage (V_{GS} > 0). The transistor becomes on-state with the accumulated charge-carriers which contribute the current flowing across the channel. In the energy level point of view, electrons can be injected from the source electrode to the lowest unoccupied molecular orbital (LUMO) energy level of the polymer semiconductor, and extracted to the drain electrode.

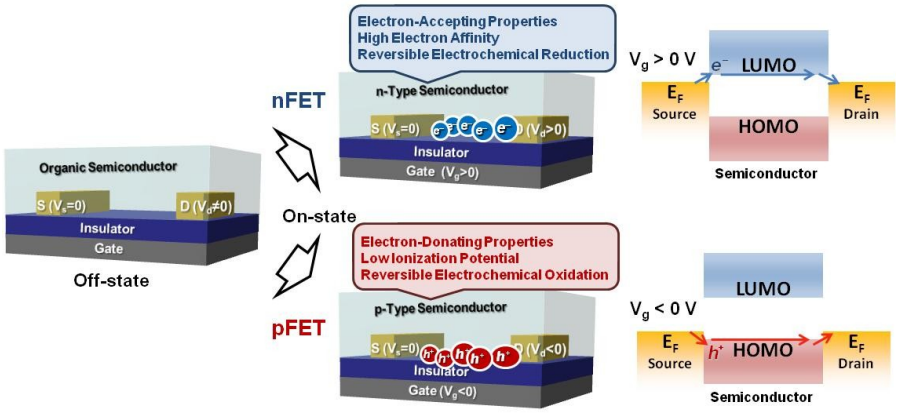

Figure 1-2. Operation mechanism of OFETs.

For a *p*-channel OFET, negative gate voltage (V_{GS} < 0) is applied to induce holes at the interface. Holes can be injected to the highest occupied molecular orbital (HOMO) energy level from the source electrode. In order to facilitate efficient charge injection/extraction and charge transport, well-matched electronic energy levels of the semiconductor and work function of the electrodes are required. It should be noted that the operation mechanism of OFETs is different from that of inorganic metal-oxide-

semiconductor FETs in which carrier inversion occurs. In OFETs, contributing charge-carriers are accumulated at the channel instead of being inverted. In other words, a *p*-channel OFET is made from a *p*-type semiconductor and an *n*-channel OFET is from an *n*-type semiconductor.

1.3.b. Electrical Characteristics and Parameters

Representative electrical characteristics of *n*-channel OFETs are shown in Figure 1-3. Output curves (Figure 1-3A) are obtained by measuring source-drain current (I_{DS}) as sweeping source-drain bias (V_{DS}) at various source-gate bias (V_{GS}). Here, the source electrode is generally grounded. This family of curves exhibits linear increase in I_{DS} at low V_{DS} (linear region; $V_{DS} << V_{GS}$), and saturation of I_{DS} at high V_{DS} (saturation region; $V_{DS} \geq V_{GS}$).[5,44-45] Another way of looking at the electrical characteristics of a field-effect transistor is transfer characteristics (Figure 1-3B), which is a plot of I_{DS} as a function of V_{GS} at fixed V_{DS}. The transfer curves are typically plotted in semi-log scale to show the current increase from off-state to on-state, which is typically several orders of magnitude. A plot of I_{DS} versus V_{GS} in the transfer curve is often accompanied by a linear scale plot of $|I_{DS}|^{1/2}$ as a function of V_{GS}, because the slope of $|I_{DS}|^{1/2}$ can be used to extract electrical parameters of the OFET.

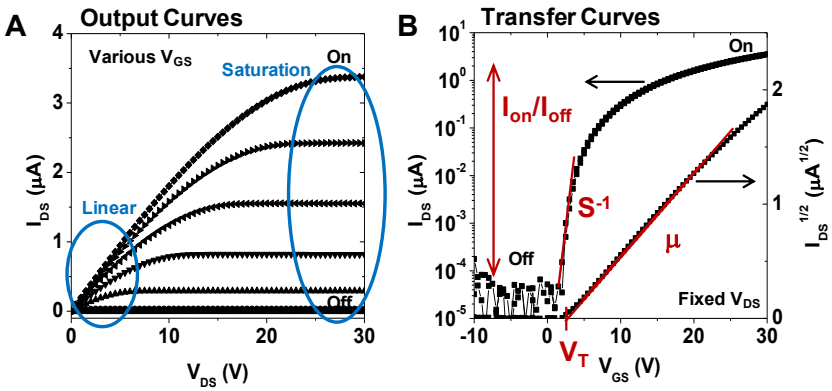

Figure 1-3. Typical electrical characteristics of *n*-channel organic field-effect transistors: (A) Output and (B) transfer curves. Electrical parameters can be extracted by using standard equations for metal-oxide-semiconductor field-effect transistors.

Important electrical parameters are field-effect mobility (μ), on/off current ratio (I_{on}/I_{off}), threshold voltage (V_T), and inverse subthreshold slope (S). Field-effect mobility, also called as charge-carrier mobility in FET, tells us how fast charge-carriers can move in the semiconductor. On/off current ratio is a ratio source-drain current at on-state to that at off-state, and represents how different current between on-state and off-state is. Threshold voltage is a switching point of the transistor, and inverse subthreshold slope shows how fast transition occurs. Channel dimensions, such as a width (W) and a length (L), and capacitance density of dielectric layer (C_i) are device parameters that define operating current and voltage levels. Correlations of the parameters in OFETs are adopted from inorganic transistor theory as followings:[5,45-46]

$$I_{DS} = \mu \frac{WC_i}{L}(V_G - V_T - \frac{V_D}{2})V_D \text{, and} \qquad \text{(Eq. 1-1; For linear region, } V_D << V_G - V_T\text{)}$$

$$I_{DS} = \mu \frac{WC_i}{2L}(V_G - V_T)^2 \text{,} \qquad \text{(Eq. 1-2; For saturation region, } V_D \geq V_G - V_T\text{)}$$

where C_i is a capacitance per unit area of gate dielectric. The equations are from the assumption of charge-sheet approximation, *i.e.*, all the charges are located at the semiconductor-insulator interface like a sheet of charges.[5] Inverse subthreshold swing (S) is defined as Eq. 1-3.

$$S = (\frac{d \log_{10} I_{DS}}{dV_G})^{-1} \text{.} \qquad \text{(Eq. 1-3)}$$

1.3.c. Device Structure and Factors Governing Performance

Figure 1-4 shows typical geometries of polymer FETs: (i) top-contact and bottom-gate, (ii) bottom-contact and bottom-gate, and (iii) bottom-contact and top-gate. Each of device structure has its own advantages and disadvantages. Top-contact/bottom-gate geometry has low contact resistance because of the large contact area between the source-drain electrodes and the semiconductor.[47] However, the electrode modification,[48-49] which often leads to high-performance operation, is impossible in the top-

contact devices. Fabrication of devices by using common photolithography is challenging due to the limited chance of having mutually exclusive solubility between a polymer semiconductor and a photoresist (*i.e.*, limited solvent orthogonality). Bottom-contact/bottom-gate geometry solves the challenges of electrode modification and photolithographic patterning, but often suffers from large contact resistance.[47] Bottom-contact/top-gate geometry offers possibilities of electrode modification, photolithographic patterning, and low contact resistance, by taking advantages of previous two geometries.[22,50-51] Yet, development of a solution processable gate insulator that has solvent orthogonality with an underlying organic semiconductor is challenging, and is also an important area of research. Figure 1-5 shows fabrication procedures of the discussed architectures of OFETs.

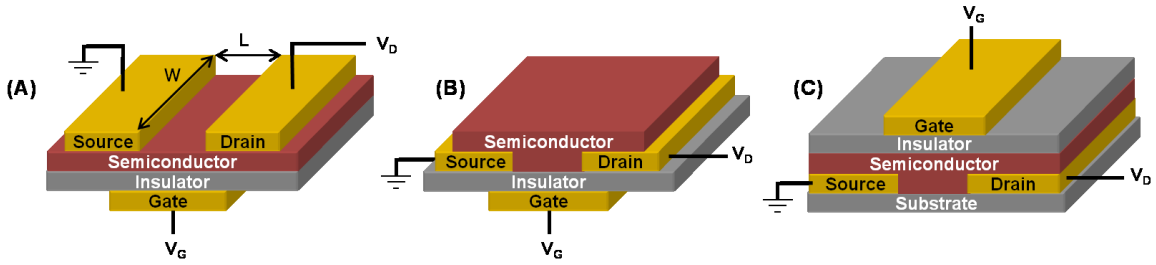

Figure 1-4. Typical OFET structures. (A) Top-contact and bottom-gate, (B) bottom-contact and bottom-gate, and (C) bottom-contact and top-gate.

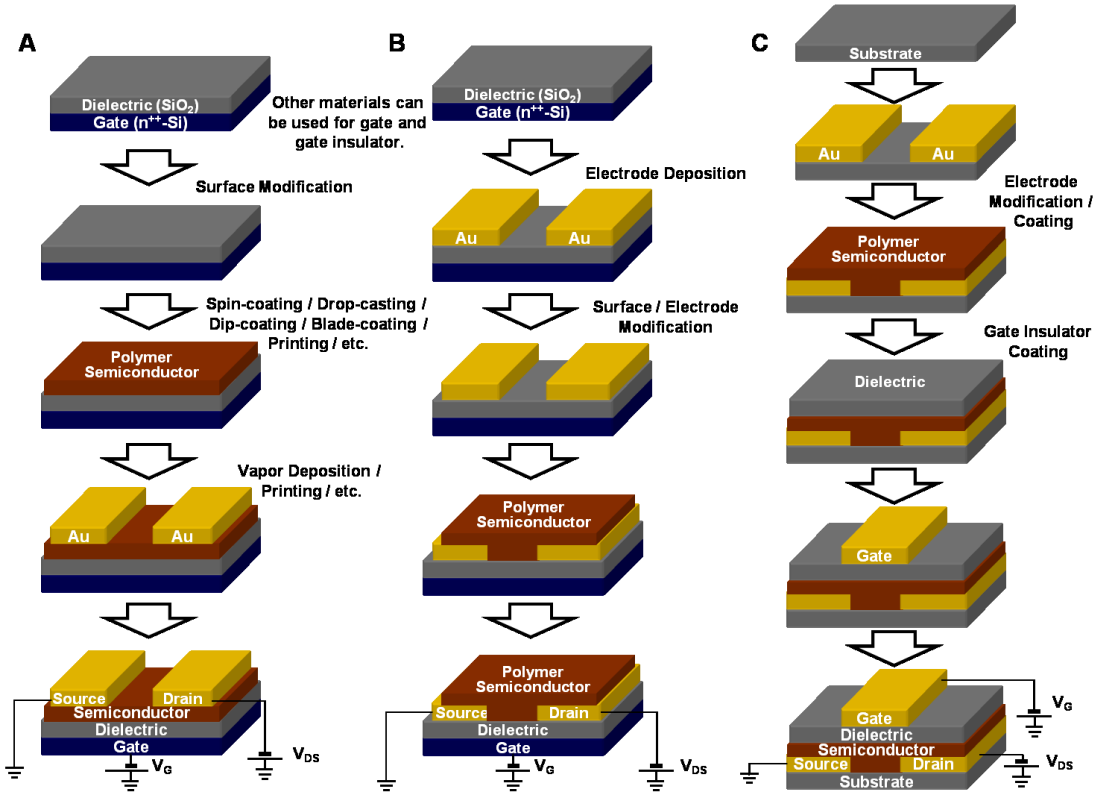

Figure 1-5. Typical fabrication procedures of polymer field-effect transistors. (A) Bottom-contact/bottom-gate geometry, (B) top-contact/bottom-gate geometry, and (C) bottom-contact/top-gate geometry.

There are several factors that affect the performance of OFETs based on polymer semiconductors as illustrated in Figure 1-6. An active layer (*i.e.*, polymer semiconductors) needs to have an extended π-conjugation and a strong interaction between neighboring π-orbitals for high-mobility charge transport.[52] Therefore, high-purity polymer semiconductors with high crystallinity, large molecular weight, and suitable electronic energy levels are required.[26,43,53-56] Careful design, synthesis, and thorough purification of chemicals and polymer semiconductors are critical. Unlike small-molecule organic semiconductors, where large crystalline domains in a thin film, and even single-crystals, can be grown with controllable manners, polymer semiconductors are less-crystalline and disordered in nature. Therefore, morphological controls of degree of crystallinity with right packing motif and domain interconnectivity in a uniform film by both design of molecular structures and selection of processing are also important.[34,41,53,57-60] For electrodes, suitable work function, either by having different metals[61] or by modifying surface a given

conducting material,[62-64] provides a low charge injection barrier, resulting in low contact resistance. Abundance and oxidative stability are practically important for choices of electrodes. As charge transport occurs at the interface of semiconductor facing dielectric, the roughness,[65] robustness,[20] capacitance,[66] chemical structure,[43,67] and dielectric constant[68-69] of the insulator affect the charge transport properties and operation of the OFETs. Therefore, engineering of semiconductor/dielectric[61,70-72] and semiconductor/electrode[48-49,73] interfaces has been applied to improve the performance of OFETs.

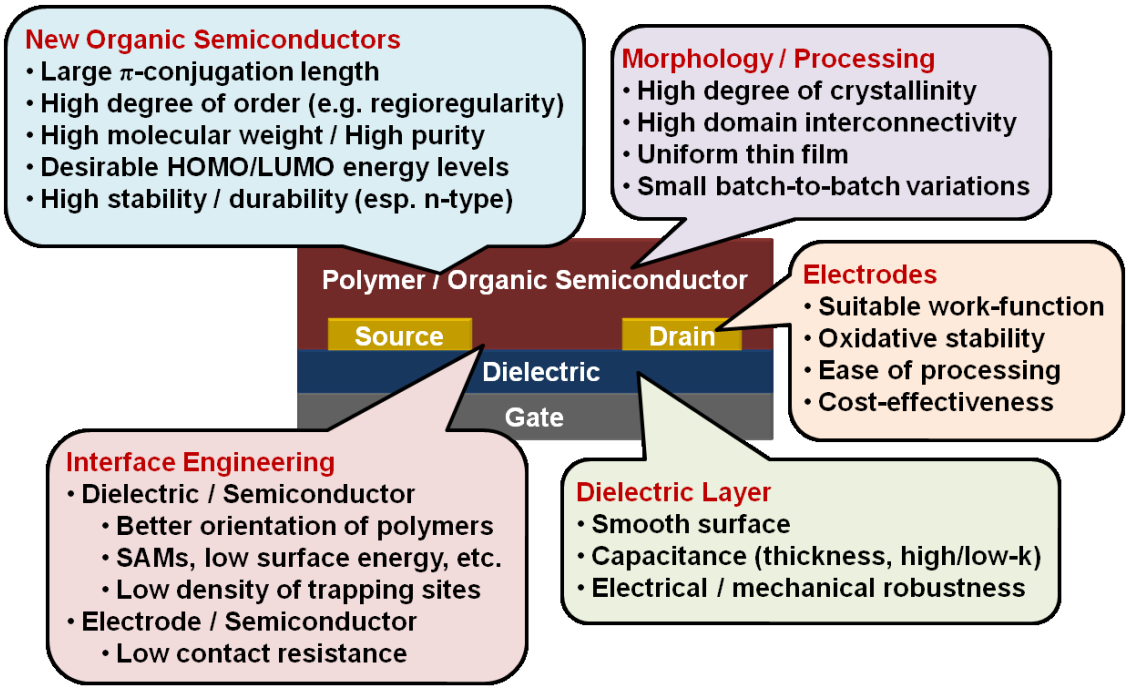

Figure 1-6. Key Factors Affecting Performance of Polymer-based OFETs.

1.4. Literature Review of Polymer Semiconductors for OFETs

In the past few decades, tremendous advancement in the field of OFETs has been achieved in terms of the performance and charge-carrier mobility. The field-effect mobility has increased from ~10^{-5} cm^2/Vs in early polymer FETs[74-75] to ~0.1–1 cm^2/Vs in current state-of-the-art FETs based on polymer semiconductors (Figure 1-7),[22,34,39,41-42,57,76-91] which is comparable to the mobility of competing

technology such as amorphous silicon. Although even higher field-effect mobility on the order of 0.1–10 cm^2/Vs has been observed in thin films and single-crystals of small-molecule organic semiconductors, for example oligoacenes (*e.g.*, pentacene,[92-93] rubrene,[94-96] TIPS-pentacene,[49] and C_8-BTBT[97-98]), oligothiophenes (*e.g.*, α-6T[99] and DFHCO-4T[100]), phthalocyanine derivatives (*e.g.*, CuPc[101] and F_{16}CuPc[102]), arylene diimides (*e.g.*, functionalized NDIs[103] and PDIs[104-105]), and fullerenes (*e.g.*, C_{60}[106-107] and PCBM[61,108]), I focus on the review of polymer semiconductors for the scope of this dissertation.

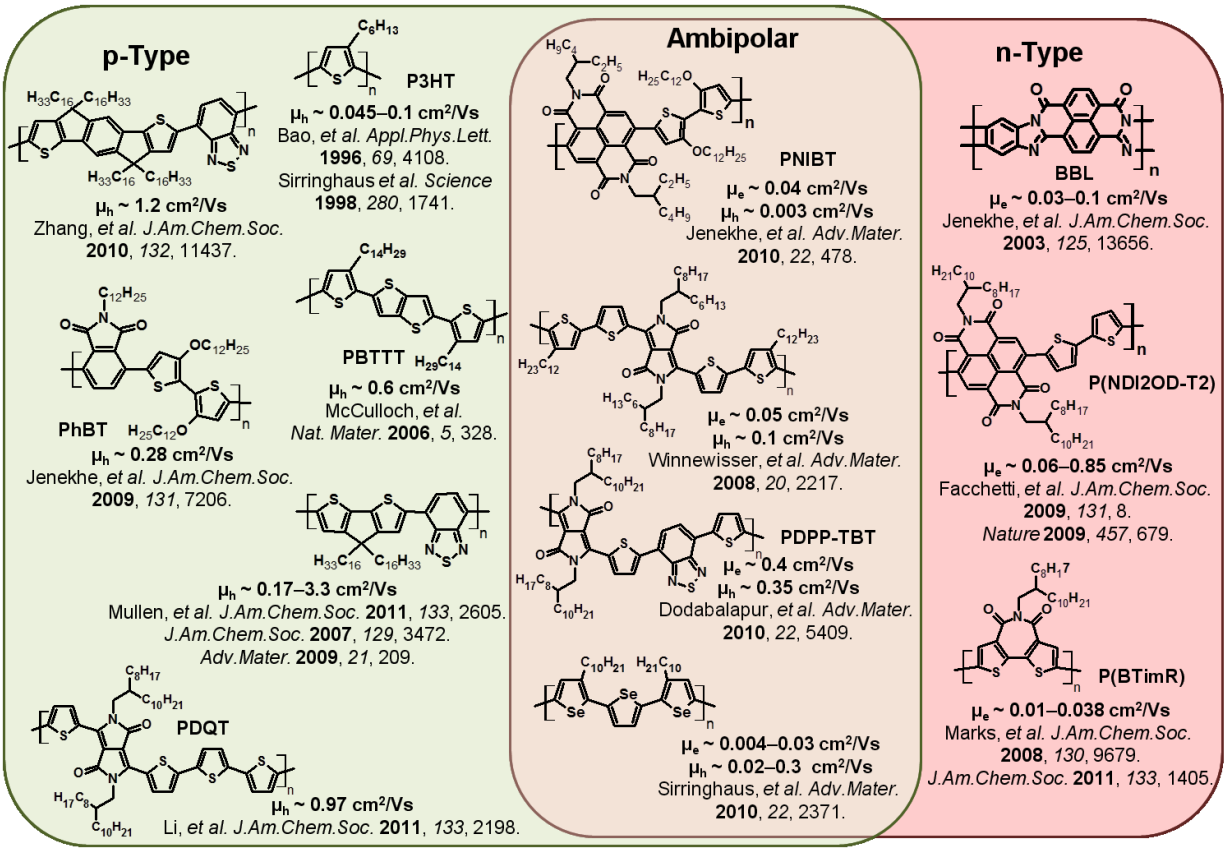

Figure 1-7. Representative polymer semiconductors with high field-effect mobility.

1.4.a. p-Type Polymer Semiconductors

The majority of the current polymer semiconductors for OFETs are *p*-type (*i.e.*, hole transporting). Early demonstration of polymer-based OFETs includes polythiophene[74] and polyacetylene,[75] all with the

hole mobility in the range of 10^{-5}–10^{-4} cm^2/Vs. PTAA with the mobility of 3.3×10^{-3} cm^2/Vs[109] and F8T2 with the mobility of ~0.02 cm^2/Vs[70] are also notable *p*-type polymer semiconductors that have been studied to understand the role of different dielectric layers and surface treatment on the hole mobility.

Among the *p*-type polymer semiconductors, polythiophene and its derivatives are undoubtedly one of the most important classes of *p*-type polymer semiconductors. Since the polymer FETs with practical high hole mobility of 0.05–0.1 cm^2/Vs are first demonstrated from regioregular poly(3-hexylthiophene) (P3HT),[76-77] enormous studies of charge transport properties and field-effect transistor performance of poly(3-alkylthiophene)s (P3ATs) as a model system have been performed to elucidate structure–processing–morphology–property relationships.[53,55,58-59,110-117] It was found that, in order to increase hole mobility of P3HT, regioregularity[53] and choice of processing solvents[59,112] are critical to have crystalline lamellar packing of P3HTs with edge-on molecular orientation, while high molecular weight is important to enhance crystalline domain interconnectivity.[54-55]

Common ways of tuning electronic energy levels and molecular packing of polymer semiconductors are to control conjugation length[78-79] and to utilize a donor–acceptor architecture in polymer semiconductors.[32-33,118-120] Many of *p*-type polymer semiconductors are designed in these ways, and are largely based on thiophene as a molecular backbone or as a electron-donating comonomer of the donor–acceptor architecture. Recent examples of significant advancement of *p*-type polymer semiconductors include PQT12 (~0.2 cm^2/Vs),[79] PBTTT (~0.06 cm^2/Vs),[78] PhBT12 (0.2–0.3 cm^2/Vs),[34] P2TDC13FT4 (~0.3 cm^2/Vs),[121] PTzQT-14 (0.2–0.3 cm^2/Vs),[83] PSOxTT (~0.1 cm^2/Vs),[86] PNDTBT (~0.5 cm^2/Vs),[122] PC12TV12T (~1.0 cm^2/Vs),[123] PDQT (~1.0 cm^2/Vs),[85] IDT-BT (~1.0 cm^2/Vs),[80] and CDT−BTZ (0.2–3.3 cm^2/Vs).[82,124]

1.4.b. n-Type Polymer Semiconductors

Development of high-mobility *n*-type polymer semiconductors is as important as advancement of high-mobility *p*-type polymer semiconductors for fabrication of high-performance complementary circuits. However, unlike inorganic semiconductors in which *n*-channel operation is more stable and exhibit higher carrier mobility, electron transporting (*n*-type) polymer semiconductors are scarce and more sensitive to environments (*i.e.*, molecular oxygen and water) compared to hole transporting (*p*-type) polymer semiconductors.

A common strategy to make *n*-type polymer semiconductors is to incorporate electron-deficient units or electron-withdrawing groups in the polymer backbone. Imide-functionalized arenes are one of the most promising building blocks among the different electron-deficient units for *n*-type polymer semiconductors. First polymer FETs with high mobility of ~0.03–0.1 cm^2/Vs in air was demonstrated from ladder-type polybenzobisimidazobenzophenanthroline (BBL).[57,125] BBL contains fused rings with rich imide and imine groups and double-stranded structure, has a low-lying LUMO energy level of (-4.0–-4.2 eV), is highly crystalline, and processable in strong acids such as methanesulfonic acid (MSA).[126-129] Non-ladder-type analog BBB showed rather low electron mobility of 10^{-6} cm^2/Vs.[57] Polymer semiconductors based on perylenetetracarboxylic diimides (PDIs),[130-131] bithiophene imides (BTIs),[89-90] and naphthalenetetracarboxylic diimides (NDIs)[22,88,132-133] are other examples that have exhibited promising n-type properties. These polymer semiconductors are readily soluble in common organic solvents, and have showed the electron mobility in the range of 0.01–0.85 cm^2/Vs.

1.4.c. Ambipolar Polymer Semiconductors

An ambipolar OFET is a transistor that can be operated in both *p*-channel and *n*-channel modes depending on the polarity at the electrodes. Although incorporation of unipolar *p*-type and *n*-type polymer semiconductors into an active layer of an OFET results in the ambipolar operation, in this section we

focus intrinsic ambipolar polymer semiconductors. It should be noted that, although ambipolar charge transport properties have been observed from many of well-known unipolar *p*-type polymer semiconductors, their strict requirements (*e.g.*, as trap-free dielectrics, low work function electrodes, air-free environments)[43] for the observation of ambipolarity excluded discussion of such cases in the generally-known unipolar polymer semiconductors in this section.

Ambipolar polymer semiconductors have a relatively narrow bandgap, with high-lying HOMO energy levels and low-lying LUMO energy levels in order to minimize charge injection/extraction barriers and support efficient electron- and hole-transport. A common strategy to tune electronic energy levels is, again, to utilize a donor–acceptor architecture in polymer semiconductors.[32-33,118-119] Ambipolar polymer semiconductors with LUMO levels of -4.0–-4.2 eV and HOMO levels of -5.1–-5.5 eV exhibited electron and hole mobilities in the range of 10^{-4} to 0.1 cm^2/Vs.[39-41,134]

First demonstration of ambipolar charge transport in polymer semiconductors is based on PIF.[36] This polyhydrocarbon has the bandgap of 1.55 eV and electron and hole mobilities of ~5×10^{-5} cm^2/Vs. After this finding, research groups have reported better performing ambipolar OFETs based on single-component polymer semiconductors, for example F8BT (~0.005 cm^2/Vs),[38] PIFDMT4 (~0.0002 cm^2/Vs),[134] PNIBT (0.003–0.04 cm^2/Vs),[41] P(DTP-BThBbT) (0.0006–0.001 cm^2/Vs),[40] PSSS (0.01–0.3 cm^2/Vs),[87] and PDA (0.02–0.1 cm^2/Vs).[135] It is interesting to note that, recently, there have been a fair number of reports regarding high-mobility ambipolar charge transport in diketopyrrolopyrrole (DPP)-based polymer semiconductors, although some other DPP-based polymer semiconductors show unipolar *p*-type characteristics. Examples of the DPP-based ambipolar polymer semiconductors include BBTDPP (~0.1 cm^2/Vs),[39] PDPP3T (0.01–0.04 cm^2/Vs),[136] HDPPTV (~0.03–0.2 cm^2/Vs),[137] and PDPP-TBT (~0.4 cm^2/Vs)[42]

1.5. Major Challenges

In the last few decades, extensive studies of polymer semiconductors and organic electronic devices have been performed by academic and industrial sectors to understand the relationships between structure, morphology, and optoelectronic properties, to improve the device performance by engineering, and to demonstrate and commercialize organic electronic products. However, there are still many challenges, such as increasing charge-carrier mobility, developing *n*-channel polymer semiconductors, enhancing stability in ambient conditions, and studying novel phenomena and applications.

Although the current organic semiconductors, even in a single crystalline form, hardly compete with inorganic crystal semiconductors (*i.e.*, single-crystalline silicon) for microprocessors in terms of charge-carrier mobility, organic electronics are still promising in different areas that make the best use of mechanical properties and processability of polymers, such as large-area displays and flexible circuits, with a moderate operation speed. However, higher charge-carrier mobility (>1 cm^2/Vs) is required to outperform the other alternative technology including amorphous silicon and metal oxide semiconductors.

Polymer semiconductors are vulnerable to external dopants such as oxygen and moisture in general.[138-141] In order for polymer FETs and associated circuits to be useful in real-world electronic applications with excellent reliability, long-term stability in working environment (*i.e.*, in air) must be ensured and the effects of atmospheric contaminants must be controlled.[17,142-143] Experimental studies have suggested that oxygen and related species have negative effects on the electrical characteristics of polymer FETs.[138,144] Considerations of thermodynamics and kinetics of doping and charge trapping caused by the external molecules should be addressed to achieve high air-stability and durability of polymer semiconductors in ambient conditions.

Novel approaches of improving basic performance of polymer semiconductor devices or introducing unique processing methodology are of interest along with designing and developing new polymer

semiconductors. Studies of ambipolar charge transport, studies of polymer semiconductor nanostructures, studies of printable electronics, and studies of dielectrics/electrodes are a few among them. These studies may lead us to realize applications that we can imagine, such as polymer-based circuits for displays and radio-frequency identification (RFID) tags, chemical/biosensors, and implanted medical devices, and that we have not imagined yet. Many applications will emerge with findings of novel systems in terms of materials and device structures.

1.6. Research Objectives and Significance

The primary objective of this research is to study relationships of structure–morphology–charge transport properties of π-conjugated polymer semiconductors, to develop high-performance field-effect transistors and circuits based on polymer semiconductors by device engineering, and to investigate ambipolar and unipolar charge transport properties of multicomponent systems, such as polymer semiconductor blends and polymer semiconductor nanocomposites. The objectives of this research focus on addressing several current issues in the field.

(i) Understanding the factors affecting the charge-carrier mobility and air-stability of polymer semiconductors to demonstrate high-performance organic field-effect transistors. Although charge-carrier mobility of polymer semiconductors has been drastically increased recently, it is still in the range of mobility of competing amorphous inorganic semiconductor technology (0.1–1 cm^2/Vs). High-mobility (>1 cm^2/Vs) with air-stability of polymer semiconductor devices, achieved by molecular design, device engineering, and processing optimization, would enable realization of polymer FET-based products in the market. For this purpose, detailed case studies of the relationships between structures, morphology, electronic energy levels, and charge transport properties of various series of polymer semiconductors are performed (Chapter 2). Hole and electron mobilities in the range of ~10^{-4}–0.28 cm^2/Vs are observed in the polymer FETs of a ladder-type polymer and various donor-acceptor alternating copolymer

semiconductors based on phthalimide, thiazolothiazole, benzobisthiazole, and naphthalenetetracarboxylicdiimide units. Stability data such as shelf stability and operational stability of some of *p*-channel and *n*-channel polymer FETs in air are also presented and the origin of the stability is discussed in views of thermodynamics and kinetics. Integration of unipolar *p*- and *n*-channel polymer FETs into a complementary circuit is demonstrated to emphasize the necessity of development of both *p*-type and *n*-type polymer semiconductors. Information obtained from this study will provide potential design criteria for developing novel polymer semiconductors with high mobility and high stability/durability.

(ii) Studying ambipolar charge transport in polymer semiconductors. Ambipolar polymer FETs may offer significant reduction of manufacturing cost by eliminating *p*- and *n*-type polymer semiconductor patterning in complementary circuits and may also introduce a new functionality of a single transistor and in the circuits. Chapter 3 discusses ambipolar charge transport in polymer semiconductor thin films. Three different strategies for realizing ambipolar polymer FETs are applied: (i) single-component polymer semiconductors, (ii) layered heterojunctions of unipolar polymer semiconductors, and (iii) bulk heterojunctions (blends) of unipolar polymer semiconductors. Single-component ambipolar polymer semiconductors follow similar morphology–transport property relationships of unipolar polymer semiconductors. Heterojunction approaches based on air-stable unipolar polymer semiconductors, for examples, polybenzobisthiazoles (PBTs), polythiazolothiazoles (PTTs), and ladder-type polybenzobisimidazobenzophenanthroline (BBL), offer outstanding stability of the ambipolar transistors. Attempts to mimic complementary logic circuits, including NOT-, NAND- and NOR-gates, from a single-type active layer without patterning are presented as well.

(iii) Engineering of polymer semiconductor/dielectric interface for enhancements of charge-carrier mobility and electrical stability. The effect of dielectric constant of a gate insulator layer on charge transport of *n*-channel polymer FETs is given in Chapter 4. The FETs based on

poly(benzobisimidazobenzophenanthroline)s (BBL and BBB) with a thin non-conjugated polymer (<100 nm) coated on a silicon dioxide gate insulator exhibited excellent charge transport properties, such as higher mobility, negligible hysteresis, and superior electrical stability, compared to the polymer semiconductor thin films on a pristine SiO_2. The field-effect mobility of electrons in BBL FETs increases exponentially with decreasing dielectric constant of the polymer dielectric buffer layer.

(iv) Studying charge transport in polymer semiconductor nanowires and nanocomposites. Nanowires and nanocomposites are of interest for fundamental understanding of charge transport in polymer semiconductors, and for potential of nanoelectronics. In Chapter 5, charge transport properties of polymer semiconductor nanowires and nanocomposites are discussed. Very low percolation threshold and unusual composition dependence of field-effect mobility are observed from self-assembled high-aspect-ratio polymer semiconductor nanowires dispersed in an insulating polymer matrix. Discussion on intra- and inter-nanowire charge transport is also given to propose the origin of the observed phenomena. The results suggest a new strategy for high-performance ambipolar charge transport with controlled morphology.

Chapter 2. High-Performance Unipolar Polymer Field-Effect Transistors

This chapter presents case studies of structure–morphology–charge transport property relationships of series of polymer semiconductors. With these polymer semiconductors, high-performance unipolar field-effect transistors (FETs) are demonstrated. Enhanced air-stability of polymer FETs are discussed in terms of energetic and kinetic factors. The results in this chapter are reprinted in part with permission from Guo and Kim, *et al.* (Copyright 2009 American Chemical Society),[34] Subramaniyan and Kim, *et al.* (Copyright 2011 The Wiley-VCH),[86] Ahmed and Kim, *et al.* (Copyright 2011 American Chemical Society),[145] Guo and Kim, *et al.* (Copyright 2012 American Chemical Society),[133] and Briseno and Kim, *et al.* (Copyright 2011 The Royal Society of Chemistry).[143]

2.1. Introduction

Achieving high-mobility and high-stability/durability is one of the most important challenges in the area of organic electronics as described in the previous chapter. In this chapter, charge transport characteristics of several unipolar *p*-type and *n*-type polymer semiconductors with high mobility and high stability are presented. Field-effect mobility on the order of ~10^{-4}–0.1 cm^2/Vs was observed from the polymer semiconductors. I have investigated effects of structural variations on the electrical properties. Specifically, effects of side chain substitutions, as exemplified by phthalimide-bithiophene copolymers (PhBTs) and poly(thiazolothiazole)s (PTTs), and donor-acceptor combinations, as exemplified by poly(benzobisthiazole)s (PBTs) and poly(naphthalenetetracarboxylic diimide)s (PNDIs), were studied. Solid-state morphology and charge transport properties in OFETs of the polymer semiconductors were characterized to reveal structure–morphology–property relationships in detail. Long-term stability of *n*-channel and *p*-channel OFETs based on ladder-type poly(benzobisimidazobenzophenanthroline) (BBL) and one of PBTs, respectively, in air has also been studied and the origins of the excellent stability are suggested. Experimental results and discussion that described here give a general guideline for designing

new high-performance polymer semiconductors. Finally, fabrication of polymer-based complementary inverters and characterization of their static-state electrical performance are described.

2.2. Experimental Methods

Materials. Most of the studied polymer semiconductors, including phthalimide-bithiophene copolymers (PhBTs),[34] poly(thiazolothiazole)s (PTTs),[86,146] poly(benzobisthiazole)s (PBTs),[145,147] poly(naphthalenetetracarboxylic diimide)s (PNDIs),[41,132] and ladder-type poly(benzobisimidazo-benzophenanthroline) (BBL),[57,148] were synthesized in house or by our collaborators. Poly(3-alkylthiophene)s (P3ATs), including poly(3-butylthiophene) (P3BT) and poly(3-hexylthiophene) (P3HT),[11,149-150] were purchased from Aldrich and American Dye Sources. Most of solvents, including toluene, chloroform, chlorobenzene, 1,2-dichlorobenzene (ODCB), 1,2,4-trichlorobenzene, methanesulfonic acid (MSA), acetone, isopropyl alcohol, and so on, were purchased from Aldrich and EMD Chemicals, and used as received. Silane agents, such as octyltriethoxysilane and octyltrichlorosilane (OTS8), were purchased from Aldrich and Gelest. Single-side-polished prime-grade heavily *n*-doped silicon wafers with a thermally grown oxide layer were purchased from Silicon Valley Microelectronics, Silicon Quest International, and WRS Materials. Gold shots (99.999%) were purchased from Aldrich and Kurt J. Lesker. Chromium-plated tungsten rods were purchased from R. D. Mathis.

Fabrication and Characterization of Field-Effect Transistors and Logic Circuits. Field-effect transistors were fabricated on heavily n-doped silicon substrates with thermally grown silicon dioxide gate insulator (100–300 nm). For bottom contact devices, gold source and drain electrodes (30–50 nm) with a thin chromium adhesive layer (1–2 nm) were patterned on the silicon dioxide by photolithography, thermal evaporation of metals, and lift-off of a photoresist layer. For top contact devices, gold source-drain electrodes (30–40 nm) were deposited by thermal evaporation through a shadow mask under high vacuum (~10^{-6}–10^{-7} Torr). Channel widths (W) and lengths (L), defined by patterned source-drain

electrodes, were 400–5000 μm and 10–200 μm, respectively. The substrates were cleaned by sequential ultrasonication in acetone and in isopropyl alcohol for 30 min each and dried by flow of nitrogen. Some of substrates were further cleaned by air-plasma treatment for 2–4 min. Hydrophobic surface of the substrate was made by forming a self-assembled monolayer of OTS8 onto the silicon dioxide surface by spin-coating (4 mM in chloroform) or vapor deposition. OTS8-treated substrates were rinsed by toluene to remove physisorbed silane agents and annealed at 100 °C for 10 min in air to ensure the complete silanization. Polymer thin films were deposited onto a substrate by spin-coating (1–3 krpm) or by drop-casting from a polymer solution. Some of the devices were annealed at various temperatures (100–250 °C) for 10–30 min under inert conditions. Gate contact pad was formed by mechanically scratching silicon dioxide at the corner of a substrate and pressing a piece of indium onto the exposed gate electrode of the doped silicon. An individual transistor on a common substrate was isolated by removing the polymer semiconductor around the device before electrical measurement. Electrical characteristics of the devices were measured by using an HP4145B semiconductor parameter analyzer under nitrogen atmosphere or a Keithley SCS4200 system in ambient air. The field-effect mobility was calculated from a saturation region by using Eq. 1-2.[5,44]

Characterization of Solid-State Morphology. Surface morphology of thin films was imaged from the devices by using a Veeco Dimension 3100 scanning probe microscopy in tapping mode. X-ray diffraction (XRD) patterns were obtained from thin films on clean glass substrates by using a Bruker AXS D8 Focus diffractometer with Cu Kα beam (40 kV, 40 mA; λ = 0.15418 nm).

2.3. Results and Discussion

2.3.a. p-Channel FETs based on Donor–Acceptor Copolymer Semiconductors

2.3.a.1. Phthalimide-based Copolymer Semiconductors (PhBTs).

A series of polymer semiconductors based on phthalimides (PhBTs) has been synthesized by Dr. Xugang Guo at the University of Kentucky.[34] PhBTs are designed to possess a donor–acceptor architecture with didodecyloxybithiophene as an electron-donating unit and phthalimide as an electron-accepting unit. Two PhBTs have different side-chains on the phthalimide unit: PhBT12 has a linear dodecyl chain and PhBTEH has a branched 2-ethylhexyl chain (Figure 2-1A). The charge-transport properties of PhBTs were investigated by fabricating OFETs with bottom-contact and bottom-gate geometry (Figure 1-4B). Devices were fabricated without any annealing procedure and tested under ambient air and light without any environmental control. The devices showed excellent current-modulation and well-resolved linear and saturation currents in *p*-channel operation as shown in Figure 2-1(B-D). Maximum saturation mobilities were 0.28 cm^2/Vs for PhBT12 and 0.036 cm^2/Vs for PhBTEH. Average hole mobilities of PhBT12 and PhBTEH, taken from over 30 devices for each polymer, were 0.17 (±0.05) cm^2/Vs and 0.017 (±0.008) cm^2/Vs, respectively. On/off current ratios of 10^4–10^5 were routinely observed from both polymers with maximum values greater than 10^6. Average threshold voltages were 24 V for PhBT12 and 31 V for PhBTEH.

XRD patterns (Figure 2-2) show 1st- and 2nd-order diffraction maxima at 2θ of 3–7 °, indicating short-range (100) lamellar ordering of PhBTs in thin films. The *d*-spacings calculated from these peaks were 31.4 Å for PhBT12 and 28.1 Å for PhBTEH. The difference implies side-chain interdigitation of PhBTEH in thin films. Wider-angle diffraction maxima are assigned to the π-stacking distances for PhBT12 (3.6 Å) and PhBTEH (3.7 Å). Although PhBT12 has slightly shorter *d*-spacing in the π-stacking axes, the calculated *d*-spacings are very similar and this difference may not have a large impact on charge

transport. However, PhBT12 gives an apparently more distinct peak suggesting better ordering in molecular scale, possibly linked to differences in OFET performance. Wide-angle X-ray diffraction (WAXD) 2D-diffraction patterns collected in transmission mode from thermally annealed, extruded fibers of both polymers indicate longer-range order with 3-dimensional registry.[34]

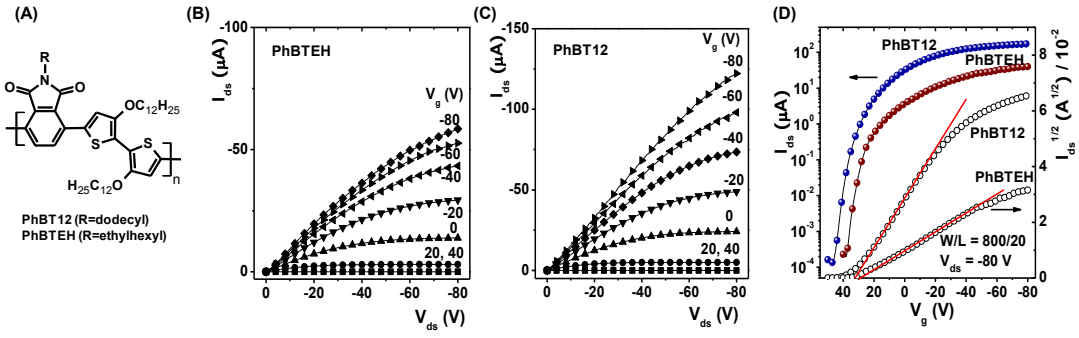

Figure 2-1. (A) Chemical structures of PhBTs. Output characteristics of OFETs based on (A) PhBTEH and (B) PhBT12. (C) Overlays of transfer characteristics of OFETs based on PhBTs. Reproduced in part with permission from Ref.[34] Copyright 2009 American Chemical Society.

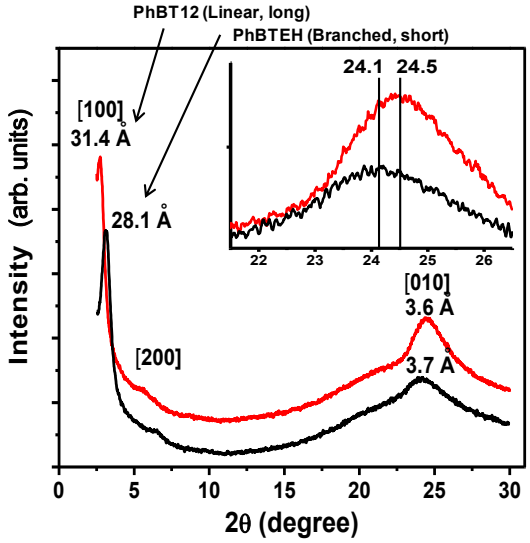

Figure 2-2. X-ray diffraction profiles of PhBT copolymer semiconductors. Reproduced in part with permission from Ref.[34] Copyright 2009 American Chemical Society.

Atomic force microscopy (AFM) images collected from the devices reveal nanofibrillar ordered domains with widths of 15–30 nm (Figure 2-3A,B,D,E). Domain boundaries are not as well-resolved in thin films from PhBT12 as from PhBTEH. The better performance of PhBT12 compared to PhBTEH is likely attributed to more extensive domain interconnectivity that leads to more efficient inter-domain charge transport.[124,151] Such enhanced domain interconnectivity might have come from the larger molecular weight of PhBT12 (207.3 kDa) compared to PhBTEH (117.3 kDa), as direct correlations have been observed between molecular weight and OFET performance of P3HT[54-55] and BBL.[56] Optical microscope images (Figure 2-3C,F) showed that PhBTEH is somewhat polycrystalline in macroscopic scale (~10 μm), whereas PhBT12 is more or less amorphous in the range, implying again the better domain interconnectivity in PhBT12 as seen in AFM images.

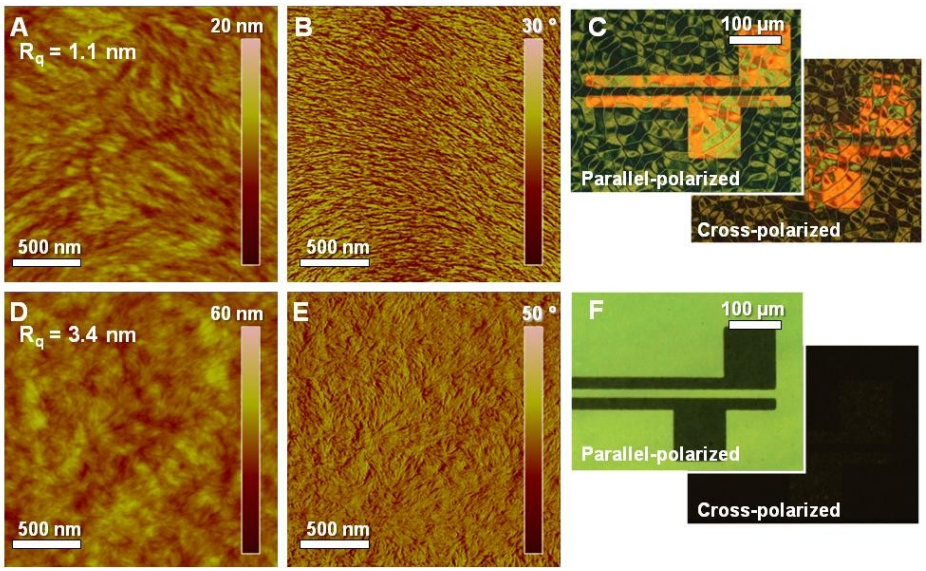

Figure 2-3. Thin film morphology of (A-C) PhBTEH and (D-F) PhBT12. (A,D) AFM Surface topography, (B,E) surface phase images, and (C,F) optical microscopy images of PhBTs. Reproduced in part with permission from Ref.[34] Copyright 2009 American Chemical Society.

2.3.a.2. Thiazolothiazole-based Copolymer Semiconductors (PTTs).

Poly(thiazolothiazole)s (PTTs) were synthesized by Dr. Selvam Subramaniyan.[86,146,152] PTTs have thiazolothiazole units with various combinations of donor moieties, linkage thiophenes, and side chains in

the polymer backbone (Figure 2-4). All of the PTTs showed *p*-type characteristics with hole mobility in the range of 7.6×10^{-3}–0.1 cm^2/Vs (Table 2-1). Here, the effects of side chains in the thiazolotothiazole polymers are investigated in detail as exemplified by PSOTT, PSEHTT, and PSOxTT.

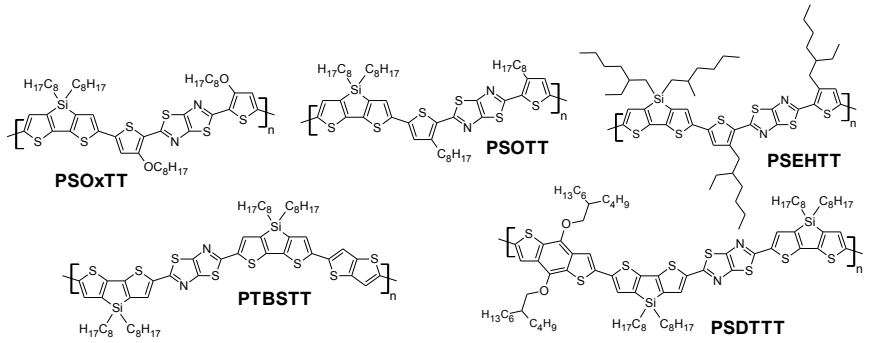

Figure 2-4. Chemical structures of thiazolothiazole-based polymer semiconductors.

PSEHTT and PSOxTT were soluble in common organic solvents such as chloroform and 1,2-dichlorobenzene at room temperature, whereas PSOTT was soluble in these solvents at higher temperatures (60–100 °C). These polymer semiconductors had number-average molecular weights of 15.5–33.9 kDa with a polydispersity index of 2.0–3.9 (Table 2-1).[86] PSOTT and PSEHTT thin films had absorption maxima at 584 and 579 nm, and shoulders at 636 and 624 nm, respectively. As expected from the increased electron-donating nature of the alkyloxy side chains of PSOxTT, its absorption spectrum is red-shifted from those of PSOTT and PSEHTT, giving a maximum at 604 nm and a shoulder peak at 649 nm. The optical bandgap of the polymer semiconductors was in the range 1.73 to 1.82 eV, calculated from the edge of the thin film absorption spectra. The optical bandgap of PSOxTT is ~0.6–1 eV larger than those of PSOTT and PSEHTT. The bandgap of PSOxTT is smaller because of the enhanced backbone planarity and stronger electron-donating property of alkyloxy-substituted thiophenes resulting in stronger donor–acceptor intramolecular interactions.[9,33-34] The HOMO/LUMO energy levels, obtained from an electrochemical method and the optical bandgap, were -5.0/-3.0 eV for PSOxTT, and -5.1/-2.9 eV for PSOTT. In the case of PSEHTT, the HOMO/LUMO energy levels were -5.1/-3.3 eV.[86]

Table 2-1. Molecular weight, electronic energy levels, and electrical parameters of polymer FETs of PTTs.

Polymer	M_n (kDa)	PDI	μ_h^{avg} (cm^2/Vs)	I_{on}/I_{off}	V_t^{avg} (V)	E_g^{opt} (eV)	HOMO (eV)
PSOxTT	24.3	2.0	0.092	10^5	-12.0	1.7	-5.0
PSEHTT	33.9	3.9	0.016	10^5	-4.4	1.8	-5.1
PSOTT	15.5	2.3	0.010	10^6	-13.4	1.8	-5.1
PSDTTT	13.1	3.4	0.0076	10^4	-19.7	1.8	-5.4
PTBSTT	-	-	0.029	10^5	-9.1	1.7	-5.3

Charge transport properties of PSOxTT, PSOTT and PSEHTT and were characterized by using bottom-contact and bottom-gate FETs on silicon substrates. As mentioned above, *p*-channel characteristics with excellent current saturation and large current modulation (I_{on}/I_{off} > 10^5–10^6) were observed (Figure 2-5). PSOxTT had a hole mobility of 0.11 cm^2/Vs whereas PSOTT and PSEHTT had hole mobilities of 0.01–0.03 cm^2/Vs. OFETs based on the three polymer semiconductors showed negligible hysteresis between forward and backward scans of output characteristics (Figure 2-5A-C), suggesting that charge trapping is not significant in the polymer semiconductors.

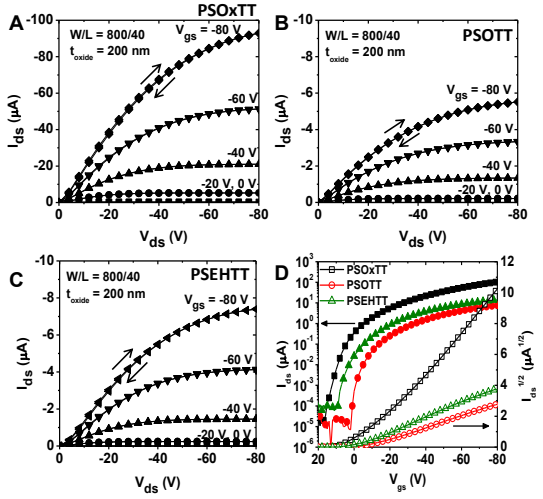

Figure 2-5. Output characteristics of (A) PSOxTT, (B) PSOTT, and (C) PSEHTT FETs. (D) Overlays of the transfer characteristics. Reproduced from Ref.[86] by permission of The Wiley-VCH.

The morphology and molecular organization of PSOxTT, PSOTT and PSEHTT thin films were investigated by X-ray diffraction (XRD).[86] Sharp diffraction peaks with a *d*-spacing of 18.9 and 17.1 Å, corresponding to the lamellar diffractions in *a*-axis, were observed in PSOxTT and PSOTT films, respectively. Interestingly, only a weak diffraction peak in *a*-axis with a d-spacing of 16.5 Å was seen in PSEHTT whereas the π-stacking in *b*-axis with a d-spacing of 3.7 Å is more prominent. This latter observation suggests that a large fraction of the PSEHTT backbones are oriented face-on relative to the substrate; that is, the π-stacking direction is preferably perpendicular to the substrate. Based on the morphological information, a factor of 4–10 higher charge-carrier mobility in PSOxTT compared to PSOTT and PSEHTT is likely from the highly crystalline edge-on orientation of PSOxTT in thin films. Higher mobility of PSEHTT compared to PSOTT may have come from the higher molecular weight of PSEHTT.[54-56]

2.3.a.3. Benzobisthiazole-based Copolymer Semiconductors (PBTs).

Poly(benzobisthiazole)s (PBTs) were synthesized by Dr. Eilaf Ahmed and Dr. Selvam Subramaniyan.[145,147] PBTs have rigid benzobisthiazole units with various combinations of donor moieties in the polymer backbone (Figure 2-6). As the benzobisthiazole unit has a weak electron-accepting property, the LUMO energy levels, estimated from cyclic voltammetry, of all the PBTs were in the narrow range of -3.3 to -3.4 eV. However, HOMO energy levels, ranging from -4.8 eV to -5.7 eV, are largely affected by the strength of electron-donating moieties. All of the PBTs showed *p*-type characteristics with hole mobility in the range of 10^{-4}–10^{-2} cm^2/Vs. All of PBTs are highly crystalline and have an edge-on orientation.[145]

The charge transport properties of the PBTs were investigated by fabricating and testing field-effect transistors using a bottom-contact/bottom-gate geometry (Figure 1-4B). Good current modulation and saturation in *p*-channel operation were seen in the current–voltage characteristics of the OFETs based on the series of PBTs as exemplified by those of PBTHDDT, PBTEHC, PBTPDT, and PBTEHS (Figure

2-7). A hole mobility ranging from 1.8×10^{-4} cm^2/Vs in PBTDTP-1 to 0.01 cm^2/Vs in PBTEHC was observed with on/off current ratio in the range of 10^3 to 10^6 and a threshold voltage in the range of -5.2 V to -28.6 V. The charge-carrier mobility, the on/off current ratio, and the threshold voltage of OFETs based on the PBTs are listed in Table 2-2. All of the PBTs exhibited similar charge transport properties with small variations in the carrier mobility and on/off current ratio as the electron-donating unit in the backbone was varied.

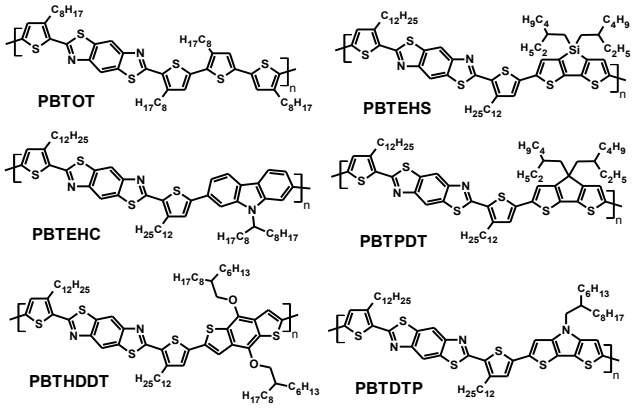

Figure 2-6. Chemical structures of benzobisthiazole-based polymer semiconductors.

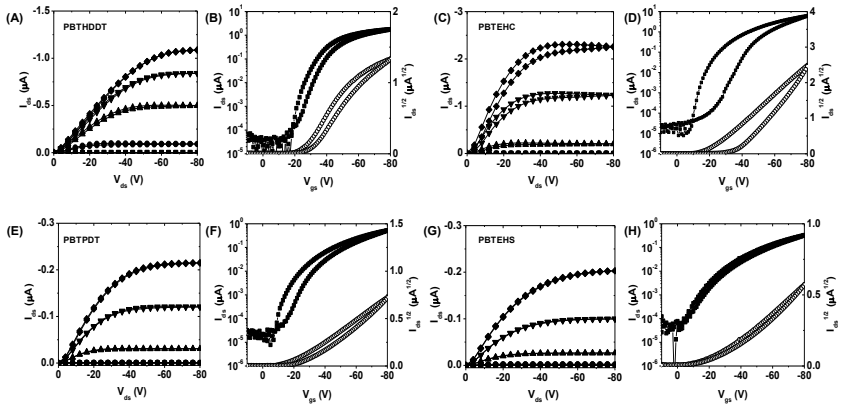

Figure 2-7. Electrical characteristics of (A,B) PBTHDDT, (C,D) PBTEHC, (E,F) PBTPDT, and (G,H) PBTEHS. Reproduced in part with permission from Ref.[145] Copyright 2011 American Chemical Society.

Significant contact resistance was observed from the output characteristics of PBTHDDT and PBTEHC devices (Figure 2-7) as indicated by the superlinearity of current increase in the linear region

(*i.e.*, low V_{ds} and under high V_{gs}). This can be explained by the low-lying HOMOs of both polymers (-5.6 – -5.7 eV), which lead to a large charge injection barrier from gold electrodes with a work function of ~5.1 eV. Nevertheless, as PBTs have highly crystalline in thin films as revealed by their XRD patterns,[145] good charge transport properties with the hole mobility as high as 0.01 cm^2/Vs were observed.

Since the molecular structure and morphology govern the charge transport properties of polymer semiconductors, it is worth comparing the properties of PBTEHS and PBTPDT, whose molecular structures differ only by one atom, a silicon atom versus a carbon atom, respectively, at the five-membered ring on the electron-donating moiety. The two polymers have similar molecular weights and electronic energy levels, such as HOMO/LUMO energy levels and optical bandgap (Table 2-2). PBTEHS and PBTPDT showed very similar charge transport properties (Figure 2-7) with a similar charge-carrier mobility of 6×10^{-4}–8×10^{-4} cm^2/Vs and a threshold voltage (-22.1 – -22.8 V). No evidence of significant effects on charge transport properties was observed by varying single atom in the molecular backbone from carbon to silicon.

Table 2-2. Molecular weight, electronic energy levels, and electrical parameters of PBTs. Reproduced in part with permission from Ref.[145] Copyright 2011 American Chemical Society.

Polymer	M_n (kDa)	PDI	μ_h^{avg} (cm^2/Vs)	I_{on}/I_{off}	V_t^{avg} (V)	E_g^{opt} (eV)	HOMO (eV)
PBTOT-1	8.1	1.9	1.9×10^{-3}	10^5	-19.0	2.0	-5.2
PBTOT-2	366.5	2.0	8.4×10^{-3}	10^6	-5.2	1.9	-
PBTEHC	6.8	1.7	9.7×10^{-3}	10^5	-15.3	2.2	-5.6
PBTHDDT	19.9	2.8	6.3×10^{-3}	10^4	-20.9	2.1	-5.7
PBTEHS	7.8	2.5	6.4×10^{-4}	10^4	-22.8	1.9	-5.1
PBTPDT	9.9	1.4	6.8×10^{-4}	10^5	-22.1	2.0	-5.1
PBTDTP-1	10.3	3.1	1.8×10^{-4}	10^4	-28.6	1.9	-
PBTDTP-2	52.4	2.8	5.3×10^{-4}	10^3	-3.7	1.8	-4.8

Field-effect transistors were fabricated from both the high and low molecular weight fractions of PBTOT and PBTDTP to assess the effect of molecular weight on charge transport of the series of polymer semiconductors. The field-effect mobility in the PBTs seems to increase by a factor of 3–5 as the molecular weight increases by a factor of 5–45. Enhancement of field-effect mobility with increasing molecular weight has been observed in other conjugated polymers including P3HT[54-55] and BBL.[56] The higher field-effect mobility in the higher molecular-weight sample can be explained by the reduced defects from chain ends and improved inter-domain charge transport.

2.3.b. n-Channel FETs based on NDI-based Copolymers (PNDIs)

2.3.b.1. Thin Film Morphology.

A series of polymer semiconductors based on naphthalenetetracarboxylicdiimide (NDI) has been synthesized by Dr. Xugang Guo at the University of Kentucky (Figure 2-8). Among the present eleven polymer semiconductors based on the NDI unit (PNDIs), nine polymer semiconductors (P1c, P2–P7, P8a, and P8b) with high to moderate solubility have been studied in detail. Solid state morphology of PNDIs was investigated by 2D wide-angle X-ray diffraction (WAXD) of polymer fibers and X-ray diffraction (XRD) scans of thin films (Figure 2-9). From the WAXD patterns of the polymers, moderate crystallinity in the π-π stacking direction with *d*-spacing of 3.9–4.0 Å was seen except P3 and P4. The head-to-head (HH) dialkyl bithiophene linkages in P3 and P4 might lead to less crystalline structures. XRD of the PNDI thin films showed a peak at 2θ of 3.8–6.0 ° which represents the diffraction of lamellar planes consisting of edge-on molecular orientation. P3 and P7, having shorter 2-ethylhexyl and *n*-octyl chains, tend to have a shorter lamellar *d*-spacing distance (~15 Å), as listed in Table 2-3. In contrast, the other polymers with longer 2-decyltetradecyl or *n*-dodecyl side chains have a longer *d*-spacing distance (>19 Å). The crystalline structures with the lamellar stacking in the polymer films and fibers imply that these PNDIs, except P3 and P4, have a large degree of backbone planarity which is critical for extended charge delocalization and efficient charge transport.[34] A peak corresponding to π-π stacking was not observed in

the XRD patterns of polymer thin films, suggesting large degree of edge-on orientation of polymer backbone planes in the films. These results are similar to a recent report on related NDI-based polymers[91] but are somewhat different from another report which observed dominant face-on orientation.[153] The discrepancy between our observation and a previous report could be due to the difference in device fabrication and film processing conditions[154] and/or the instrumental limitation of the sensitivity,[153] as described in literature.

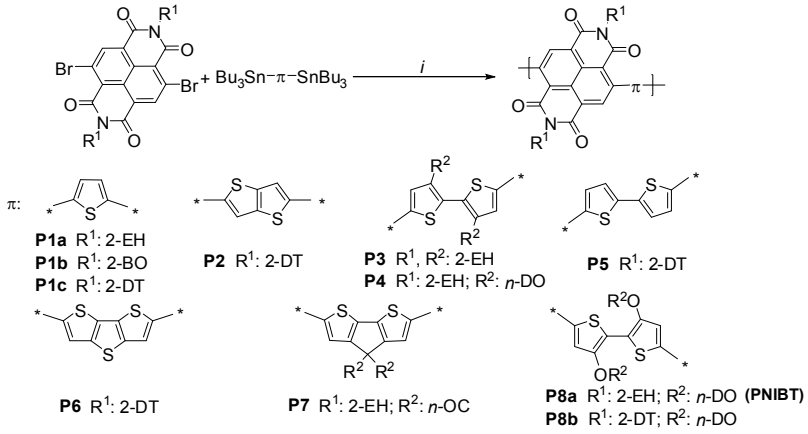

Figure 2-8. Synthetic scheme and chemical structures of the NDI-based polymer semiconductors. Reproduced with permission from Ref.[133] Copyright 2012 American Chemical Society.

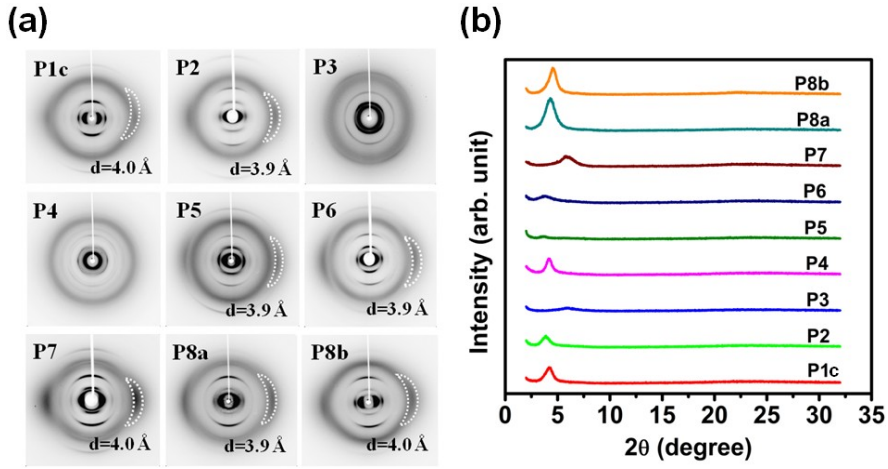

Figure 2-9. (a) 2D wide-angle X-ray diffraction (WAXD) of extruded polymer fibers and (b) θ–2θ X-ray diffraction (XRD) profiles of polymer thin films. Reproduced with permission from Ref.[133] Copyright 2012 American Chemical Society.

The recently reported results of X-ray single-crystal structures of oligothiophene-NDI donor-acceptor co-oligomers[155] can provide insights into the crystalline structure and molecular packing of PNDIs. The single crystal structures of such model systems revealed a monoclinic primitive lattice with slipped face-to-face stacking of π-planes of the molecules. The intermolecular distance in the single crystal is very small (3.2–3.3 Å). It was observed that intermolecular orbitals overlap between NDI in one molecule and thiophene rings in the adjacent molecule.[155] The close intermolecular distance is driven by strong interaction between two large aromatic molecules, which is also expected in the present PNDIs.

Table 2-3. Solid-state morphological parameters of NDI copolymers. Reproduced in part with permission from Ref.[133] Copyright 2012 American Chemical Society.

	π-π spacing [a] (Å)	Lamellar spacing [b] (Å)	Surface roughness [c] (Å)
P1c	4.0	20.9	16.7
P2	3.9	22.7	9.3
P3	–	14.7	6.4
P4	–	21.0	10.9
P5	3.9	23.8	13.1
P6	3.9	23.3	7.5
P7	4.0	14.8	33.2
P8a	3.9	20.6	26.8
P8b	4.0	19.2	13.5

[a] Calculated from WAXD patterns of extruded fibers. [b] Calculated from θ–2θ scans of thin films. [c] Root-mean-square roughness measured from AFM topographic images (5 μm × 5 μm).

Surface morphology of the PNDIs was investigated by AFM imaging of the thin films (Figure 2-10). The surfaces of thin films of P1c, P2, P5, P7, P8a, and P8b exhibited diffused nanofibrillar morphology. The root-mean-square surface roughness (R_q) of the polymer thin films, determined from AFM topographic imaging, is summarized in Table 2-3. Such well-interconnected nanofibrillar morphology[83] has been suggested to result in high mobility in OFETs based on polymer semiconductors, such as poly(3-alkylthiophene)s,[59,156] and phthalimide[34] or NDI-containing polymer semiconductors.[41] Very high

roughness (2.7–3.3 nm) and large number of aggregates on the surfaces of P7 and P8a thin films are due to the high molecular weight of the polymers and consequently relatively low solubility in chloroform/dichlorobenzene solvent mixtures (90/10; vol/vol).

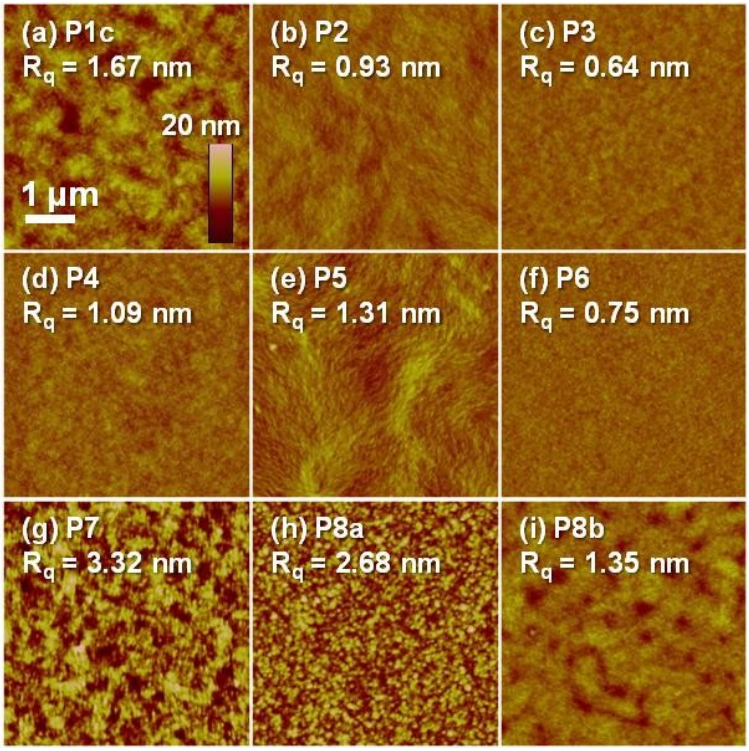

Figure 2-10. Topographical atomic force microscopy images of polymer thin films. R_q represents a root-mean-square roughness. Image size: 5 µm × 5 µm. Vertical scale: 20 nm. Reproduced with permission from Ref.[133] Copyright 2012 American Chemical Society.

2.3.b.2. Charge Transport Properties.

OFETs were fabricated and tested in order to investigate charge transport properties of the PNDIs. A summary of the OFET electrical parameters, including average electron mobility (μ_e^{avg}), average hole mobility (μ_h^{avg}), threshold voltage (V_t), and on/off current ratio (I_{on}/I_{off}), is presented in Table 2-4. As expected from their low-lying LUMO energy levels of the polymers (-3.8 – -3.9 eV), the OFETs fabricated from PNDIs showed good *n*-channel characteristics (Figure 2-11) with clear current modulation and electron mobility as high as 0.069 cm^2/Vs (P5). The highest average electron mobility

was 0.033 cm^2/Vs of P5 transistors, which is slightly lower than that of P(NDI2OD-2T) in same device architecture.[88] P6 and P8a also showed high electron mobilities of ~10^{-2} cm^2/Vs. A comparison of the electron mobility of P8a (μ_e=0.023 cm^2/Vs) to that of P8b (μ_e=9.9×10^{-4} cm^2/Vs) shows that the bulkier the side chains on the imide group are, the lower is the carrier mobility,[34] which is similar to the carrier mobility difference between P5 with bulkier 2-decyltetreadecyl chains and P(NDIOD-2T) with 2-octyldecyl chains.

It should be noted that the electron mobilities of the nine PNDIs spread over 3 orders of magnitude despite the very similar LUMO energy levels, suggesting that other factors such as solid-state morphology can also influence the charge transport properties. For example, the head-to-head (HH) linkage of the bithiophene unit in P3 and P4 induces substantial backbone torsion. This torsion in the electron-donating unit (thiophene derivatives) not only affects HOMO energy level without changing the LUMO energy level, but also influences the geometric/electronic structures of the LUMO. A comparison between P3 and P4 also provides evidence of the effects of side chain substitutions. P3 and P4 have different alkyl side chains on thiophene units (2-ethylhexyl for P3 and n-dodecyl for P4), but share the same side chains on imide group (2-ethylhexyl), similar molecular weight (78.7 kDa for P3 and 73.0 kDa for P4), and essentially identical electronic energy levels (-3.87 eV for P3 and -3.82 eV for P4). P4 with linear side chains shows two orders of magnitude higher electron mobility than P3 with branched side chains (10^{-2} vs. 10^{-4} cm^2/Vs). The difference likely comes from the different degrees in steric hindrance and overlap of molecular orbitals, caused by the linear and branched side chains, although the π-π stacking diffraction peak in P3 and P4 was not detected from our XRD experiments. Top-contact devices (Figure 1-4A) of PNDIs showed 1.2–3 fold higher electron mobilities than bottom-contact devices (Figure 1-4B), except in the cases of P1c, P3, and P7. The increase in the electron mobility is likely from lower contact resistance in the top-contact/bottom-gate OFETs compared to the bottom-contact/bottom-gate devices, as described in the previous chapter.[47]

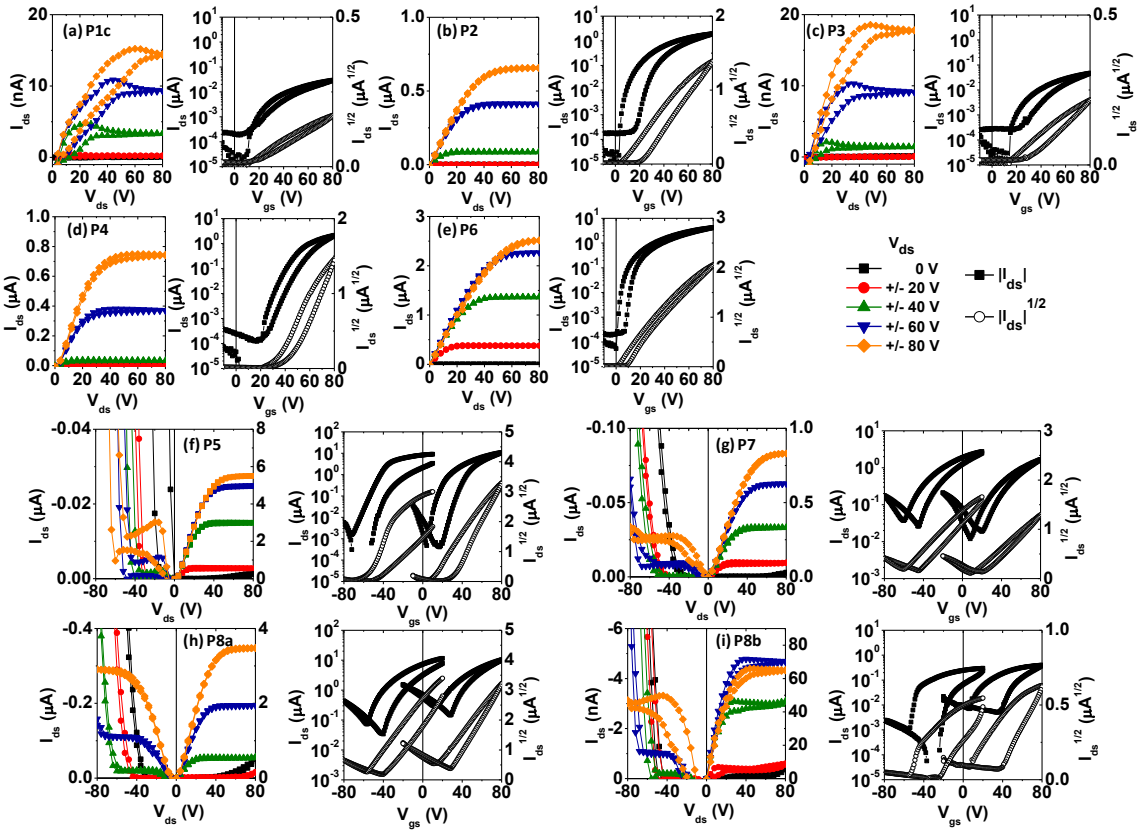

Figure 2-11. Output and transfer characteristics of PNDI transistors with top-contact geometry. Reproduced in part with permission from Ref.[133] Copyright 2012 American Chemical Society.

By incorporating various electron-donating units in the donor–acceptor copolymers, the HOMO levels of PNDIs can be tuned over a wide range, while keeping the LUMO energy levels constant (Figure 2-12). The change of HOMO energy level resulted in transition from *n*-type to ambipolar charge transport, although the electron transport is still dominant (*i.e.*, the majority charge-carriers are electron; $\mu_e/\mu_h > 1$). Figure 2-12 summarizes the HOMO/LUMO energy levels of the present PNDIs and the observed average electron and hole mobilities. The polymers with weaker electron-donating units (P1c, P2, P3, P4, P5, and P6) had low-lying HOMO energy levels (-5.9 – -5.7 eV) and exhibited dominant electron-transport properties in OFETs. On the other hand, polymers with stronger electron-donating units (P7, P8a, and P8b) showed high-lying HOMO energy levels (-5.5 – -5.3 eV), which resulted in substantial ambipolar charge transport with low μ_e/μ_h. Well-matched electronic energy levels of organic semiconductors with

the work function of electrodes are required to reduce energetic barriers, resulting in efficient charge injection/extraction in both unipolar and ambipolar OFETs.[35] This trends are similar to the previously reported OFETs based on the model systems of NDI-thiophene oligomers that the hole mobility became increased as the electron-donating strength of counits increased, which was accompanied by higher-lying HOMO energy level.[155] These results demonstrate the effectiveness of donor-acceptor copolymer approach with various moieties to tune electronic energy levels, and therefore control the polarity of the majority charge carriers in the materials.

Table 2-4. Electrical parameters of bottom-gate field-effect transistors based on PNDIs. Reproduced in part with permission from Ref.[133] Copyright 2012 American Chemical Society.

Polymer	Device geometry [a]	μ_e^{avg} (cm^2/Vs) [b]	μ_h^{avg} (cm^2/Vs) [b]	μ_e / μ_h	$V_{t,e}$ (V) [b]	$V_{t,h}$ (V) [b]	I_{on}/I_{off}
P1c	TC	8.6×10^{-5}	–	–	9.4	–	10^2–10^3
	BC	1.5×10^{-3}	–	–	25.9	–	10^3
P2	TC	3.6×10^{-3}	–	–	13.9	–	10^4
	BC	1.2×10^{-3}	(3.3×10^{-5}) [c]	(35.3) [c]	0.3	(-39.9) [c]	10^3–10^4
P3	TC	8.6×10^{-5}	–	–	12.0	–	10^3
	BC	2.3×10^{-4}	–	–	20.2	–	10^3
P4	TC	0.012	–	–	24.9	–	10^4–10^5
	BC	5.3×10^{-3}	8.9×10^{-6}	590.3	11.6	-37.5	10^2–10^4
P5	TC	0.033	(3.6×10^{-4}) [c]	(90.7) [c]	5.5	(-56.1) [c]	10^3–10^4
	BC	0.023	(2.1×10^{-3}) [c]	(11.2) [c]	-0.8	(-40.1) [c]	10^2–10^3
P6	TC	9.6×10^{-3}	–	–	-0.8	–	10^4–10^5
	BC	8.0×10^{-3}	7.6×10^{-4}	10.4	-12.1	-43.4	10^2–10^3
P7	TC	4.4×10^{-3}	6.6×10^{-4}	6.6	0.2	-34.8	10^2
	BC	5.6×10^{-3}	1.0×10^{-3}	5.6	9.6	-22.8	10^2
P8a	TC	0.023	2.8×10^{-3}	8.3	3.1	-30.3	10^2
	BC	0.014	3.3×10^{-3}	4.2	25.8	-13.4	10^2
P8b	TC	9.9×10^{-4}	7.4×10^{-6}	134.0	0.46	-19.8	10^2
	BC	8.0×10^{-4}	8.5×10^{-5}	9.4	16.5	-27.0	10^2

[a] TC: Top-contact. BC: Bottom-contact. Both cases have a bottom-gate structure. [b] Average of 4–10 devices. Polymer films were thermally annealed at 150 °C for 30 min. [c] Hole transport was occasionally observed in some devices. Hole mobility and threshold voltage of p-channel mode are on average of those from devices with ambipolar characteristics.

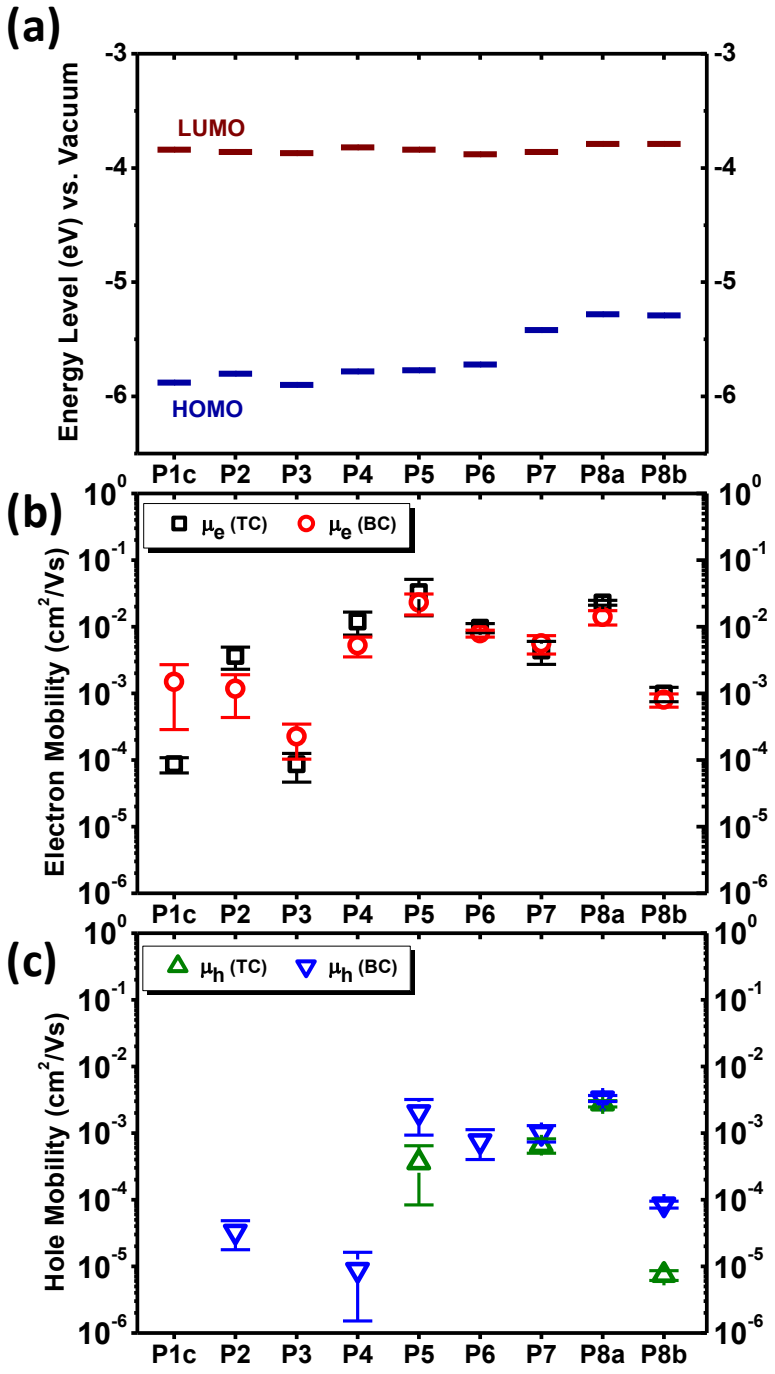

Figure 2-12. (a) Electronic energy levels of NDI copolymer semiconductors. (b) Average electron mobility of NDI copolymer semiconductors in both top-contact (TC; black square) and bottom-contact (BC; red circle) OFET architectures. (c) Average hole mobility of NDI copolymer semiconductors in TC device (green upward triangle) and BC device (blue downward triangle). Error bar represents one standard deviation. Reproduced with permission from Ref.[133] Copyright 2012 American Chemical Society.

For those materials which showed ambipolar characteristics (P7, P8a, and P8b), the electron mobility tends to decrease and hole mobility to increase when bottom-contact geometry is applied (Table 2-4), resulting in a lower μ_e/μ_h ratio. Besides, bottom-contact devices of P2, P4, and P6 exhibited ambipolar charge transport whereas top-contact devices showed unipolar electron transport. The appearance/enhancement of hole mobility cannot be explained by reduction of contact resistance in bottom-gate/top-contact devices compared to bottom-gate/bottom-contact ones. Another factor that results in the difference of charge carrier mobilities between top-contact and bottom-contact devices might have come from the surface modification and the change of a work function the electrodes during the substrate preparation. Plasma treatment on gold electrodes has been shown to increase the work function higher than 5.1 eV.[157] The electronic energy difference between gold electrodes and LUMO energy levels of PNDIs get larger after plasma treatment, whereas the difference with rather low-lying HOMO energy levels gets smaller. Although the devices in multiple batches were carefully fabricated, small unintentional variation in device processing conditions cannot be ruled out as a possible factor in large standard deviations in charge-carrier mobility in the bottom-contact devices of PNDIs with lower-lying HOMO energy levels (-5.7 – -5.9eV). It should be noted that, in the cases of P2 and P5, some of the devices showed ambipolar characteristics whereas other batches had unipolar electron transport properties. Such occasional ambipolarity in NDI-based polymers have also been reported by others, although the origin is not yet understood.[22]

The OFETs based on the present series of PNDIs showed good shelf stability as the electron mobility decrease by a factor of 1–3 when stored in ambient air for a few weeks. However, the electron mobility typically dropped by 2–3 orders of magnitude when the OFETs were tested in air without any environmental control (Table 2-5; Figure 2-13), indicating that they are not operationally stable in ambient conditions. Charge carriers in *n*-type organic semiconductors are anions, which are generally vulnerable to ambient air species, especially to moisture and oxygen,[138,140] and only few polymer-based *n*-

channel OFETs have showed good operational stability in air.[57,134,146,158] The top-gate OFET structure offers enhanced device stability because of the encapsulating nature of multilayers of the gate dielectric and electrode.[22,50,159] It is worth mentioning that the hole mobilities of P5 and P8b were increased after air-exposure. The increase in hole mobility is likely caused by unintentional doping of the polymer semiconductors by extrinsic molecules.

Table 2-5. Stability and Durability of Bottom-Gate/Top-Contact (BG/TC) OFETs Against Ambient Air. Reproduced in part with permission from Ref.[133] Copyright 2012 American Chemical Society.

Polymer	Condition [a]	μ_e^{avg} (cm^2/Vs)	μ_h^{avg} (cm^2/Vs)	$V_{t,e}$ (V)	$V_{t,h}$ (V)
P1c	As fabricated, N_2	8.6×10^{-5}	–	9.4	–
	Stored in air, tested in N_2	5.7×10^{-5}	–	43.6	–
	Tested in air	–	–	–	–
P2	As fabricated, N_2	3.6×10^{-3}	–	13.9	–
	Stored in air, tested in N_2	2.7×10^{-3}	–	41.5	–
	Tested in air	1.9×10^{-6}	–	64.1	–
P3	As fabricated, N_2	8.6×10^{-5}	–	12.0	–
	Stored in air, tested in N_2	8.4×10^{-5}	–	34.7	–
	Tested in air	–	–	–	–
P4	As fabricated, N_2	0.012	–	24.9	–
	Stored in air, tested in N_2	2.2×10^{-3}	–	21.4	–
	Tested in air	3.0×10^{-5}	–	57.0	–
P5	As fabricated, N_2	0.033	–	5.5	–
	Stored in air, tested in N_2	0.015	1.9×10^{-3}	-1.7	-51.8
	Tested in air	2.6×10^{-4}	3.4×10^{-3}	-11.5	-0.4
P6	As fabricated, N_2	9.6×10^{-3}	–	-0.8	–
	Stored in air, tested in N_2	0.012	–	39.8	–
	Tested in air	4.4×10^{-5}	–	62.9	–
P7	As fabricated, N_2	4.4×10^{-3}	6.6×10^{-4}	0.2	-34.8
	Stored in air, tested in N_2	2.6×10^{-3}	3.4×10^{-4}	14.6	-30.9
	Tested in air	3.5×10^{-6}	2.1×10^{-4}	-0.2	13.3
P8a	As fabricated, N_2	0.023	2.8×10^{-3}	3.1	-30.3
	Stored in air, tested in N_2	6.7×10^{-3}	1.3×10^{-3}	18.5	-5.4
	Tested in air	3.6×10^{-5}	6.3×10^{-4}	59.7	28.9
P8b	As fabricated, N_2	9.9×10^{-4}	7.4×10^{-6}	0.46	-19.8
	Stored in air, tested in N_2	7.0×10^{-4}	1.8×10^{-5}	7.4	-5.6
	Tested in air	–	1.8×10^{-5}	–	1.1

[a] Devices were initially tested under inert nitrogen atmosphere within a few hours after fabrication. Then, the devices were taken out and stored in ambient lab conditions for 2–4 weeks, transferred back to the glove-box, and tested to check shelf life-time. Finally, the devices were brought out and tested again in air without any encapsulation or environmental control such as humidity.

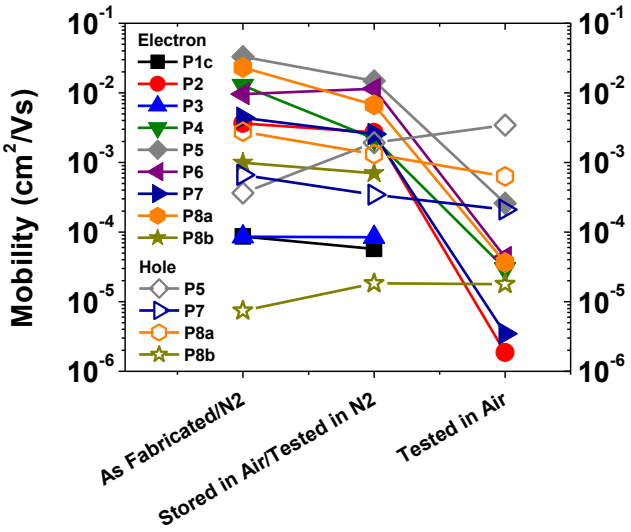

Figure 2-13. Air-stability of PNDI-based OFETs. Devices were fabricated and tested in nitrogen environment. After initial testing, they were brought out from the inert conditions and stored in ambient air for 2–3 weeks, then transferred into the nitrogen-filled drybox and tested. Finally, the devices were tested in ambient air without any environmental control.

2.3.c. Stability and Durability of Polymer FETs in Air

2.3.c.1. Stability of n-Channel BBL FETs.

As discussed above, polymer semiconductors, especially electron transporting polymer semiconductors, tend to be affected by external molecules such as oxygen and water.[138-141] Polymer FETs will be useful only when they reliably work for designated period of time in typical operating conditions (*i.e.*, in ambient air).[17,142] Most of the current *n*-channel polymer transistors only show stable performance under controlled atmosphere (*i.e.*, in an inert gas, in air with low humidity, or with encapsulation) with very few exceptions; furthermore, there has been no study of air-stability and durability of *n*-channel polymer transistors for a practical period of time (>1 year). This poses a challenge for the realization of durable all-polymer complementary inverters and logic circuits. I have examined BBL FETs and found that ambient atmosphere in the laboratory does not affect the performance of the devices.

Figure 2-14A is an overlay of transfer characteristics of as-fabricated and aged OFETs based on representative *n*-type and *p*-type polymer semiconductors, BBL and P3HT, respectively. It clearly demonstrates that *n*-channel BBL transistors outperform *p*-channel P3HT transistors. Output characteristics of BBL transistors shown in Figure 2-14B also indicates excellent stability of BBL in air. Long-term air-stability of *n*-channel polymer transistors without encapsulated device structures is rare in literatures[57,88] and is more often observed in *p*-type organic semiconductors[78-79,145,147] or in *n*-type small-molecule organic semiconductors.[102-103,140,160] Figure 2-14(C-E) illustrates the stability of an *n*-channel BBL transistor for 4 years without any noticeable change in electron mobility or device characteristics, whereas a *p*-channel P3HT transistor rapidly degrades in a matter of several days and essentially lose field-effect mobility after several weeks. While the electron mobility of a BBL transistor remained constant ($\sim 1\times10^{-4}$–6×10^{-4} cm^2/Vs), the mobility of P3HT transistor dropped by more than four orders of magnitude from an original mobility of 7.2×10^{-4} cm^2/Vs to a mobility below $\sim10^{-8}$ cm^2/Vs. The on/off current ratio of the BBL transistor was typically on the order of 10^4 throughout the measurements, whereas that of the P3HT transistor decreased from 10^3 to less than 10 over time. Fluctuation of threshold voltage of the P3HT transistor is much severe compared to that of the BBL transistor.

The excellent stability and durability of *n*-channel operation in BBL films are considered to be from the low-lying LUMO energy levels and highly crystalline nature of BBL. BBL has showed an excellent robustness in air against thermooxidative decomposition.[148] The rich nitrogen and oxygen heteroatoms in BBL give rise to excellent electron accepting properties such as reversible *n*-type doping, ability to accept up to two electrons per repeat unit,[127-128] and a low-lying LUMO energy level of 4.0–4.2 eV.[126-129] Air-stability in part originates from the low-lying LUMO energy level in combination with a large overpotential for oxidation of organic semiconductor anion.[138,140] Moreover, the excellent stability of the performance of BBL FETs in ambient atmosphere can further be explained by its more positive reduction

potential ($E_{red,BBL}$= -0.4 V vs. SCE) compared to water at neutral pH ($E_{red,H2O}$= -0.66 V vs. SCE)[138] which makes the BBL anion energetically stable in the presence of moisture.

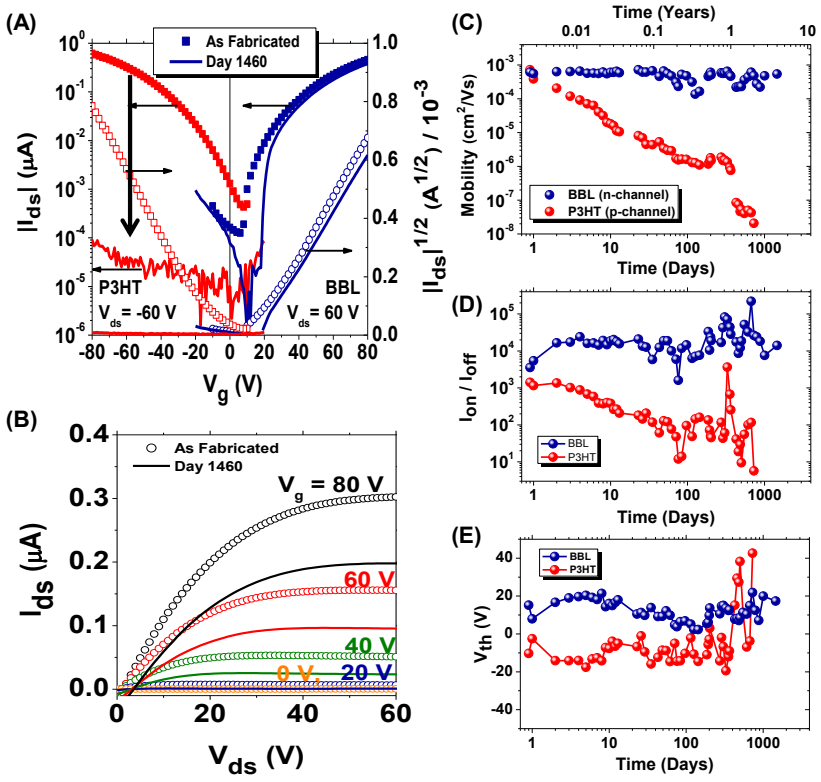

Figure 2-14. Air-stability of representative polymer semiconductors, P3HT (*p*-type) and BBL (*n*-type). (A) Overlays of transfer characteristics of P3HT and BBL transistors as fabricated and after stored for 1460 days in air. (B) Overlays of output characteristics of BBL transistors as fabricated and after stored for 1460 days in air. (C) Field-effect mobilities, (D) on/off current ratios, and (E) threshold voltages of BBL and P3HT transistors as a function of air-exposure time. Devices were fabricated and tested in air without humidity control (relative humidity = 20–70 %). Reproduced from Ref.[143] by permission of The Royal Society of Chemistry.

Along with the energetic characteristics of BBL, the solid state morphology can also be attributed to the other origin of the stability of BBL. Solid-state morphology of BBL thin films has been characterized by AFM, TEM, and XRD.[143,161-163] In AFM phase image, nanoscale sheets in the range of 50–125 nm randomly oriented throughout the film were observed.[143] Highly crystallinity of BBL has also been observed from XRD and TEM with electron diffraction. A strong in-plane (010) diffraction consistent

with an interplanar π-stacking distance of ~3.4 Å which is in agreement with the literature value of 3.36–3.37 Å.[129,162] The short distance corresponds to the face-to-face interchain packing along the *b*-axis direction of the unit cell.[162] The peak of (100) diffraction was determined to be ~7.9 Å which corresponds to the side-to-side packing of BBL chains down the surface normal (equivalent to the *a*-axis of the unit cell). This *d*-spacing is in a good agreement with the previously proposed distance of 7.87–7.93 Å.[129,162]

The high degree of crystallinity of BBL, as a result of the rigid and planar ladder structure[57,148,163-164] and efficient π-stacking, is advantageous not only for optimal charge transport,[57,129,163] but also for providing a physical barrier against the diffusion of molecular oxygen into the polycrystalline polymer matrix. It is well-established that molecular oxygen is one of the reasons for device degradation in OFETs and particularly in *n*-channel transistors,[35,43,138,144] and solid-state packing effects have been previously suggested for explaining air stability in highly crystalline small organic *n*-type semiconductors.[48,140-141] In a previous study that characterized the gas permeation, diffusion, and sorption in highly crystalline BBL polymer films,[164] it was found that only certain penetrants (*i.e.*, gases) of sufficiently small size can diffuse into BBL films. The kinetic diameter (*i.e.*, molecular size) of the gas needs to be smaller than the intermolecular *d*-spacing of BBL. For instance, the kinetic diameter of molecular oxygen is 3.46 Å while the *d*-spacing of BBL is in the range of 3.37–3.40 Å.[164] The fact that molecular oxygen has a larger diameter than the *d*-spacing of BBL suggests that the gas is impenetrable to the crystalline BBL film. This is expected in regions of high molecular order such as the crystalline domains observed in the BBL thin films. Small fraction of imperfect packing may very well result in selective diffusion of oxygen resulting in the small fluctuations of mobility in the course of the periodic measurement over extended time. A study of the electron transport of BBL FETs in an atmosphere with various partial pressure of oxygen (0.02–750 torr) provides a direct evidence of the minimal effect of molecular oxygen on electron transport in BBL.[143] The initial BBL FETs measured under vacuum showed a field-effect electron mobility of 0.004 cm^2/Vs. The electron mobility of BBL remained constant from vacuum up to 40 torr of oxygen

pressure (0.004 cm^2/Vs) and decreased slightly to 0.0025 cm^2/Vs at 750 torr of oxygen pressure.[143] It should be noted that the kinetic diameter of molecular H_2O is very small (~2.65 Å),[165] and therefore the electron transport properties of BBL thin film can be affected by the humidity of ambient conditions. Although the BBL is energetically stable against H_2O, high humidity can lower the overpotential for oxidation of organic semiconductor anion and affect the electron transport properties of BBL thin film (Figure 2-14C,D,E).

In the case of P3HT, reported π-stacking distance is ~3.7 Å,[76] which is larger than the kinetic diameter of oxygen and water. P3HT is relatively more flexible and also has a much lower glass transition temperature (T_g = 12 °C)[166-167] than BBL (T_g > 500 °C).[168] Therefore, extrinsic small molecules, such as oxygen, ozone, and water, can easily diffuse into the thin film and present between P3HT molecules, resulting in chemical degradation of molecular backbone, unintentional doping, and/or formation of charge-trapping sites.[138,144,169] Amorphous region between crystalline domains in P3HT thin films would especially allow diffusion of such reactive penetrants. Presence of trace amounts of impurities in the commercially available sample of P3HT might also facilitate the degradation process cause by the penetrants. This result suggests that, although *p*-type polymer semiconductors are generally less vulnerable against formation of charge traps, long-term air-stability and durability can be substantially increased by inducing kinetic barriers to the penetrants in the polymer semiconductors.[145,147]

2.3.c.2. Stability of p-Channel PBTOT FETs.

I have also investigated the stability and durability of OFETs fabricated from a highly crystalline *p*-type polymer semiconductor based on a benzobisthiazole unit, PBTOT. The electrical parameters such as hole mobility, on/off current ratio, and threshold voltage, of PBTOT OFETs were recorded as a function of time in ambient air conditions (Figure 2-15). The OFETs were initially tested in a nitrogen-filled dry box, brought out and tested in air, and then stored and periodically tested in ambient laboratory conditions. Figure 2-15(A-C) shows that the carrier mobility, threshold voltage, and the on/off current

ratio essentially remained the same for 2 years. A slight change in the initial carrier mobility measured in nitrogen (0.009 cm^2/Vs) compared with the first measurement in air (0.007 cm^2/Vs) was observed. The carrier mobility measured after 721 days was 0.006 cm^2/Vs. Similarly, a slight variation in the initial threshold voltage measured in nitrogen (-5 V) compared to the first measurement in air (-18 V) was observed and after 4 days it stabilizes at -13 V for up to 721 days. Figure 2-15(D,E) shows slight changes in the transfer and output characteristics of days 1 and 721 measurements in air. The remarkable durability of the PBTOT devices is from both thermodynamic and kinetic origins, as seen above in *n*-type polymer semiconductor, BBL. PBTOT has low-lying HOMO energy level (-5.2 eV) and consequent resistance to unintentional oxidation in air. PBTOT also has a high degree of crystallinity in thin films which enables kinetic barrier to oxygen and moisture diffusion and resistance to oxidation.

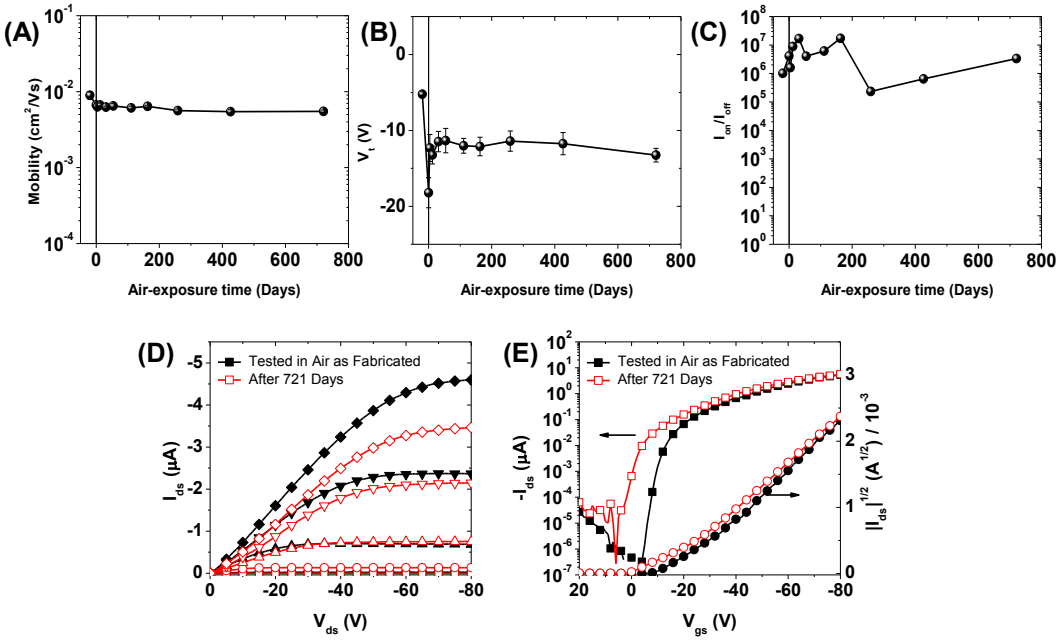

Figure 2-15. Air-stability of a *p*-type polymer semiconductors, PBTOT. (A) Hole mobility, (B) threshold voltage, and (C) on/off current ratio as a function of air-exposure time. Overlays of (D) output and (E) transfer characteristics of PBTOT transistors as fabricated and after stored for 721 days in air. Devices were stored and tested in air. Reproduced with permission from Ref.[145] Copyright 2011 American Chemical Society.

These experimental results of highly stable BBL and PBTOT transistors are in good agreement with previous reports found in literature. Most of the current high-mobility *n*-type and *p*-type polymer semiconductors have a π-stacking distance of 3.6–3.9 Å along the *b*-axis and the *d*-spacing along the *a*-axis of 15.6–31.4 Å due to the presence of solubilizing alkyl side chains.[34,78-79,82,86,90,145,147,153,170-171] Although these packing distances are larger than the kinetic diameters of the molecular oxygen and water, some of the polymer semiconductors have showed better durability than P3HT in air without encapsulating layers.[78-79,88,145,147,171] The better durability of those polymers compared to P3HT is from a result of a combination of superior electrochemical stability due to suitable HOMO/LUMO energy levels, highly crystalline morphology, and/or the rigid molecular structures of fused aromatic rings in the backbone that limit the rate of diffusion of the penetrants. Therefore, a careful design of the molecular structure of polymer semiconductors is essential to tackle both energetic and kinetic aspects of the degradation mechanisms and to realize highly stable and durable polymer semiconductors and organic electronic devices.

2.3.d. Complementary Circuit Applications of Polymer FETs

Complementary metal-oxide-semiconductor (CMOS) technology utilizes multiple *n*-channel and *p*-channel FETs to build digital logic circuits which perform a logic calculation of binary information (represented by 0 and 1), and have played an essential role in development of current information technology.[44] Low power-dissipation and high performance are some of the major advantages of digital CMOS technology over non-complementary ones.[5,21,35,44,142,172] Power consumption is minimized in a CMOS circuit because the component transistors are selectively turned on only when the circuit is switching, otherwise they are off at steady state, minimizing the current flowing through the circuit. The better performance of a CMOS circuit, such as sharp switching, high stability, and large noise-immunity, arises because every elemental transistor actively contributes to the function of the circuit.[44,172-173]

Although most of electronic devices operate dynamically under a given frequency range depending on the applications, only static characteristics are mainly focused here.

Figure 2-16 shows symbols of FETs and a few examples of circuit diagrams of the most simple complementary logic gates. Voltages at the terminal electrodes turn each transistor on or off selectively, inducing the current flow through a certain pathway of the circuit and resulting in the targeted output voltage, which is close to either the supplied voltage (V_{dd}; represents signal 1) or ground (represents signal 0), of the logic operation. For example, the input signal is inverted after NOT gate operation (from 0 to 1, or from 1 to 0). The output signal of NAND gate is 0 only when two input signals are 1; otherwise the output is 1. The NOR operation results in 1 only when the input signals are both 0. Complementary NOT gate requires one *n*-channel and one *p*-channel transistors, and two-terminal complementary NAND and NOR gates require two *n*-channel and two *p*-channel transistors each.

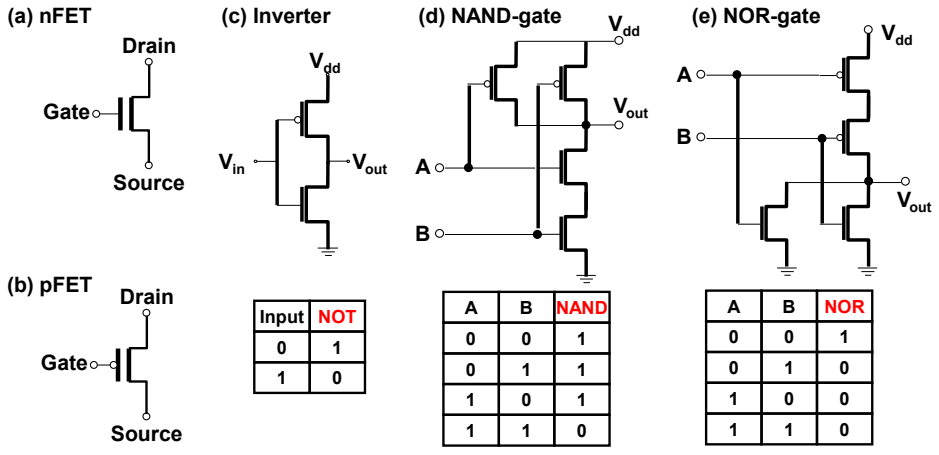

Input	NOT
0	1
1	0

A	B	NAND
0	0	1
0	1	1
1	0	1
1	1	0

A	B	NOR
0	0	1
0	1	0
1	0	0
1	1	0

Figure 2-16. Symbols of (a) *n*-channel and (b) *p*-channel transistors. Diagrams of complementary circuits and their corresponding truth tables: (c) an inverter, (d) a NAND logic gate, and (e) a NOR logic gate.

For proof-of-principle, complementary inverters based on polymer semiconductors were fabricated by integrating an *n*-channel BBL transistor and a *p*-channel P3HT transistor with same geometrical factors (W=1000 μm, L=100 μm, t_{SiO2}=200 nm). Both OFETs showed similar mobilities of 6.2×10^{-4}–7.9×10^{-4} cm^2/Vs (Figure 2-17A). Figure 2-17B shows the static voltage transfer characteristics of the P3HT/BBL

complementary inverter. One can observe excellent voltage switching characteristics with a voltage gain as high as 14 in the first and third quadrant of the output versus input voltages depending on the polarity of the supply voltage. The transfer characteristics show symmetrical gate threshold switching (V_m) at nearly half of the supply voltage ($V_m = V_{dd}/2$). The symmetry is a result of the equally-matched mobilities and absolute values of threshold voltages of the *p*- and *n*-channel transistors.[142] The switching thresholds of the inverters can be estimated graphically and analytically. In a graphical method, the intersection of the transfer curve and $V_{out}=V_{in}$ line gives the trip voltage, as shown in Figure 2-17B. In an analytical method,[44] one can calculate the values using Eq. 2-1 for the 1st quadrant:

$$V_m = \frac{V_{TOn} + (V_{dd} + V_{TOp})\sqrt{\frac{1}{k_R}}}{1+\sqrt{\frac{1}{k_R}}}, \qquad \text{(Eq. 2-1)}$$

and Eq. 2-2 for the 3rd quadrant:

$$V_m = \frac{V_{TOp} + (V_{dd} + V_{TOn})\sqrt{k_R}}{1+\sqrt{k_R}}, \qquad \text{(Eq. 2-2)}$$

where $k_R = k_n/k_p$, which is the ratio of transconductance parameters $k_{n,p}=\mu_{n,p}C_iW/L$, and V_{TOp}, V_{TOn} are the threshold voltages of the individual *p*- and *n*-channel transistors.[44] These equations are derived under the assumption that both transistors are in saturation region when the inverter is in the transition state. The calculated threshold voltages V_m for 1st and 3rd quadrants ($V_{dd}=\pm 80$ V) were 34.7 V and -45.3 V, respectively, in agreement with the graphically derived trip voltages of 41 V and -39 V. It is obvious from the voltage transfer characteristics in Figure 2-17B that there is some degree of hysteresis in the forward and reverse voltage sweeps, especially in the 1st quadrant where *n*-channel transistor drives. The hysteresis can be attributed to the hysteresis of the OFETs with traps at the dielectric/semiconductor interface,[43,67] and have caused the deviations between the calculated and graphically derived trip voltages.

Figure 2-17B also shows current (I_{dd}) flowing through the complementary inverter as a function of input voltage. It is clear that high current, and therefore high power dissipation, is seen only when the inverter is switching. In order to highlight the high-performance and low-power consumption of the complementary inverter, I also fabricated non-complementary inverter based on *p*-channel P3HT transistors with same channel dimensions (Figure 2-18). Both depletion-type inverter, where the gate of the load transistor is connected to the output terminal, and enhancement-mode-type inverter, the gate of the load transistor is connected to the power supply terminal, showed large I_{dd} at a static state of $V_{in} \sim$ -80 V. The depletion-type inverter exhibited a positively shifted trip voltage although switching was fairly sharp. The enhancement-load-type inverter showed very poor switching as well as large I_{dd} at a static state.

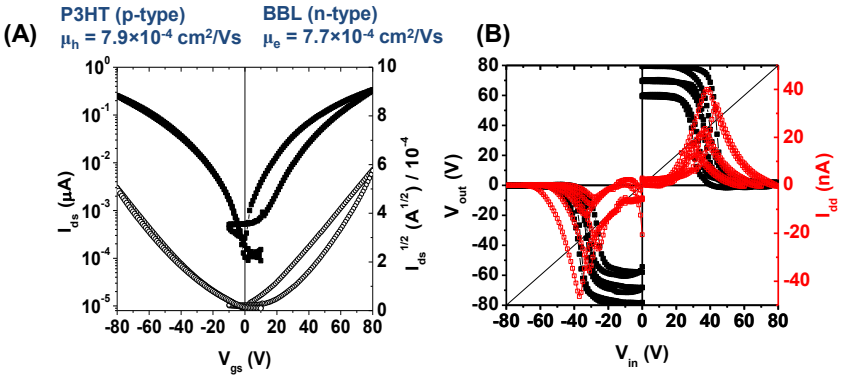

Figure 2-17. (A) Transfer characteristics of P3HT and BBL transistors. (B) Voltage output characteristics and current in a complementary inverter based on the P3HT and BBL transistors.

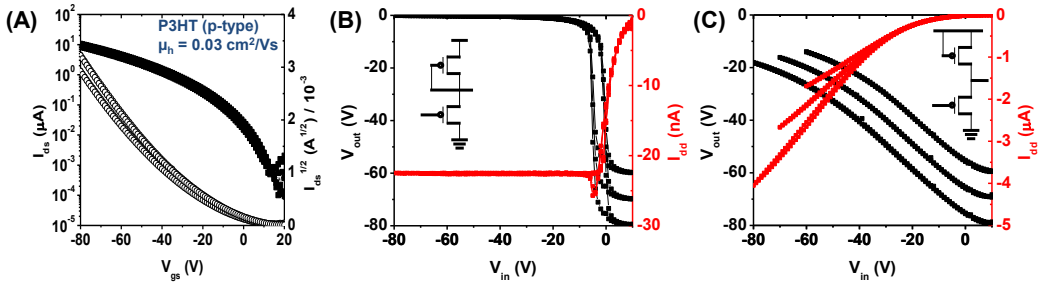

Figure 2-18. (A) Transfer curves of a P3HT transistor. (B,C) Voltage and current characteristics of P3HT-based inverters: (B) depletion-type and (C) enhancement-load-type. Channel dimensions are identical.

On a design perspective of a circuit into which multiple transistors are integrated, power–delay product (PDP), a figure of merit that represents how much of power the circuit dissipates ($P \sim C_L V_{dd}^2 f$, where P is power dissipation, C_L is load capacitance, and f is clock frequency) and how fast the switching occurs (delay, τ), becomes important to validate the technology.[44] Although the current stage of studies of polymer semiconductors and polymer-based OFETs focuses on the investigation of charge transport properties of polymer semiconductors by using fairly large device dimensions and voltages (*e.g.*, C_i=11–33 nF/cm^2, W=100–5000 μm, L=40–200 μm, $|V_{ds}|$=50–100 V, $|V_{dd}|$=40–100 V, and so on), it will eventually become critical to study scaling issues and develop suitable device geometry, dielectric materials, electrodes and contacts, and related processing technology.

2.4. Conclusions

In summary, I have investigated the charge transport properties of various polymer semiconductors, including PhBTs, PTTs, PBTs, PNDIs, and BBL, to gain insights of structure–morphology–property relationships. Specifically, effects of donor-acceptor combinations and side chain substitutions were studied. Field-effect mobility in the range of ~10^{-4}–0.1 cm^2/Vs was observed from the polymer semiconductors.

Effects of side chain substitutions were studied from both PhBTs and PTTs. Both series of polymer semiconductors showed high hole mobility of 0.01–0.2 cm^2/Vs depending on the side chains. Phthalimide units incorporated into alkoxythiophene polymer backbones exhibited extended conjugation and π-stacking characteristics. Morphological studies revealed that small changes of side chains affected the solid-state morphology of PhBTs. The crystallinity in short range and long range as well as the domain interconnectivity induced by side chains played an important role on the charge transport. In a study on PTTs, the different aspects of side chain substitution effects on charge transport properties were investigated. Backbone planarization and intramolecular charge transfer resulted in higher mobility in

PSOxTT by significantly enhanced crystallinity with edge-on orientation as well as well-matched electronic energy levels.

Effects of relative strengths of electron-donating and electron-accepting units in the polymer semiconductors were also studied by maintaining electron-acceptor units (either BTs or NDIs) and varying electron-donating units. Bandgaps of the donor–acceptor polymer semiconductors were effectively tuned by inducing various degree of intramolecular charge transfer. LUMO energy levels were essentially same throughout each series of copolymers, whereas HOMO energy levels varied by ~0.9 eV with different donor strengths. Hole transporting properties of the polymer semiconductors were affected by the variation of HOMO levels. Morphological factors such as crystallinity of the polymer semiconductors turned out to be critical for charge transport as well.

Studies of long-term air-stability of the selected polymer semiconductors, namely BBL, P3HT, and PBTOT, were also performed to enlighten the approaches for highly stable/durable polymer semiconductors. The results suggest that oxidative stability can be introduced by tuning LUMO energy levels for *n*-type polymer semiconductors and HOMO levels for *p*-type polymer semiconductors. High-crystallinity with short packing distances of the polymer semiconductors with rigid molecular structures can offer extended stability, as a diffusion barrier can be formed against diffusion of external molecules such as oxygen and moisture.

Finally, polymer semiconductor-based complementary inverters were demonstrated. The advantages of complementary approach, such as excellent switching characteristics with a high voltage gain, large noise-tolerance, and very low power consumption, are observed and discussed by comparing the performance of *p*-channel OFET-based inverters.

Chapter 3. Ambipolar Polymer Field-Effect Transistors

This chapter investigates ambipolar field-effect transistors based on polymer semiconductors. The results in this chapter are reprinted in part with permission from Kim, *et al*. (Copyright 2010 The Wiley-VCH),[41] Wu and Kim, *et al.* (Copyright 2011 American Chemical Society),[137] and from Kim, *et al*. (Copyright 2010 American Chemical Society).[146]

3.1. Introduction

Ambipolar OFETs, which are capable of both *p*-channel and *n*-channel operations, have been gaining great interest as an alternative approach to mimicking complementary metal-oxide-semiconductor (CMOS) digital integrated circuits without patterning of *p*-type and *n*-type polymer semiconductors.[35-41,43,134,174-189] Enhanced circuit performance compared to unipolar circuits can be achieved while reducing complexity of the fabrication because of the multifunctional operation of ambipolar OFETs. Ambipolar transistors are also of interest in fundamental studies of charge transport in organic semiconductors[35,43,190] as well as the development of efficient light-emitting transistors.[38-39,191-194]

Since the first demonstration of ambipolar charge transport in a bilayer OFET of small-molecule semiconductors,[174] ambipolar OFETs have been realized by using various approaches (Figure 3-1), including layered heterojunctions of unipolar organic semiconductors,[174,181-186,195-196] blends (or bulk heterojunctions) of unipolar organic semiconductors,[36,177-180,191] single active materials with asymmetric metal electrodes of different work-functions,[193] and single-component organic semiconductors with a common electrode.[36-41,43,100,134-135,175-176,187-189,197-198] Charge-carrier mobilities in the range of 10^{-6} to 0.1 cm^2/Vs have been reported in the ambipolar OFETs.

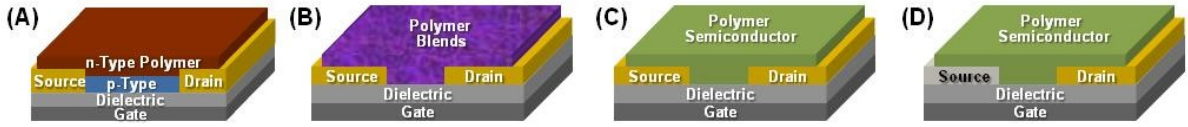

Figure 3-1. Approaches to ambipolar charge transport in OFETs. (A) Multilayer heterojunctions, (B) bulk heterojunctions, (C) a single-component semiconductor with symmetric metal electrodes, and (D) a device with asymmetric metal electrodes.

An important advantage of the layered heterojunction approach is that semiconductor channels are well-defined in separate layers with inherent motifs of molecular packing. Because each semiconductor covers whole channel area, charge transport in *n*-type (or *p*-type) polymer semiconductor is not limited by the presence of *p*-type (or *n*-type) polymer semiconductor in principle. It may also be possible to embed light-emitting devices, vertical and lateral heterojunction diodes, and solar cells into the circuits at the same time with materials having a desirable functionality.[184,199-201] However, most heterojunction OFETs studied to date are based on thermally-evaporated small molecules[174,182-184] or externally-transferred films of polymers which add additional steps in the fabrication process.[185-186] Making ambipolar OFETs and their complementary circuits from solution-processed *n*/*p* polymer/polymer heterojunctions is highly attractive but it remains challenging to achieve because of the difficulty of finding polymer semiconductors with mutually exclusive solubility. Issues of Interfacial morphology and charge injection barrier also need to be addressed in the multilayer structures.

Blend (or bulk heterojunction) approach enables various combinations of well-studied unipolar semiconductors as long as the constituent polymer semiconductors have a common solvent (typically an organic solvent or an acid solvent). It is especially attractive not only for developing ambipolar transistors but also for increasing efficiency of organic solar cells.[202-203] However, there are still issues such as difficulties in control of phase separation of the blend and in achieving percolation for charge transport.

The effective charge-transport channel area is inevitably reduced by the presence of multiple semiconductors, resulting in lower charge-carrier mobilities and source-drain current.

Devices with asymmetric metal electrodes with different work-functions may introduce good charge transport across single-component or multicomponent semiconductor channels.[193] However, complicated patterning process with a precise alignment is required for fabrication of devices with different metal electrodes. Stability of a metal with a low work-function is another issue to be tackled in this approach. As a result, this approach is very challenging and impractical, although it may be a good platform for investigating charge injection and extraction to/from organic semiconductors.

Polymer semiconductors with donor–acceptor architecture have been of long interest as a means towards ambipolar charge transport and multifunctional properties for organic electronics.[32-33,118] Narrow bandgap can be achieved from the donor–acceptor approach as a result of intramolecular charge transfer.[32-33,118-119] Simple spin-coating of such low-bandgap polymer semiconductors onto a substrate with commonly used source-drain metal electrodes can offer high-performance ambipolar OFETs. Very recently, donor–acceptor polymer semiconductors with sufficiently low-lying LUMO levels (-4.0 – -4.2 eV) and high-lying HOMO levels (-5.1 – -5.5 eV) were found to be promising semiconductors in ambipolar OFETs, exhibiting electron and hole mobilities in the range of 10^{-4} to 0.1 cm^2/Vs.[39-41,134] Controls of solubility, crystallinity, and energy levels by chemical design to achieve a good processability and high charge-carrier mobilities are challenges of this approach.

In this chapter, I demonstrate the solution-based fabrication of high-performance ambipolar transistors and complementary circuits based on single-component ambipolar polymer semiconductors, multilayers of unipolar polymer semiconductors, and blends of unipolar polymer semiconductors. Electron and hole mobilities of 0.001–0.04 cm^2/Vs and 0.001–0.2 cm^2/Vs, respectively, are achieved in the ambipolar OFETs. Complementary logic circuits, including an Inverter (NOT-gate), and two-terminal NAND- and

NOR-gates, based on ambipolar OFETs show good switching characteristics. I have also investigated the effects of annealing temperature and exposure to the air on the charge transport properties.

3.2. Experimental Methods

Materials. Polymer semiconductors studied here, PNIBT, HDPPTV, HDPPPV, PPTPV, BBL, PBTOT, PSOTT, and PSOxTT, were synthesized as reported.[41,86,146-148,204] Molecular weights of the polymer semiconductors were 113 kDa for PNIBT, 154 kDa for HDPPTV, 206 kDa for HDPPPV, 78.5 kDa for PPTPV, 722 kDa for PBTOT, 15.5 kDa for PSOTT, and 24.3 kDa for PSOxTT. The BBL sample used in this study has an intrinsic viscosity of 7.0 dL/g in methanesulfonic acid (MSA) at 30 °C and a typical electron mobility of 0.001–0.002 cm^2/Vs in air.[56,129,177-178] P3HT with a molecular weight of ~54 kDa was purchased from Aldrich.

Device Fabrication and Characterization. OFETs and circuits were fabricated as typical coplanar structures on silicon substrates. Heavily *n*-doped silicon with 200–300 nm thermal oxide acted as a common gate with a dielectric layer as well as the substrate. Gold source and drain electrodes (40–60 nm) with a thin underlying chromium adhesive layer (1–2 nm) were patterned by conventional photolithography, thermal evaporation, and lift-off process. Channel width and length were 800–5000 μm and 20–100 μm, respectively. The substrates were cleaned by ultrasonication with acetone and isopropyl alcohol and dried by flow of nitrogen. Some of devices were treated with a self-assembled monolayer of octyltrichlorosilane (OTS8) by vapor deposition or spin-coating after furhter cleaning of substrates by plasma treatment (100 W for 2–4 min). The substrates were then washed with toluene to remove physisorbed silane agents. Polymer semiconductor thin films (~5–50 nm) were deposited from a solution in chloroform, 1,2-dichlorobenzene, 1,2,4-trichlorobenzene, or methanesulfonic acid by spin-coating (1000–3000 rpm for 30–60 s) onto the substrates. BBL films deposited from an acid solution were immediately immersed in methanol, water, and/or dimethylsulfoxide for ~1–8 hours to remove the acid

solvent. The removal of the acid was continued until the washing medium became neutral pH. The films were thermally annealed on a temperature-controlled hot-plate for 10 min under inert conditions. Devices were tested by using an HP4145B semiconductor parameter analyzer under nitrogen environment or by using a Keithley 4200 semiconductor characterization system in air. Electrical parameters, including field-effect mobility and threshold voltage, were calculated by using the standard saturation region equation (Eq. 1-2). The plots of $|I_{ds}|^{1/2}$ versus V_{gs} with appropriate biases, where the device shows the current saturation in output curves (*i.e.*, large, positive V_{gs} and V_{ds} for calculation of μ_e, and negative biases for μ_h) were used.[41] Because the opposite type of charge carriers can be involved in the operation under certain voltage biases,[205] inappropriate selection of data may cause an over-estimation of carrier mobilities. The capacitance of the SiO_2 was used in the calculation of mobilities in both upper- and lower-layer of the channel of multilayer heterojunction transistors.

Morphology and Photophysical Properties Characterization. Surface morphology of thin films was imaged directly from the devices by using a Veeco Dimension 3100 scanning probe microscopy in tapping mode. Samples for photophysics and X-ray diffraction were prepared on freshly cleaned glass substrates. Absorption spectra were taken on a Perkin-Elmer Lambda 900 UV/Vis/NIR spectrometer. X-ray diffraction patterns were obtained on a Bruker AXS D8 Focus diffractometer with Cu Kα beam (40 kV, 40 mA; λ = 0.15418 nm). Scanning electron microscope (SEM) imaging was done by using a FEI Sirion SEM with an accelerating voltage of 5 kV.

3.3. Results and Discussion

3.3.a. Single-Component Ambipolar Polymer FETs

3.3.a.1. Naphthalenediimide–Bithiophene Copolymer Semiconductor (PNIBT).

PNIBT (P8a) is one of the NDI-based polymer semiconductors (PNDIs) discussed in the previous chapter, and has an alternating donor–acceptor architecture consisting of electron-donating dialkoxybithiophene and electron-accepting NDI units (Figure 3-2A). As seen above and in literature, NDI-based copolymers have so far proved to be good *n*-channel transistor materials,[22,88] and the incorporation of the highly electron-rich dialkoxybithiophene is expected to enhance p-channel charge-transport.[34] PNIBT is readily soluble in chloroform, but less soluble in 1,2-dichlorobenzene. Differential scanning calorimetry (DSC) scans of PNIBT indicated no obvious thermal transitions, up to 350 °C. Optical absorption spectroscopy of PNIBT thin films annealed at 100 °C revealed a broad absorption band centered at 853 nm with an optical bandgap of 1.16 eV. HOMO and LUMO energy levels derived from cyclic voltammetry were -5.1 and -3.7 eV, respectively.

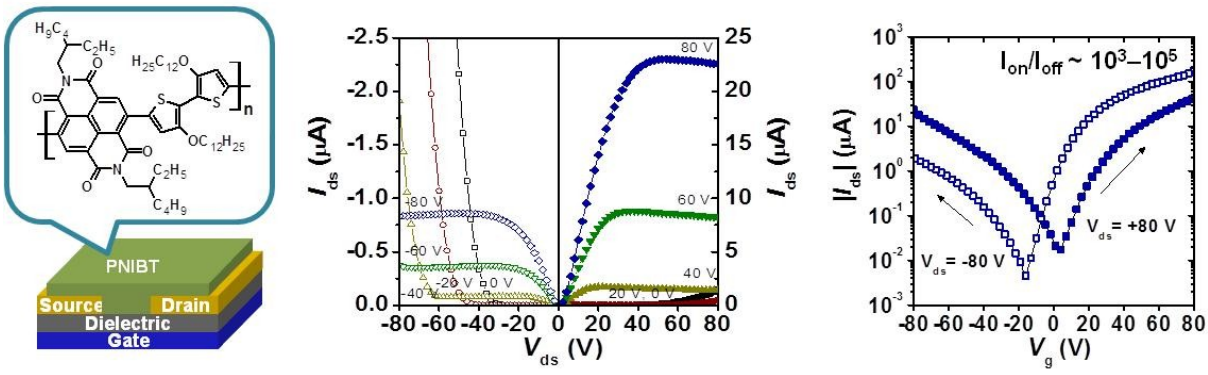

Figure 3-2. (A) Chemical structure of the copolymer PNIBT. (B) Schematic of field-effect transistors. (C) Output and (D) transfer characteristics of the polymer field-effect transistor after annealing at 200 °C. The saturation mobilities in the specific device are 0.042 cm^2/Vs for electrons and 0.0026 cm^2/Vs for holes. Reproduced from Ref.[41] by permission of The Wiley-VCH.

PNIBT transistors with bottom-contacts and bottom-gate were fabricated by spin-coating of the polymer solution in chloroform onto a substrate that are hydrophobically modified by an octyltrichlorosilane monolayer (Figure 3-2B). The PNIBT devices showed typical ambipolar features, such as diode-like current increase (when $|V_{ds}| >> |V_{gs}–V_t|$) with current saturation at high gate voltage in output curves (Figure 3-2C) and V-shape transfer curves with a narrow off-state (Figure 3-2D). Such current–voltage characteristics of ambipolar transistors arise from the controlled injection of both holes and electrons into a common channel.[177] The PNIBT OFETs showed excellent current modulation with on/off current ratios of 10^3–10^5 at large source-drain bias (V_{ds} = ± 80 V), compared to that typically reported ($\leq 10^3$) for ambipolar OFETs with comparable mobilities ($>10^{-3}$ cm^2/Vs).[37-40,178,191,193-194] The charge-carrier mobilities were calculated using the saturation region equation (Eq. 1-2).[5,44] The linear-fit was applied to the plots of $|I_{ds}|^{1/2}$ as a function of V_{gs} in the saturation region (V_{ds}~V_{gs}) for both n-channel and p-channel operations (Figure 3-3A). Electron mobility as high as 0.04 cm^2/Vs and hole mobility as high as 0.003 cm^2/Vs were obtained. It is interesting that the electron mobility in these PNIBT transistors is about one order of magnitude larger than the hole mobility, considering that the injection barrier for electrons (~1.4 eV) is substantially higher than for holes (~0 eV) from the gold electrodes with a work function of 5.1 eV. Charge trapping at the semiconductor/dielectric interface, often implicated for poor electron transport due to trapping of electrons by hydroxyl groups,[43] is also ruled out as the origin of the observed asymmetry in carrier mobilities. It is likely that the donor–acceptor molecular structure of PNIBT intrinsically supports ambipolar charge-transport with high carrier mobilities.

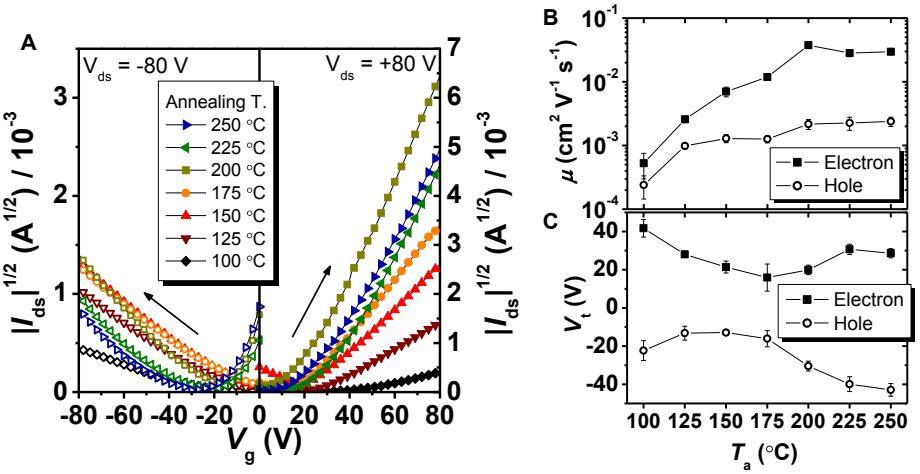

Figure 3-3. (A) Square-root of source-drain current vs. gate voltage curves at various annealing temperatures (T_a). (B) Saturation mobility and (C) threshold voltage as a function of annealing temperature. Reproduced from Ref.[41] by permission of The Wiley-VCH.

The lack of a clear T_g or melting temperature in the DSC scans of PNIBT implied that thermal annealing would not influence its order/morphology and therefore performance within devices. However, the annealing temperature (T_a = 100–250 ºC) has notable effects on the ambipolar PNIBT transistors. Figure 3-3A shows the transfer curves of the ambipolar PNIBT OFETs, $|I_{ds}|^{1/2}$ versus V_g, as a function of the annealing temperature, T_a. The saturation electron and hole mobilities extracted from these transfer curves are shown in Figure 3-3B as a function of T_a and also collected in Table 3-1. As T_a increased from 100 °C to 200 °C, the mobility increased monotonically from 5×10^{-4} to 0.03–0.04 cm^2/Vs for electrons and from 2×10^{-4} to 0.002–0.003 cm^2/Vs for holes (Figure 3-3B). About two orders of magnitude enhancement in electron mobility is observed while the hole mobility improved by a factor of 10. No significant change in the charge-carrier mobilities was observed at T_a higher than 200 °C. The threshold voltages (V_t) for *n*-channel mode decreased from 42 V to 16 V as T_a increased from 100 °C to 175 °C, then increased to 29 V at higher T_a (Figure 3-3C). For *p*-channel operation, V_t shifted from -22 V to -13 V to -43 V, when the temperature increased from 100 to 150 to 250 °C. Unlike charge-carrier mobility and

threshold voltage, the on/off current ratios of the *p*- and *n*-channel modes were not affected by the annealing temperature. Parameters of the PNIBT OFETs as a function of T_a are summarized in Table 3-1.

Changes in the optical absorption and morphology of PNIBT thin films as a function of T_a clarify the observed improvement of the ambipolar transistors with increased annealing temperature. Figure 3-4A shows the UV/Vis/NIR absorption spectra of PNIBT thin films annealed at temperatures from 100 to 250 °C. A significant bathochromic shift in the absorption is observed as T_a was increased. The optical absorption maximum (λ_{max}) seen at 853 nm for PNIBT thin films annealed at 100 °C is shifted to 980 nm after annealing at 175–200 °C. At higher T_a, the 980-nm absorption peak became dominant while the feature at 853 nm is reduced to a shoulder. The higher-energy absorption maximum also shifted from 418 nm to 441 nm as T_a increased from 100 to 250 °C. The optical bandgap determined from the absorption-edge of PNIBT changed from 1.16 to 1.07 eV as T_a was varied (100–250 °C). The observed absorption spectral shifts suggest changes in polymer backbone planarity and/or packing arrangement.

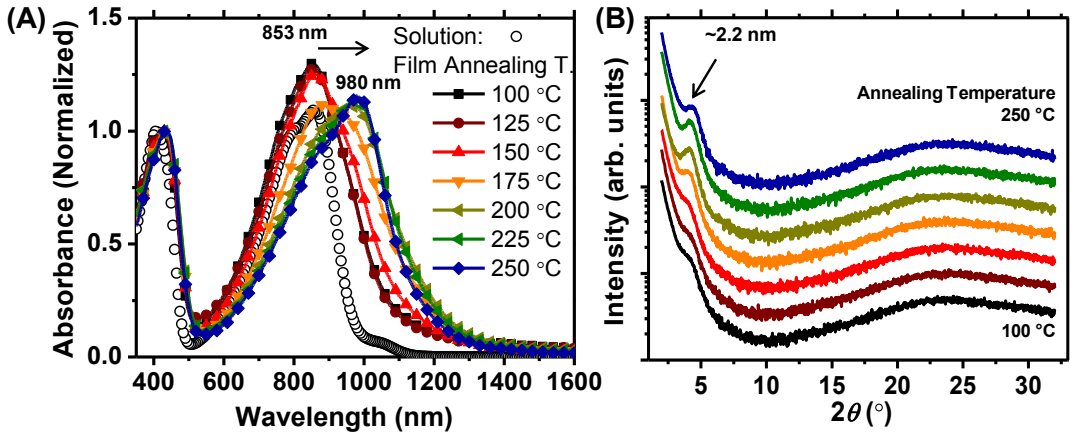

Figure 3-4. (A) UV/Vis/NIR absorption spectra, and (B) X-ray diffraction patterns of PNIBT annealed at various temperatures. Absorption data are normalized at the peak around 430 nm. Reproduced from Ref.[41] by permission of The Wiley-VCH.

X-ray diffraction (XRD) spectra were measured from films annealed at the same temperatures employed for the optical absorption study (Figure 3-4B). The diffraction plots are relatively featureless suggesting short-range order at best. On going from T_a = 150 ºC to 175 ºC, there is an apparent step-change as a broad feature at 2θ = 4.1 ° becomes a clear diffraction maximum. The corresponding *d*-spacing of this peak is ~2.2 nm, which could reasonably be assigned to the spacing between polymer backbones filled by alkyl side chains (lamellar spacing). The polymers are likely kinetically trapped in a lower state of order during spin coating. Although no thermal transition was detected by DSC, there is apparently some increase in polymer backbone mobility between 150–200 ºC, allowing relaxation to a somewhat more ordered state.

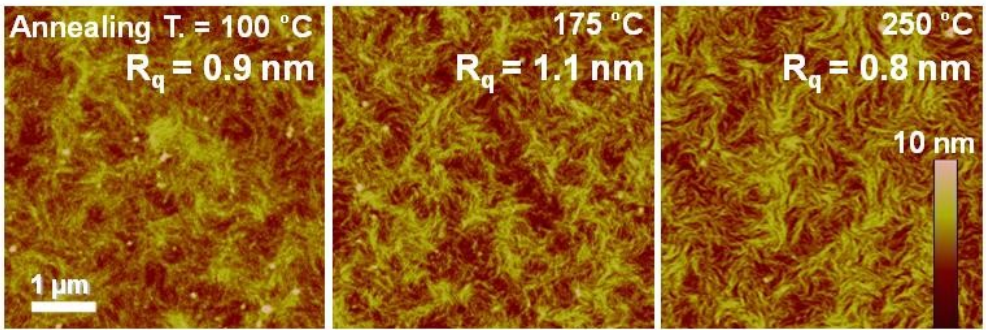

Figure 3-5. Topographic AFM images of PNIBT thin films after annealing at: (A) 100 °C; (B) 175 °C; and (C) 250 °C. Corresponding root-mean-square roughness (R_q) values are 0.9 nm, 1.1 nm, and 0.8 nm, respectively. Reproduced from Ref.[41] by permission of The Wiley-VCH.

Figure 3-5 shows the surface morphology of the ambipolar devices as revealed by topographic atomic force microscopy (AFM). Entangled nanofibrillar structures with a broad distribution of widths of ~20–100 nm were clearly seen throughout the whole range of T_a. Root-mean-square surface roughness values (R_q) ranged from 0.8 to 1.1 nm. The edge of the nanofibers tended to be sharper with higher T_a, but no other obvious morphological difference was seen in PNIBT thin films annealed at various temperatures (Figure 3-5). The highly entangled nanostructures seen in the surface morphology of PNIBT thin films, in addition to the local ordering of the polymer as indicated from optical absorption and XRD spectra,

appear to facilitate domain-interconnectivity essential to high charge-carrier mobility, similar to recent observations in other high-mobility polymers.[34,124,151]

The ambipolar PNIBT transistors were integrated on a common substrate to demonstrate complementary inverters. An inverter consists of two connected transistors and enables the switching of an input signal (*i.e.*, V_{in}) to an output signal (*i.e.*, V_{out}), and is thus a valuable building block of digital circuits for data processing.[44] The two transistors in a complementary inverter share a common gate which acts as an input terminal and a common drain as the output terminal. The remaining two electrodes of the transistors are biased to power-supply (V_{dd}) for the load device and ground for the driver device. Here, the power and ground terminals are interchangeable because the elemental PNIBT transistors are virtually identical.

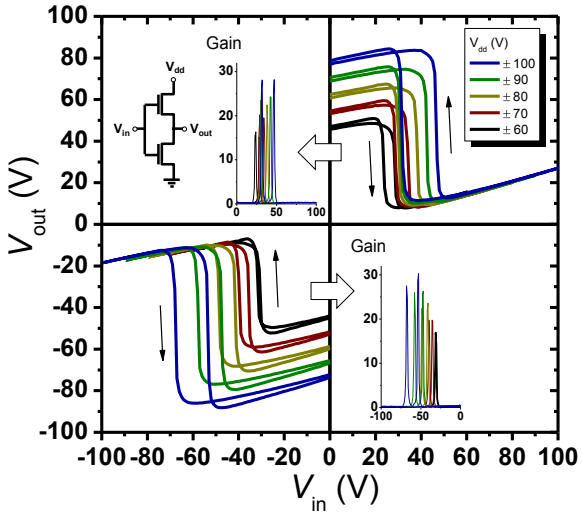

Figure 3-6. Voltage transfer characteristics of a complementary PNIBT inverter (annealed at 250 °C) with various supplied voltages. Insets show a circuit diagram and the plots of gains ($-dV_{out}/dV_{in}$) corresponding to the voltage transfer curves. Reproduced from Ref.[41] by permission of The Wiley-VCH.

Figure 3-6 shows the voltage transfer characteristics (V_{out} vs. V_{in}) of the inverters with various supplied voltage, V_{dd}. The inverters exhibited an excellent switching of V_{out} at V_{in} near the half of V_{dd}. At the

steady-state where V_{in} is either near 0 V or near the supplied voltage, V_{out} has an offset from the ideal output voltage (V_{dd} or 0 V). The amount of offset decreases as V_{in} approaches the switching point. The observed offsets of V_{out} are typical for inverters from ambipolar transistors,[36] mainly because of the narrow off-state and high current at the gate voltage near 0 V in the transistors. The minima of I_{ds} in the transfer curves of the transistors are shifted from 0 V of the gate. Voltage gain ($-dV_{out}/dV_{in}$) as high as 30 was recorded from the inverters (Figure 3-6; Table 3-1). The sharp switching is one of the main advantages of complementary logic gates. Similar switching characteristics were observed from the first and third quadrants depending solely on the polarity of applied biases. This means that the constituent transistors have comparable performance and there is negligible variation in the capability of the transistors on a common substrate. The high gain comes from the high charge-carrier mobilities of both holes and electrons in the new copolymer semiconductor, despite the difference of a factor of 10 in the mobility values. However the asymmetry of the mobilities (Figure 3-3B), in combination with the asymmetry of threshold voltages (Figure 3-3C) in *p*- and *n*-channel modes, might cause hysteresis between forward and reverse sweeps.[44]

Table 3-1. Absorption maxima of thin films and electrical parameters of PNIBT transistors and inverters annealed at various temperatures. Reproduced from Ref.[41] by permission of The Wiley-VCH.

T_a (°C) [a]	λ_{max} (nm)	E_g^{opt} (eV)	μ_e^{avg} (cm^2/Vs) [b]	μ_h^{avg} (cm^2/Vs) [b]	$V_{t,e}^{avg}$ (V) [b]	$V_{t,h}^{avg}$ (V) [b]	$Gain_{max}$ [c]
100	853	1.16	5.3×10^{-4}	2.4×10^{-4}	41.7	-22.3	16.0
125	853	1.16	2.6×10^{-3}	9.8×10^{-4}	28.0	-13.2	25.8
150	860	1.12	7.0×10^{-3}	1.3×10^{-3}	21.4	-12.9	25.9
175	879	1.06	1.2×10^{-2}	1.3×10^{-3}	15.9	-16.1	26.3
200	962	1.05	3.8×10^{-2}	2.2×10^{-3}	19.9	-30.4	28.9
225	979	1.05	2.8×10^{-2}	2.3×10^{-3}	30.7	-39.9	29.7
250	980	1.07	3.0×10^{-2}	2.4×10^{-3}	28.6	-42.9	30.3

[a] Annealing temperature. [b] Average values of 7–8 devices. Calculated from the plot of $I_{ds}^{1/2}$ vs. V_g, according to the saturation current equation. [c] Maximum value of $-dV_{out}/dV_{in}$ at V_{dd}=±100 V.

3.3.a.2. Diketopyrrolopyrrole (DPP)-based Copolymer Semiconductors.

The charge transport properties of DPP-based poly(arylene vinylene)s were investigated by fabricating and characterizing OFETs. Figure 3-7 shows chemical structures of the copolymer semiconductors and representative current–voltage characteristics of OFETs based on HD-PPTV. HD-PPTV and PPTPV showed ambipolar transporting features.[35-36,41,177] A hole mobility of 0.20 cm^2/Vs and electron mobility of 0.03 cm^2/Vs were obtained from HD-PPTV. The larger injection barrier for electrons from the gold electrodes might have resulted in one order of magnitude lower electron mobility.

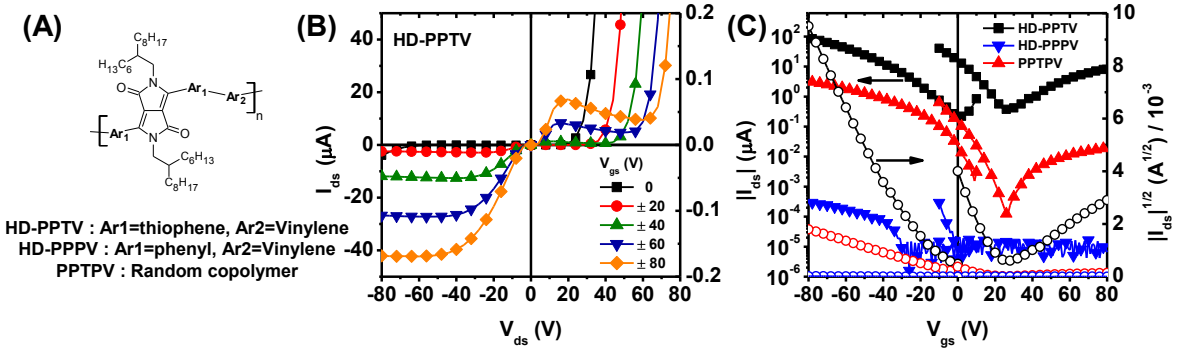

Figure 3-7. (A) Chemical structures of DPP-based copolymer semiconductors. (B) Output characteristics of the field-effect transistor based on HD-PPTV after annealing at 150 °C. (C) Overlays of representative transfer curves (V_{ds}=±80 V) of the transistors of HD-PPTV, HD-PPPV, and PPTPV. Reproduced with permission from Ref.[137] Copyright 2011 American Chemical Society.

Figure 3-8 shows the annealing temperature dependence of hole and electron mobilities in HD-PPTV transistors. The electrical parameters of devices without air-exposure are collected in Table 3-2. The average hole mobility was in a narrow range of 0.091–0.17 cm^2/Vs and the electron mobility was 0.012–0.015 cm^2/Vs with current on/off ratios of 10^2–10^3. The threshold voltages are -9.0 to -1.6 V for *p*-channel operation and 22.7–32.1 V for *n*-channel mode. These asymmetric threshold voltages are commonly seen in ambipolar OFETs based on DPP-containing polymers.[39,136,189] Unlike PNIBT discussed above, the measured mobilities are insensitive to the annealing temperature (T_a). It is believed that thermal annealing

did not have a substantial influence on charge transport due to the lack of a clear glass transition or melting transition in the DSC scans of HD-PPTV. It should be noted that a brief exposure of devices to air before testing (for less than 2 min) caused decrease of both hole and electron mobilities by factors of 1.5–3 and 2–14, respectively, resulting in the average mobilities of 0.04–0.12 cm^2/Vs for holes and 0.001–0.006 cm^2/Vs for electrons. The large decrease of electron mobility is likely from the relatively high-lying LUMO energy level (-3.34 eV) which makes the polymer vulnerable to dopants in air.

In the case of HD-PPPV, the average hole mobility of 4.9×10^{-7} cm^2/Vs was obtained and electron transport was not observed in the OFETs. A major reason for the lack of electron transport in HD-PPPV is its high-lying LUMO level (-3.1 eV), resulting in a large injection barrier for electrons from the gold electrodes. In addition, the largely amorphous nature of HD-PPPV thin film also accounts for the poor charge transport in the material. PPTPV, a random copolymer of monomers of HD-PPTV and HD-PPPV, showed intermediate average hole and electron mobilities of 3.9×10^{-4}–2.2×10^{-3} and 2.9×10^{-6}–2.3×10^{-5} cm^2/Vs, respectively, after annealing at 110−200 °C. The highest average mobilities in PPTPV OFETs were observed after annealing at 150 °C (Table 3-2).

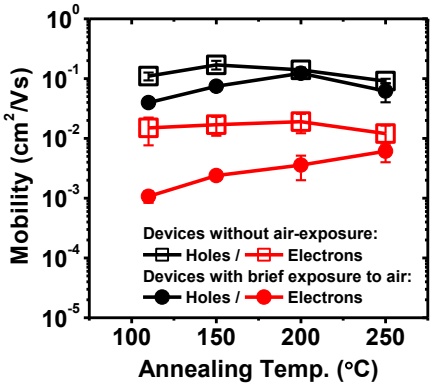

Figure 3-8. Effects of the annealing temperature and air-exposure on field-effect mobility of HD-PPTV. Reproduced with permission from Ref.[137] Copyright 2011 American Chemical Society.

Based on XRD patterns,[204] HD-PPTV has a strong (100) diffraction peak at 4.8 °, corresponding to a d-spacing of 18.5 Å. This d-spacing corresponds to a stacking distance governed by the 2-hexyldecyl side chains, suggesting that the HD-PPTV exhibits a lamellar crystalline packing in a thin film. The broad band centered at 22.7 ° is related to the π–π stacking distance (3.9 Å). In contrast, HD-PPPV did not show any diffraction peak in the XRD pattern suggesting an amorphous nature of the film. Interestingly, the random copolymer PPTPV shows a weak diffraction peak at 4.9 °, corresponding to a d-spacing of 18.0 Å. This means that PPTPV has some degree of crystallinity with a lamellar packing structure, similar to HD-PPTV. The crystallinity correlates well with charge carrier mobility discussed above.

Complementary logic circuits were also fabricated and demonstrated by integrating multiple HD-PPTV transistors. Figure 3-9 shows the voltage transfer characteristics of the NOT, NAND, and NOR gates with supplied voltage (V_{dd}) of ±80 V. Signal switching in an ideal inverter occurs at a half of V_{dd}. However, the inverter based on HD-PPTV showed switching at the voltages more positive than $V_{dd}/2$ due to the positive and asymmetric threshold voltages of individual transistor in *p*- and *n*-channel operations. Nevertheless, the inverters showed sharp switching characteristics with the voltage gain ($-dV_{out}/dV_{in}$) of 15–27.

Table 3-2. Electrical parameters of HD-PPTV, HD-PPPV, and PPTPV transistors without air exposure. Reproduced with permission from Ref.[137] Copyright 2011 American Chemical Society.

Material	T_a [a] (°C)	μ_h [b] (cm^2/Vs)	μ_e [b] (cm^2/Vs)	$V_{t,h}$ [b] (V)	$V_{t,e}$ [b] (V)	I_{on}/I_{off}
HD-PPTV	110	0.11	0.015	-5.9	24.5	10^2–10^3
	150	0.17	0.017	-5.5	22.7	10^2–10^3
	200	0.14	0.019	-1.6	28.8	10^2–10^3
	250	0.091	0.012	-9.0	32.1	10^2–10^3
HD-PPPV	150	4.9×10^{-7}	-	-9.8	-	10^1
PPTPV	110	3.9×10^{-4}	2.9×10^{-6}	3.9	17.9	10^2–10^3
	150	2.2×10^{-3}	2.3×10^{-5}	-2.6	16.4	10^2–10^3
	200	1.5×10^{-3}	1.9×10^{-5}	-9.3	24.2	10^2–10^3

[a] The polymer film was annealed at T_a for 10 min. [b] Average of 5–6 devices.

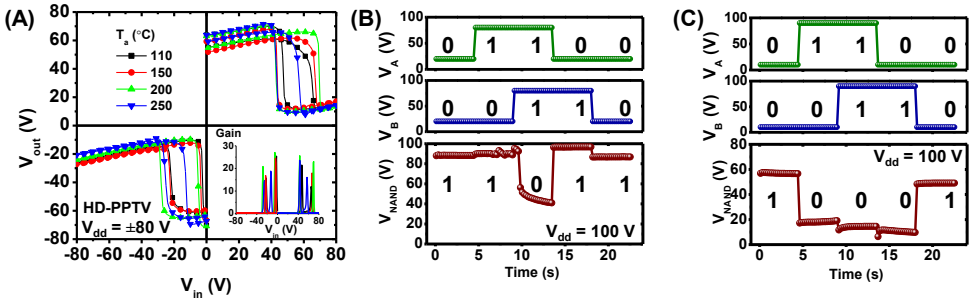

Figure 3-9. Voltage transfer characteristics of complementary inverter, NAND-gate, and NOR-gate based on HD-PPTV. The inset of (A) shows the plot of gains ($-dV_{out}/dV_{in}$) that corresponds to the voltage transfer curves. For (B) and (C), truth tables are overlaid to show the logic operation. Reproduced in part with permission from Ref.[137] Copyright 2011 American Chemical Society.

3.3.b. Layered Polymer Heterojunctions for Ambipolar FETs

Well-defined *n*/*p* heterojunctions of the polymers in Figure 3-10 can be sequentially prepared by solution-based processing, because BBL is soluble in MSA but not in chlorinated aromatic solvents whereas P3HT, PBTOT, and PSOTT are soluble in the latter solvents. During the coating process, no evidence of dewetting of polymeric thin film was observed (Figure 3-11). Figure 3-12 shows UV/Vis absorption spectra of thin films of the polymer semiconductors and their bilayered heterojunctions. The absorption spectra of the heterojunctions are simple superposition of the spectra of the component polymers, showing that the heterojunctions were formed from sequential deposition without degradation. No evidence of ground-state charge-transfer at the heterojunctions was observed. The *n*/*p* polymer/polymer heterojunctions were spatially not well-resolved in SEM images (Figure 3-10d) due to the very thin films (≤ 25 nm) and low contrast between polymer semiconductors. The *n*/*p* bilayer heterojunctions offer the potential to effectively use the full channel area in OFETs, allowing the achievement of electron and hole mobilities close to those of the constituent polymer semiconductors (see below).

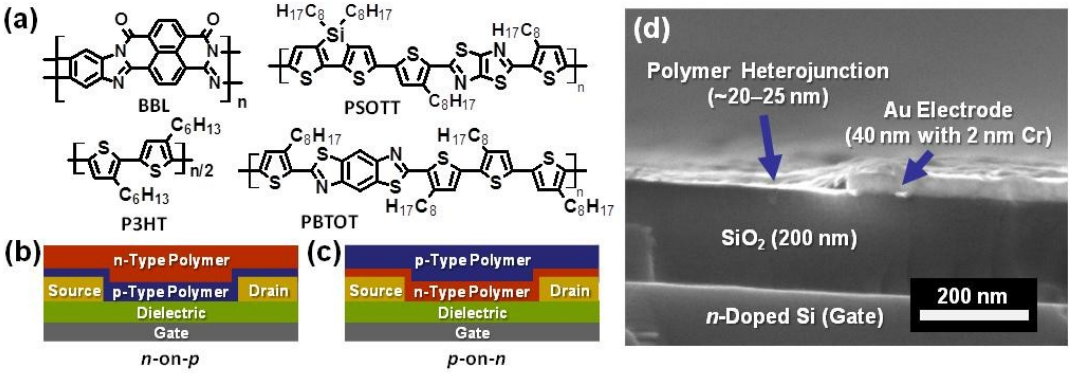

Figure 3-10. (a) Molecular structures of the n-channel (BBL) and p-channel polymer semiconductors (P3HT, PBTOT, and PSOTT). (b-c) Schematics of ambipolar field-effect transistors based on *n*/*p* polymer heterojunctions: (b) *n*-on-*p* and (c) *p*-on-*n* bilayers. (d) A cross-sectional scanning electron microscope image of a transistor based on BBL-on-PBTOT heterojunction. Reproduced with permission from Ref.[146] Copyright 2010 American Chemical Society.

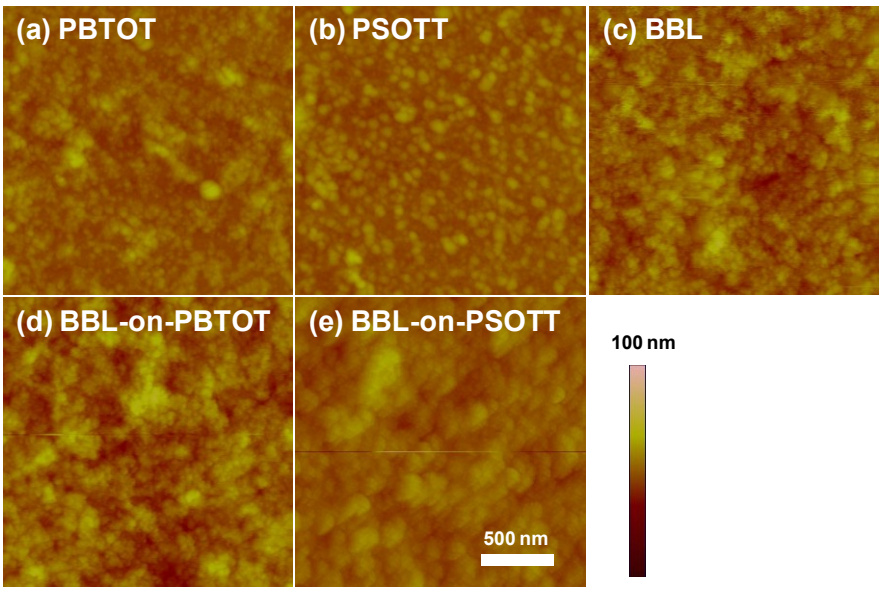

Figure 3-11. AFM topographic images of (a) PBTOT, (b) PSOTT, (c) BBL, (d) BBL-on-PBTOT, and (e) BBL-on-PSOTT.

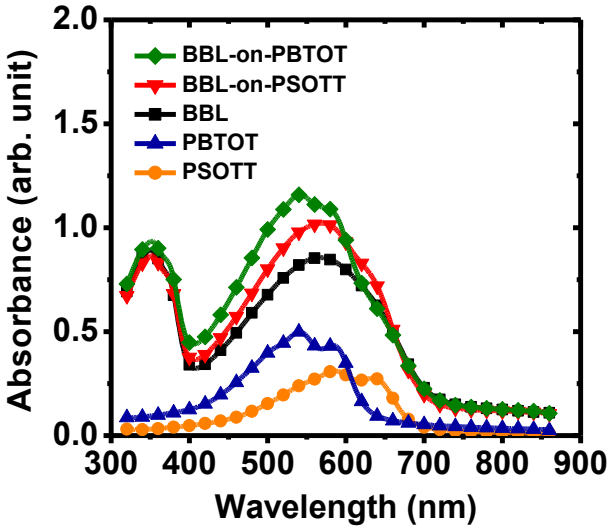

Figure 3-12. Absorption spectra of thin films of BBL, PSOTT, and PBTOT, and heterojunctions of BBL-on-PSOTT and BBL-on-PBTOT. Reproduced with permission from Ref.[146] Copyright 2010 American Chemical Society.

Figure 3-13 and Figure 3-14 show the electrical characteristics of the OFETs from the *n*/*p* polymer heterojunctions. Clear *I*–*V* characteristics of linear and saturation regions at high V_{gs} and superlinear current increase of typical ambipolar OFETs at low V_{gs} were observed in the output curves (Figure 3-13),[35] confirming the formation of channels for holes and electrons with well-defined *n*/*p* heterojunctions following sequential spin coating. Both electron mobility (μ_e) and hole mobility (μ_h) of *n*-on-*p* devices are in the range of ~10^{-3}–10^{-2} cm^2/Vs. The similarity of mobilities to those of single-layer OFETs comes from the fact that charge transport occurs in thin conduction sheet defined by the channel dimensions (*W* and *L*). Average electron and hole mobilities in BBL-on-PBTOT are 0.0051 cm^2/Vs and 0.0078 cm^2/Vs, respectively. BBL-on-PSOTT showed a higher average hole mobility of 0.012 cm^2/Vs, whereas the observed average electron mobility was 0.0058 cm^2/Vs. The on/off ratios of the OFETs are ~10^3 with low V_{ds} (±10 V), whereas the ratios become ~10 when V_{ds}=±80 V (Figure 3-14). Average threshold voltages for *n*- and *p*-channel modes are 4.3 V and -10.1 V in BBL-on-PBTOT, and 19.8 V and 5.9 V in BBL-on-PSOTT, respectively. In P3HT-on-BBL devices, the mobilities are rather low and

asymmetric compared to the other systems (Figure 3-13c). The electron mobility of 0.002 cm^2/Vs is similar to the previously reported values of BBL on SiO_2.[177-178] It is interesting that μ_e in *n*-on-*p* devices is generally higher than in *p*-on-*n*, despite potential electron-injection barriers of *n*-on-*p* devices. The higher μ_e might come from the absence of electron-trapping silol groups[43] covered by OTS8 and *p*-type polymers. The very low mobility of holes (~10^{-5} cm^2/Vs) in P3HT-on-BBL devices can be attributed to the fact that the underlying BBL layer is relatively thick (~20–30 nm) and rough (R_q~5 nm). A thick underlying layer can act as a barrier for hole injection,[174] and a rough interface scatters the charge carriers in the *p*-channel,[65] resulting in the much lower hole mobility in P3HT. It should be noted that corrections for contact resistance and capacitance change caused by the presence of a bottom-channel layer have not been made in the calculation of the mobility of the top channel.

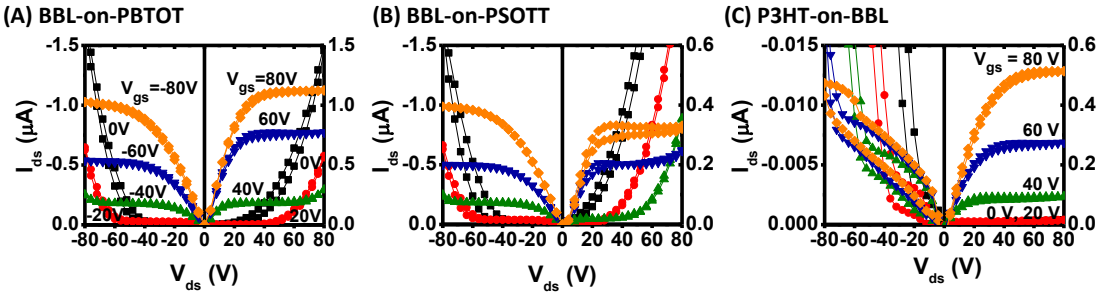

Figure 3-13. (a-c) Output characteristics of *n*/*p* bilayer heterojunction transistors: (a) BBL-on-PBTOT, (b) BBL-on-PSOTT, and (c) P3HT-on-BBL. Reproduced with permission from Ref.[146] Copyright 2010 American Chemical Society.

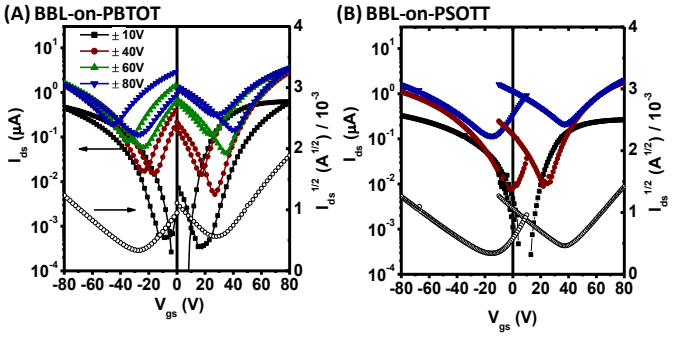

Figure 3-14. Transfer curves of bilayer transistors based on (A) a BBL-on-PBTOT and (B) a BBL-on-PSOTT transistors. Charge-carrier mobilities were calculated from the slope of $I_{ds}^{1/2}$ at V_{ds} = ±80 V. Reproduced in part with permission from Ref.[146] Copyright 2010 American Chemical Society.

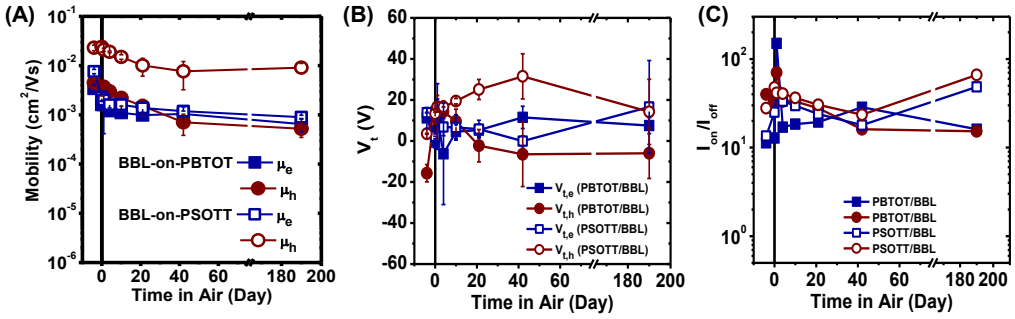

Figure 3-15. Electrical parameters of layered polymer heterojunction ambipolar field-effect transistors as a function of time after air-exposure. (A) field-effect mobilities, (B) threshold voltages, and (C) on-off current ratios. Devices were initially testes in inert conditions (data points before day 0), and then stored and tested in ambient lab conditions. Reproduced with permission from Ref.[146] Copyright 2010 American Chemical Society.

Field-effect mobilities of electrons and holes in the *n*/*p* heterojunction OFETs in air have been tracked for more than 6 months (Figure 3-15), demonstrating good stability. The OFET mobilities were initially measured in nitrogen and then stored and periodically tested in air. The hole mobilities in PBTOT and PSOTT *p*-layers decreased from 0.0045 and 0.023 cm^2/Vs to 0.0007 and 0.0077 cm^2/Vs, respectively, after 42 days stored and tested in air. The mobilities measured after 190 days in air were 0.0005 cm^2/Vs and 0.0093 cm^2/Vs, respectively. Although in general *p*-type semiconductors are energetically less susceptible to external dopants that result in degradation of the carrier mobility than *n*-type materials, very thin layer (≤10 nm) of electrically active *p*-channel may be vulnerable to dopants due to the lack of kinetic barrier for diffusion of oxidant molecules to the charge accumulation channel.[141] On the other hand, the electron mobilities in both systems were initially dropped from 0.003–0.008 cm^2/Vs to 0.001–0.002 cm^2/Vs and stabilized with little fluctuations over time. The good air-stability observed here is consistent with the observation in OFETs based on single-layer unipolar semiconductors as described in Chapter 2.

Complementary logic gates, including NOT, NAND, and NOR circuits, based on the integrated ambipolar OFETs exhibited sharp switching as shown in Figure 3-16. Circuit diagrams of an inverter (NOT-gate) consisting of two transistors, and two-input NAND and NOR circuits with four transistors each are shown in Figure 3-16A. The circuits consist of identical ambipolar OFETs from BBL-on-PBTOT *n*/*p* heterojunctions with the same geometric factors (C_i=17 nF/cm^2, W=5000 μm, and L=100 μm). Voltage transfer characteristics of the inverter showed sharp switching, which is typical for complementary circuits,[35] with a high gain ($-dV_{out}/dV_{in}$) of 16–18 reproducibly obtained at V_{dd}=±80 V (Figure 3-16B). The output voltage offsets from V_{dd} and 0 V are also typical for logic circuits based on ambipolar transistors.[35,41] Some degree of hysteresis is likely due to the threshold voltage difference of *n*- and *p*-channel modes in the individual OFETs.

In the logic circuits of NAND and NOR gates, good switching characteristics were also observed, as shown in the output voltages plotted with the corresponding input voltages V_A and V_B (Figure 3-16C,D). High and low voltages at the terminals represent signals 1 and 0, respectively. The truth tables are included in Figure 3-16C,D to clarify the logic operations. It should be noted that the NAND gate based on the ambipolar transistors is converted into the NOR gates, and *vice versa*, by simply swapping terminals of V_{dd} and ground since the constituent transistors are identical. The results demonstrate that ambipolar OFETs can be used for designing and constructing various complementary circuits. Because the ambipolar transistors and circuits are fabricated by simple solution processes, the devices presented here could ultimately be printable and the approach should be applicable to real electronic devices as the technology further develops.

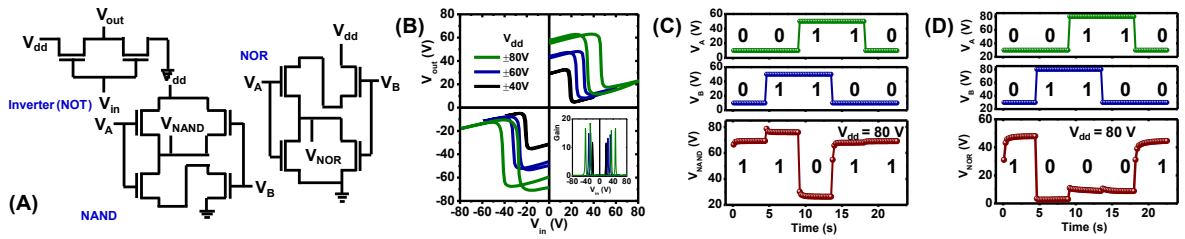

Figure 3-16. (A) Circuit diagrams of a complementary inverter, and NAND and NOR logic gates. (B) Voltage transfer characteristics of an inverter. (C-D) Output voltages of complementary logic gates and the truth tables with corresponding input voltages V_A and V_B: (C) NAND, and (D) NOR gates. The transistors in the circuits are based on BBL-on-PBTOT heterojunctions. Reproduced with permission from Ref.[146] Copyright 2010 American Chemical Society.

3.3.c. Polymer Blends for Ambipolar FETs

Bulk heterojunction approach, or polymer semiconductor blend, is a simple method to achieve ambipolar charge transport based on unipolar polymer semiconductors. However, only few examples of bulk heterojunction ambipolar transistors have been reported in part due to the scarcity of *n*-type polymer semiconductors.[177-178,180,206] Although BBL is a good candidate for *n*-type materials in such polymer blend-based ambipolar transistors, limited solubility of BBL requires specific *p*-type counterpart such as acid-soluble polymer semiconductors.[177-178] PSOxTT (Figure 3-17A) is a *p*-type polymer semiconductor with high mobility of ~0.1 cm^2/Vs,[86] and is soluble in both organic solvents and methanesulfonic acid. Therefore, bulk heterojunction thin films of BBL and PSOxTT can be deposited by spin-coating of a blend of two polymers in the acid, followed by the acid solvent extraction with water. It should be noted that the blend of BBL and PSOxTT can be coated on an OTS8-treated substrate resulting in the good charge transport properties, even though pure BBL film was not able to be coated onto the hydrophobic surface. A thin film with pure PSOxTT from a methanesulfonic acid solution was cracked and delaminated from a substrate during the deprotonation step. Therefore, PSOxTT films were made from chloroform solution for characterization.

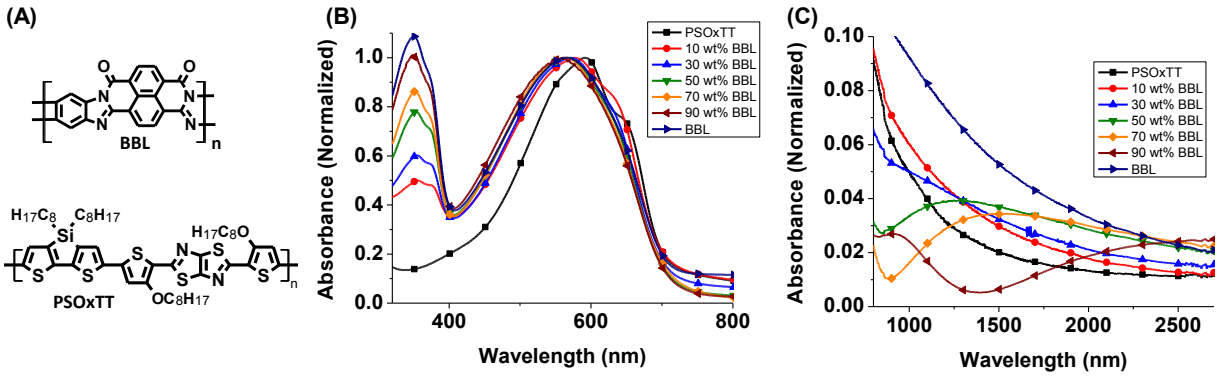

Figure 3-17. (A) Chemical structures of BBL and PSOxTT used for bulk heterojunction ambipolar OFETs. (B-C) Optical absorption spectra of BBL/PSOxTT in (B) ultraviolet/visible region, and (C) near-infrared region.

Figure 3-17(B,C) shows optical absorption spectra of BBL/PSOxTT bulk heterojunction thin films. BBL has characteristic absorption peaks at 563 nm and 350 nm, whereas PSOxTT has a maximum peak at 600 nm and a shoulder at 650 nm. As BBL composition decreased, lowest energy absorption peak red-shifted by 17 nm and a shoulder at 620 nm evolved. A BBL absorption at 350 nm also decreased with lower BBL composition. Interestingly, a thin film with 30 wt% BBL has an absorption shoulder at 1000 nm. This shoulder evolves as a peak and red-shift to 1290 nm (50 wt%) and to 1584 nm (70 wt%) as the BBL composition increases. A thin film with 90 wt% BBL has a further red-shifted peak at 2650 nm and a new peak at 920 nm. Although these peaks are likely from charge transfer between electron-donating PSOxTT and electron-accepting BBL, the exact origin of these peaks in the blends is not understood yet. Due to the absence of strong fluorescent emission of both BBL and PSOxTT, photoluminescence emission spectrum was not obtained.

Surface morphology of the bulk heterojunction films was imaged by using AFM as shown in Figure 3-18. Thin films with larger composition of BBL (70–90 wt%) have relatively smooth surface (R_q ~ 8.5–10.1 nm). The surface roughness increased to 14.5 nm, to 25.6 nm, and to 32.4 nm, when BBL composition decreased to 50 wt%, to 30 wt%, and to 10 wt%. Phase images clearly show the presence of larger domains with lower composition of BBL (Figure 3-18). In order to quantify domain sizes, two-

dimensional isotropic power spectral density based on the AFM images was used (Figure 3-18F). Thin film with 10 wt% BBL showed a peak at 1 μm^{-1} of spatial frequency. The frequency increased to ~3 μm^{-1} as the composition of BBL increased to 90 wt%, suggesting decrease in the domain size.

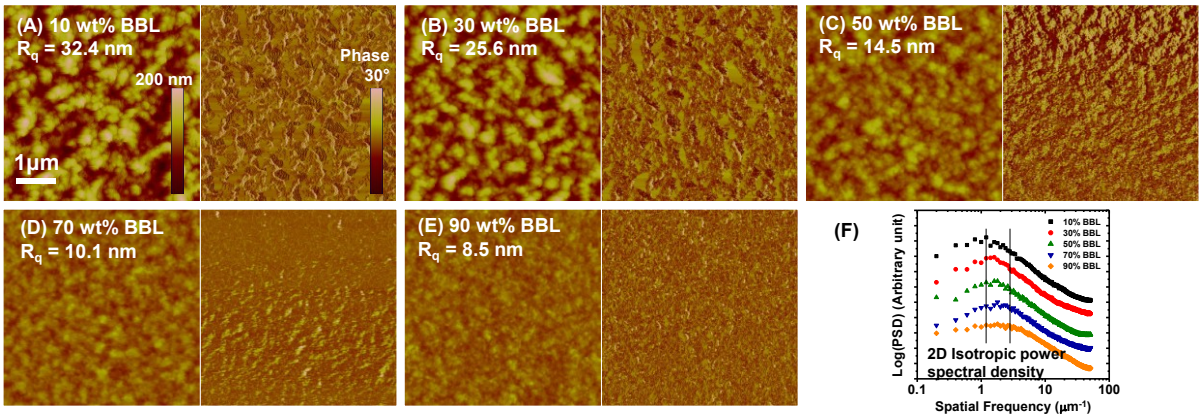

Figure 3-18. (A-E) AFM topography and phase images of BBL/PSOxTT bulk heterojunction thin films: (A) 10 wt%, (B) 30 wt%, (C) 50 wt%, (D) 70 wt%, and (E) 90 wt% of BBL. (F) Two-dimensional isotropic power spectral density of the corresponding images.

X-ray diffraction patterns (Figure 3-19) show that the BBL/PSOxTT blends do not have detectable crystallinity, whereas thin films of pure BBL and PSOxTT have distinct diffraction peaks as reported.[86,143] The absence of diffraction peak is likely related to the limited movement of a polymer chain in solid state caused by high rigidity of the constituent polymer semiconductors and rapid removal of an acid solvent during deposition process of the blend thin film from a homogeneous acidic solution. Homogeneous blends are quenched into solid with a well-intermixed state of PSOxTT and BBL, resulting in the lack of periodicity in atomic and molecular scales.

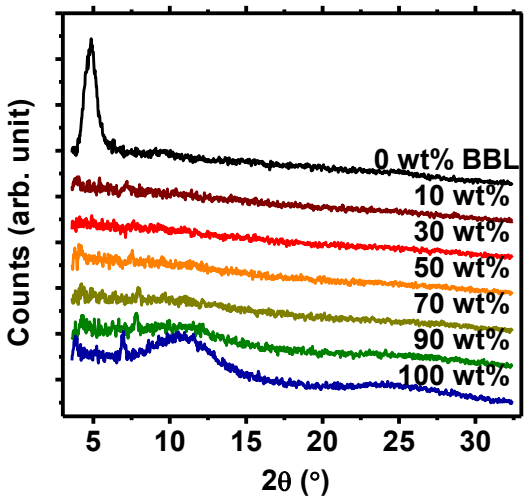

Figure 3-19. XRD patterns of BBL/PSOxTT bulk heterojunction thin films.

Figure 3-20 shows electrical characteristics of a BBL/PSOxTT bulk heterojunction thin film transistor (50 wt% BBL) and the compositional dependence of the field-effect mobility and the threshold voltage. Symmetric ambipolar charge transport characteristics with a good current modulation and saturation were observed in both output and transfer curves (Figure 3-20A,B). The average electron and hole mobilities are 2.9×10^{-3} cm^2/Vs and 1.6×10^{-3} cm^2/Vs, respectively. These mobilities are comparable to the values found in the other polymer-blend-based ambipolar OFETs.[177-178,180,206] The electron mobility shows positive dependence of BBL composition in the bulk heterojunctions, having the mobility up to 0.004 cm^2/Vs with 90 wt% BBL (Figure 3-20C). On the other hand, the hole mobility peaks at 50 wt% BBL (50 wt% PSOxTT), and lowers at lower and higher compositions of PSOxTT. For example, films with 10 wt% of PSOxTT and 90 wt% of PSOxTT have the hole mobility of 4.7×10^{-4} cm^2/Vs and 3.3×10^{-4} cm^2/Vs, respectively. Decrease in hole mobility with lower composition of the *p*-type polymer semiconductor can be understood by having smaller effective charge transport pathways (*i.e.*, channel area) for holes. However, low hole mobility with dominant amount of PSOxTT might be somewhat counter-intuitive. Unlike very rigid ladder-type BBL, PSOxTT tends to form aggregates in an acid solvent and during

deprotonation process, resulting in a limited interconnection between PSOxTT domains and limited percolation of hole transport pathways.

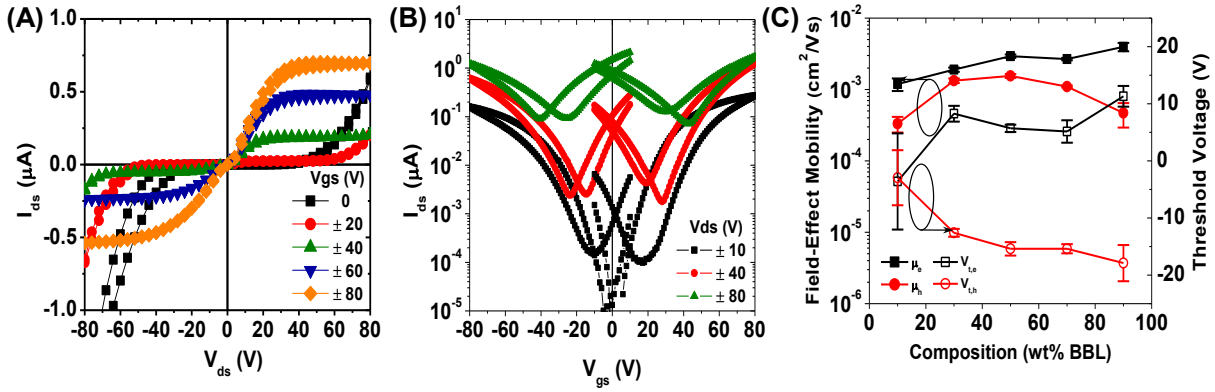

Figure 3-20. (A) Output and (B) transfer characteristics of BBL/PSOxTT (1:1 wt ratio) bulk heterojunction ambipolar FETs. (C) Compositional dependence of field-effect mobilities and threshold voltages of BBL/PSOxTT bulk heterojunction ambipolar transistors.

As shown in Figure 3-21, a complementary inverter was also fabricated based on the bulk heterojunction ambipolar transistors (50 wt% BBL). The inverter showed good switching characteristics with a voltage gain as high as 21. Large hysteresis between forward and backward scans was observed. Such large hysteresis is believed to be in part from variation in performance of two constituent transistors, and in part from the hysteresis of individual transistors as shown in Figure 3-20.

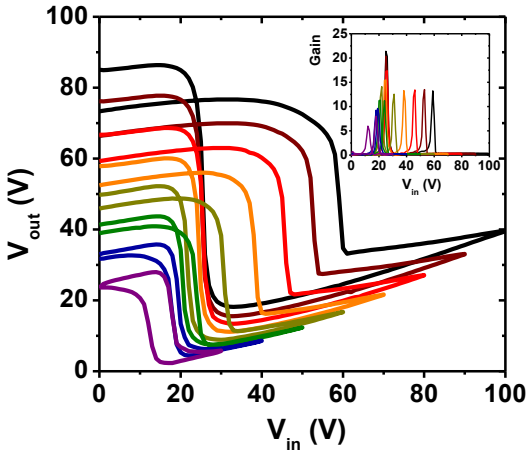

Figure 3-21. Voltage output characteristics of an inverter based on BBL/PSOxTT blend OFETs.

3.4. Conclusions

In summary, I have investigated ambipolar charge transport properties based on donor–acceptor copolymer semiconductors, multilayer polymer semiconductor heterojunctions, and polymer blends of unipolar polymer semiconductors. High-mobility ambipolar transistors and their complementary circuits were fabricated by using a common gold electrode. Charge-carrier mobilities of 0.03–0.04 cm^2/Vs for electrons and 0.003–0.2 cm^2/Vs for holes were achieved in the single-component polymer transistors. Multilayer polymer/polymer heterojunctions, realized by utilizing solvent orthogonality of BBL and *p*-type polymer semiconductors, showed mobilities of 0.003–0.02 cm^2/Vs which are close to those in their component unipolar semiconductors was achieved in air without encapsulation. Polymer blend transistors were also demonstrated to show balanced charge-carrier mobilities of ~10^{-3} cm^2/Vs. Furthermore, simple logic circuits, such as NOT, NAND, and NOR gates, were also demonstrated based on the ambipolar OFETs, exhibiting good signal switching characteristics and a high voltage gain. These results suggest that high-performance complementary circuits can be achieved via solution-processed ambipolar polymer OFETs.

Chapter 4. Enhanced Performance of n-Channel Polymer FETs by Use of Dielectric Buffer Layer

This chapter investigates effects of a polymer dielectric buffer layer on electron transport properties of n-channel polymer FETs. The results in this chapter are reprinted in part with permission from Kim, *et al*. (Copyright 2011 American Institute of Physics).[69]

4.1. Introduction

Development of high performance *n*-channel organic field-effect transistors (OFETs) fabricated by a solution-based processing has been one of the main challenges in organic electronics.[17,22,57,207-208] Because engineering of the gate insulator is one of the promising means to enhance the performance of the OFETs,[207] the effects of the polymer dielectric layer on the performance of OFETs have been studied by varying the chemical functionality,[67] roughness,[209] viscoelasticity,[210] surface energy,[211] and dielectric constant (k) of the insulator.[109,212-213] These properties of the dielectric layer appear to affect the device performance by influencing film growth and morphology as well as through energetic interactions between charge carriers and the dielectric medium. However, studies of effects of the polymer buffer layer on charge transport in organic semiconductors have been largely limited to vacuum-deposited small molecules, including pentacene,[67,209-211,213-215] perylenetetracarboxylic diimide,[216] and fullerene.[107] Energetic, viscoelastic, and topographic properties of the buffer layer inevitably affect the morphology of the organic semiconductor during film deposition, and thus the deconvolution of various factors affecting charge transport remains challenging. Systems with sequential solution-based deposition of dielectrics and organic semiconductors have not been well-studied because most of the insulating polymers, except for a few crosslinked ones, are highly soluble in organic solvents, and are easily destroyed by a solution of the organic semiconductor. Also, the scarcity of *n*-type polymer semiconductors[17] hinders detailed

investigation of electron transporting in *n*-channel OFETs. Although top-gate approach has been proposed and can be used to avoid such limitations, the possibilities of interfacial intermixing and morphological changes during solution-processing remain.[22,109,212]

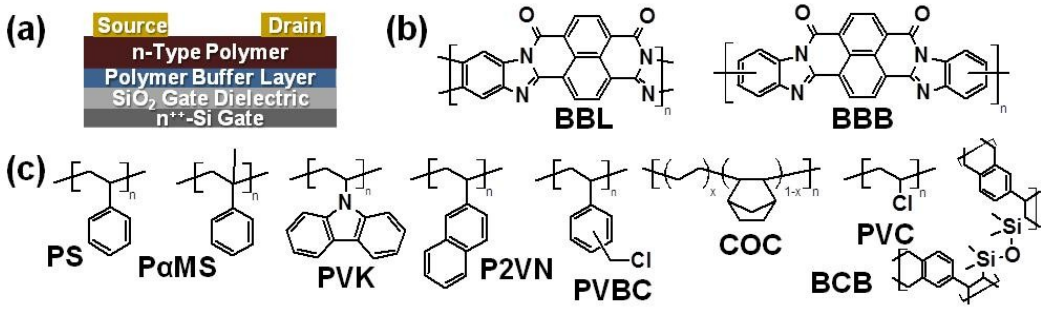

Figure 4-1. (a) Schematic cross-section of n-channel OFET with a dielectric polymer buffer layer. (b) Molecular structure of the n-type polymer semiconductors, BBL and BBB. (c) Molecular structures of the dielectric polymers studied. Reprinted with permission from Ref.[69] Copyright 2011, American Institute of Physics.

Here, the effect of low-*k* polymer dielectric buffer layer of the gate insulator on the charge transport in n-channel polymer thin film transistors was investigated (Figure 4-1). It is found that the field-effect mobility of electrons in ladder-type poly(benzobisimidazobenzophenanthroline) (BBL) FETs increased exponentially with decreasing dielectric constant of the polymer dielectric buffer layer. The *n*-type polymer semiconductor BBL offered a unique opportunity to perform the present experiments by virtue of its solution processability from methanesulfonic acid (MSA) at room temperature,[57,143,146,178] which is orthogonal to the organic solvents from which the polymer dielectric layers were spin-coated.

Various polymer dielectrics, including polystyrene (PS), poly(α-methylstyrene) (PαMS), poly(2-vinylnaphthalene) (P2VN), poly(vinylcarbazole) (PVK), poly(vinylchloride) (PVC), poly(vinylbenzyl chloride) (60/40 mixture of 3- and 4-isomers; PVBC), cyclic olefin copolymer (ethylene-norbornene copolymer; COC), and crosslinked divinyltetramethylsiloxane-bis(benzocyclobutene) (BCB), with the dielectric constants ranging from 2.35 to 3.40,[214,217-220] were used to fabricate the polymer dielectric buffer layers (Figure 4-1) and thus to study the effects of the dielectric constant of the buffer layer on charge

transport. Absence of alkyl side-chains on the BBL backbone is also advantageous to investigate the effects of an adjacent dielectric material without the convoluted effects of the side-chains. The effects of roughness, viscoelasticity, and surface energy of the polymer buffer layer can be minimized during film deposition. Therefore consideration of domain growth[210-211] is excluded from the investigation of dielectric/electron interactions in OFETs.

4.2. Experimental Methods

OFETs with top-contact and bottom-gate geometry were made on a heavily *n*-doped silicon wafer with a 200 nm-thick SiO_2. A polymer buffer layer was deposited by spin-coating the solution (COC, PS, PαMS, P2VN, and PVBC in toluene; BCB in mesitylene; PVK in chlorobenzene; and PVC in 1,2-dichlorobenzene) on top of a plasma-cleaned substrate and dried under vacuum at 60 °C. The *n*-channel semiconductors, BBL and BBB, was spin-coated from a solution in MSA onto the substrate in air, and immediately washed by dipping the film in water or methanol for 4–5 times over 2–3 hours to remove the acid solvent.[146] The BBL film (20–40 nm thick) was dried under vacuum at 60 °C for 8–12 hours and annealed at 150 °C for 10 minutes under argon environment unless otherwise specified. The color of BBL and BBB is red in a solution in MSA, purple in a washing medium as a swollen film, shiny gold-brown when dried. The transistors were finished by depositing 40 nm-thick gold source/drain electrodes through a shadow mask to define the transistor channel (width/length=1000 μm/100 μm). The OFETs were characterized at room temperature under nitrogen by using an HP4145B (or in ambient air by using a Keithley 4200) semiconductor parameter analyzer. The capacitance per unit area of the gate dielectric was measured from an MIM structure (n^{++}-Si/SiO_2/polymer/Au) by using an HP4284A LCR meter.

4.3. Results and Discussion

4.3.a. Effects of a Polymer Dielectric Buffer Layer on Transistor Performance

The polymer buffer layer formed on the SiO_2 substrate was very smooth (Figure 4-2). The film thickness and root-mean-square roughness of the polymer buffer layers were 3.7–75.2 nm and 0.2–0.7 nm, respectively, measured by atomic force microscopy. The experimentally measured capacitance per unit area of the gate dielectric was in the range of 12.1–16.8 nF/cm^2. Calculation of the capacitance density was also done from the dielectric constant and thickness of SiO_2 and the polymer buffer layer. The measured and calculated capacitances were in good agreement within 5%. The static contact angle of water on the polymer buffer layers was in the range of 82–96 °, which is much higher than that on plasma-cleaned SiO_2 without any buffer layer (~0 °).

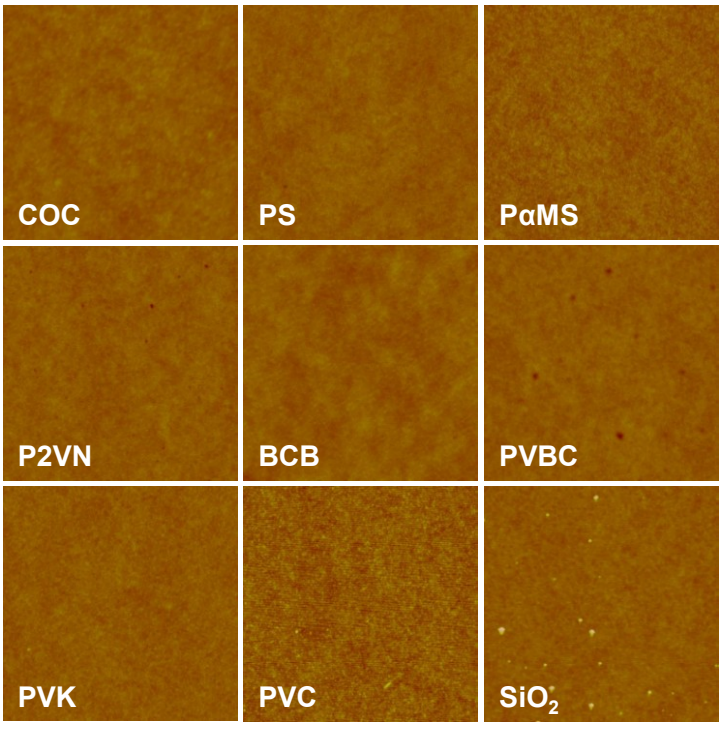

Figure 4-2. Atomic force microscopy topographic images of a polymer buffer layer on a SiO_2 substrate, as well as the image of SiO_2. Image size: 2 μm by 2 μm; Vertical scale: 20 nm.

Output and transfer characteristics of the BBL transistors with a PS buffer layer showed excellent current modulation and saturation, as shown in Figure 4-3. The on/off current ratios were in the range of 10^3–10^4. Forward and backward voltage sweeps are overlaid to emphasize the negligible hysteresis of the devices. Other polymer buffer layers also showed similar current (*I*)–voltage (*V*) characteristics with negligible hysteresis. In order to quantify the performance of OFETs with various polymer dielectric buffer layers, the field-effect electron mobility was calculated from the saturation region of *I*–*V* characteristics at V_{ds}=80 V. The electron mobility as high as 0.028 cm^2/Vs was recorded from the devices with a PS buffer layer. The electron mobility of 6–30 devices was 0.018 cm^2/Vs, 0.020 cm^2/Vs, and 0.016 cm^2/Vs for PS, COC, and BCB buffer layers, respectively. These mobilities are 44–56 times enhanced compared to the electron mobility of control devices with a bare SiO_2 as the dielectric layer (3.6×10^{-4} cm^2/Vs). OFETs with PαMS and P2VN have the electron mobility of 0.017 cm^2/Vs and 0.013 cm^2/Vs, respectively. Unlike the low-*k* (*k*<2.7) polymer dielectrics, devices with PVK, PVBC, or PVC buffer layer had a rather low average mobility on the order of 10^{-4}–10^{-3} cm^2/Vs. Electrical and other physical parameters of devices with various polymer dielectric buffer layers are summarized in Table 4-1.

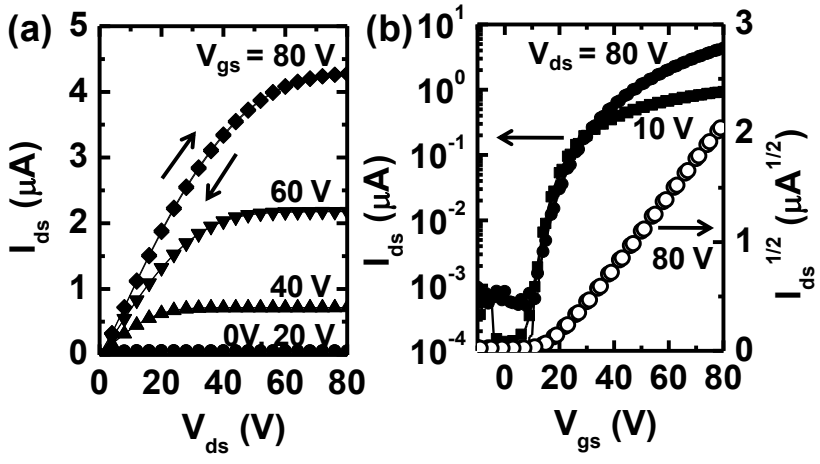

Figure 4-3. (a) Output and (b) transfer characteristics of n-channel BBL transistors with a PS buffer layer. Reprinted with permission from Ref.[69] Copyright 2011, American Institute of Physics.

Table 4-1. Summary of buffer layer thickness, roughness, contact angle, and electrical parameters.

Buffer Polymer	k [a]	Solvent	t (nm) [b]	R_q (nm) [c]	θ_{H2O} (°) [d]	C_i (nF/cm^2) [e]	μ_e (cm^2/Vs) [f]	I_{on}/I_{off} [g]	V_t (V) [h]	n [i]
COC	2.35	toluene	22.8	0.3	95.3	14.0	0.020 ±0.002	10^4	14.2 ±1.6	6
PS	2.55	toluene	43.0	0.3	90.3	13.1	0.018 ±0.004	10^4	17.5 ±9.1	30
PαMS	2.6	toluene	26.1	0.5	92.3	14.9	0.017 ±0.002	10^4	21.6 ±5.3	12
P2VN	2.6	toluene	30.8	0.3	89.3	14.4–14.8	0.013 ±0.002	10^3–10^4	11.2 ±5.2	12
BCB	2.65	mesitylene	17.5	0.6	86.3	15.0–16.3	0.016 ±0.006	10^4	11.8 ±4.1	18
PVBC	2.9	toluene	31.7	0.3	84.3	15.1–15.8	0.0058 ±0.001	10^3	24.6 ±18.0	12
PVK	3.0	chlorobenzene	11.7–14.4	0.4	90.7	16.0–16.4	0.0050 ±0.002	10^3–10^4	12.3 ±1.1	16
PVC	3.4	dichlorobenzene	14.9	0.7	82.7	15.9	5.2×10^{-4} $\pm1\times10^{-5}$	10^2–10^3	15.4 ±2.1	6
–	(SiO_2) 3.9	–	–	0.5	~0	17.0	3.6×10^{-4} $\pm2\times10^{-4}$	10^1–10^2	9.9 ±6.8	16

[a] k, dielectric constant obtained from literature (COC,[219] PS,[217] PαMS,[217] P2VN,[214] BCB,[220] PVBC,[218] PVK,[217] PVC,[217] SiO_2[107]); [b] t, thickness of buffer layer; [c] R_q, root-mean-square roughness; [d] θ_{H2O}, water contact angle; [e] C_i, capacitance per unit area; [f] μ_e, average field-effect electron mobility (± one standard deviation); [g] I_{on}/I_{off}, on-to-off current ratio; [h] V_t, average threshold voltage (± one standard deviation); [i] n, number of OFETs tested.

Figure 4-4(a) shows the field-effect electron mobility (μ) as a function of the dielectric constant (k) of the polymeric buffer layer in semi-log scale. The electron mobility is described by $\mu=A\exp(-B\,k)$: i.e. the mobility increased exponentially with decreasing dielectric constant. Such a dependence of the mobility on the dielectric constant of the polymeric buffer layer can be explained by the energetic expense caused by the interaction between charge-carriers in the organic semiconductor and dipoles at the adjacent dielectric layer.[109] A similar relationship, *i.e.* increase in μ with decreasing k, has been previously reported from amorphous *p*-type polymer semiconductors[109] and a rubrene single crystal,[221] but it is contradictory to the report on a polymer semiconductor with long alkyl side-chains where the carrier mobility was independent of k.[22,212] Since the former *p*-type organic semiconductors lack side-chains, similar to *n*-type BBL, the contradictory result of the latter is likely from the screening effect of alkyl chains (see below).

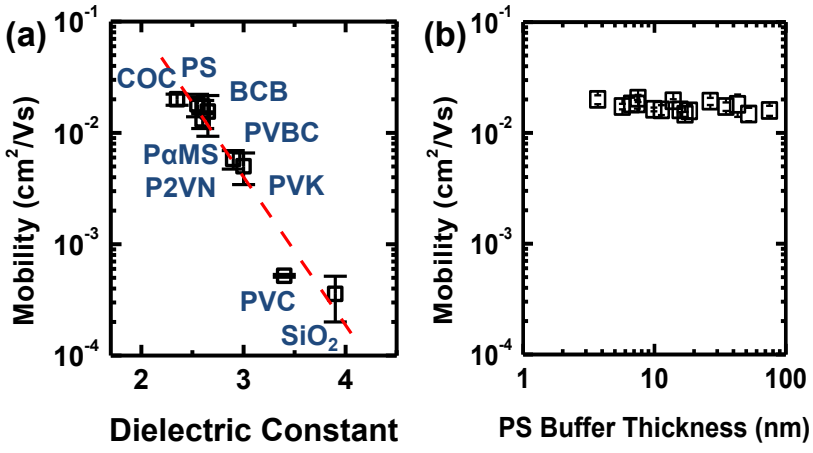

Figure 4-4. (a) Field-effect electron mobility as a function of dielectric constant of the polymer dielectric buffer layer. Dashed line is a fitting equation: $\mu = A \exp(-B\ k)$. (b) Electron mobility as a function of thickness of the PS buffer layer. Reprinted with permission from Ref.[69] Copyright 2011, American Institute of Physics.

The exponential dependence of charge-carrier mobility has been seen in charge transport models of organic semiconductors, such as the Arrhenius-type thermally activated transport model ($\mu=\mu_{A0}\exp(-E_A/k_BT)$).[109,207] Significant interaction between charge-carriers and dipoles can be considered to increase activation energy, E_A. The observed effect of the dielectric constant of the buffer layer on electron mobility is described by $\mu=A\ \exp(-B\ k)$. The pre-exponential factor A and the constant B define how highly the mobility depends on the dielectric constant at room temperature. Linear fit (Figure 4-4a) of the semi-log plot of the mobility (μ) vs dielectric constant (k) resulted in A=39.9 cm^2/Vs and B=3.07 at room temperature. This result suggests that the room-temperature field-effect mobility may be as high as 1.85 cm^2/Vs in a device with vacuum (or air) as the dielectric layer (k=1).

The dependence of the mobility on the thickness of the buffer layer was also studied by varying the PS buffer thickness from 3.7 nm to 75.2 nm, in order to estimate a minimum thickness of a buffer layer that affects charge transport in organic semiconductors. The electron mobility was essentially identical throughout the range of buffer layer thickness (Figure 4-4b), suggesting that the influence of a dielectric layer on charge transport in organic semiconductor is localized within a short range from the

heterointerface of the semiconductor/insulator system. Analytical modeling on amorphous *p*-type polymer semiconductor has showed that the range of static dipolar disorder can be even less than 1 nm.[222] This explains why some polymer semiconductors with long alkyl chains show dielectric-constant independence of the carrier mobility.[22,212] Our result shows that the low-*k* buffer layer could be as thin as a few nanometers in a high-*k*/low-*k* multilayer gate systems for high-performance, low-voltage operation.[223] The buffer layers have similarly low surface roughness (0.2–0.7 nm), precluding us from finding any correlation between the mobility and roughness (Table 4-1).

Effects of annealing temperature (T_a) and deprotonation medium on electron mobility and threshold voltage were investigated on BBL FETs with a PS buffer layer (Figure 4-5). When water is used to remove the acid solvent, MSA, the mobility increases with increasing T_a and saturates to 0.014–0.018 cm^2/Vs when $T_a \geq 150$ °C. The threshold voltage also reduces significantly from 56 V without annealing to 18–27 V after annealing. However, when methanol is used for removal of MSA, the electron mobility and threshold voltage are 0.019–0.023 cm^2/Vs and 11–15 V, respectively, and are independent of the T_a. This observation of different annealing temperature dependence also suggests that presence of water in the thin films of polymer semiconductors have deteriorating effects on the charge transport properties, as discussed in Chapter 2. Although the devices are dried under dynamic vacuum for overnight, the trace amount of H_2O molecules can present in the thin film, resulting in large number of traps against electron transport. High temperature ($T_a \geq 150$ °C) is required to remove the water molecules from the BBL thin films.

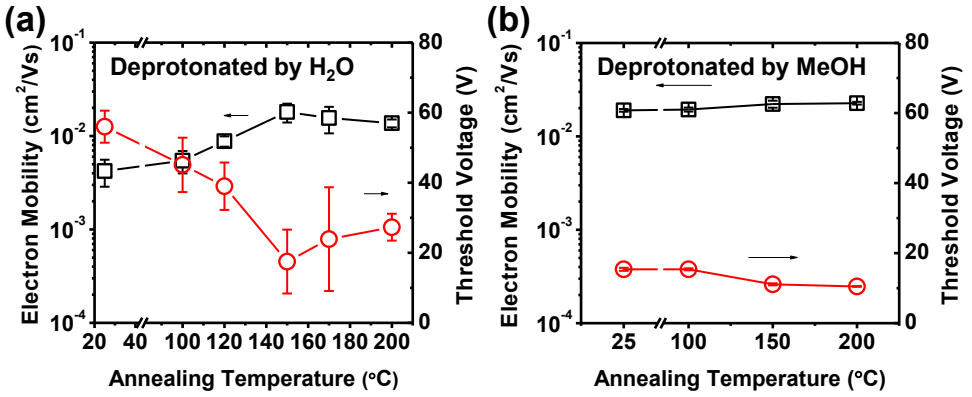

Figure 4-5. Annealing temperature dependence of electron mobility and threshold voltage of BBL FETs with a PS buffer layer after removal of the acid solvent, MSA, by (a) water, and (b) methanol.

The effectiveness of the polymer buffer layer is also observed in a non-ladder-type analogous polymer semiconductor, BBB (Figure 4-6). BBB is also free from alkyl side-chains, and processable in acid solvent. Reported electron mobility on a silicon dioxide gate without any buffer layer was on the order of 10^{-6} cm^2/Vs in air.[57] Insertion of a PS buffer layer resulted in the electron mobility of 1.5×10^{-3} cm^2/Vs and the threshold voltage of 15.2 V under nitrogen environment. In ambient air, the electron mobility decreases to 2.4×10^{-4} cm^2/Vs, which is still 2 orders of magnitude higher than the device without buffer layer.

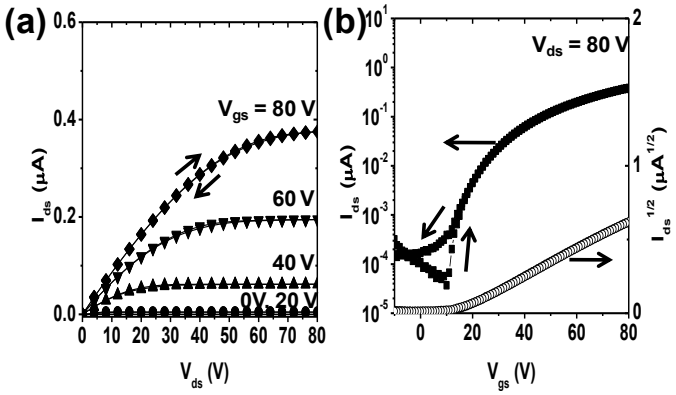

Figure 4-6. (a) Output and (b) transfer curves of a BBB transistor with a PS buffer layer.

4.3.b. Enhancement of Electrical Stability and Durability

The polymer dielectric buffer layer not only enhances field-effect mobility but also stabilizes the electrical characteristics. Voltage shifts under forward and backward scans and under multicycling test should be minimized in order to achieve a reliable operation of integrated circuits. The BBL transistors without any buffer layer suffered from large hysteresis and voltage shift, as shown in Figure 4-7a,b. On the other hand, the hysteresis was reduced to 0–4 V by inserting a polymer buffer layer. The largest hysteresis of 4 V was observed from devices with PVK as a buffer layer. The multicyclic voltage shift was also reduced to 0 V as exemplified by the transistors with a PS buffer layer that show identical characteristics of 1000 cycles of gate voltage sweep between 0 V and 80 V at V_{ds}=80 V, recorded for 7 hours (Figure 4-7d,e). The stable cyclic operation is considered to be from the absence of charge trapping sites, such as carbonyl and hydroxyl groups, in the buffer layer (Figure 4-7c,f).[67,107] Impurities such as mobile ions in SiO_2 are also effectively screened by the polymer buffer layer.

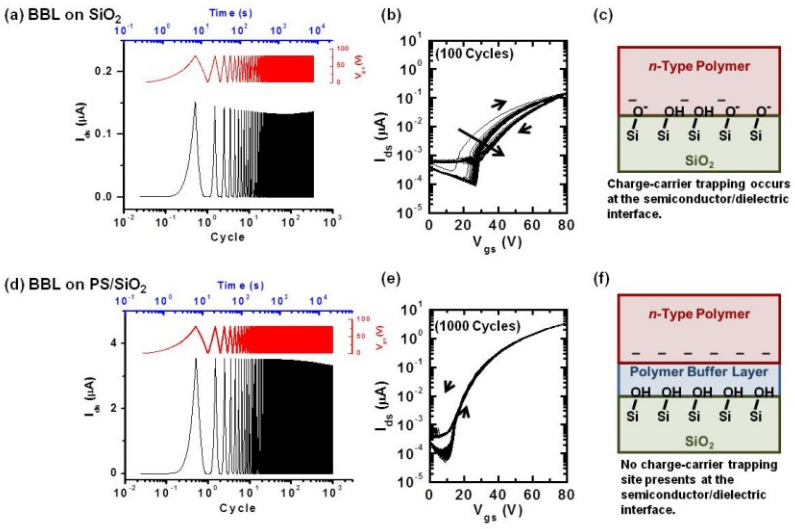

Figure 4-7. Multicyclic stability of *n*-channel OFETs. (a-c) BBL OFET without any buffer layer: drain current as a function of cycle (a), overlays of transfer curves (b), and origin of large hysteresis (c). (d-f) BBL OFET with a PS buffer layer: drain current as a function of cycle (d), overlays of transfer curves (e), and origin of small hysteresis (f). V_{ds} was fixed at 80 V for both cases. Reprinted in part with permission from Ref.[69] Copyright 2011, American Institute of Physics.

Combination of high-durability of BBL in air[57,143,146,178] and high-stability of OFETs with polymer buffer layer results in the remarkable air-stability of the n-channel devices in terms of field-effect mobility (Figure 4-8). Although initial changes of the mobility was observed as the BBL and BBB OFETs were taken out from inert conditions to ambient air, the mobility and the threshold voltage are stabilized to ~2×10^{-3} cm^2/Vs for BBL and ~2×10^{-4} cm^2/Vs for BBB, when stored and periodically tested in air over 195 days. I have also exposed the BBL devices under extreme conditions. The BBL transistors were tested as fabricated under nitrogen, brought into a chamber, exposed to air-plasma for 5 minutes, and tested under nitrogen again. Although the mobility decreased by a factor of 3 from 0.020 (±0.0006) cm2/Vs to 0.0066 (±0.0002) cm^2/Vs (Figure 4-9), the devices were functioning without hysteresis even after the plasma treatment, proving the ruggedness of the devices.

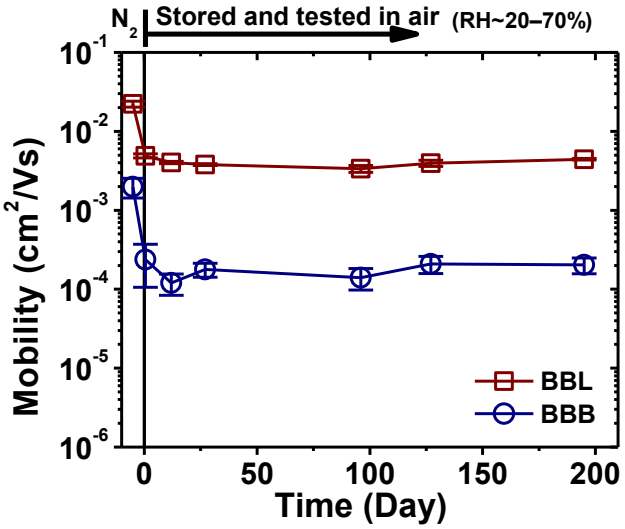

Figure 4-8. Electron mobility and threshold voltage of BBL and BBB transistors with a 43.0 nm-thick PS buffer layer as a function of time in air. Devices were stored and periodically characterized in air for durability test.

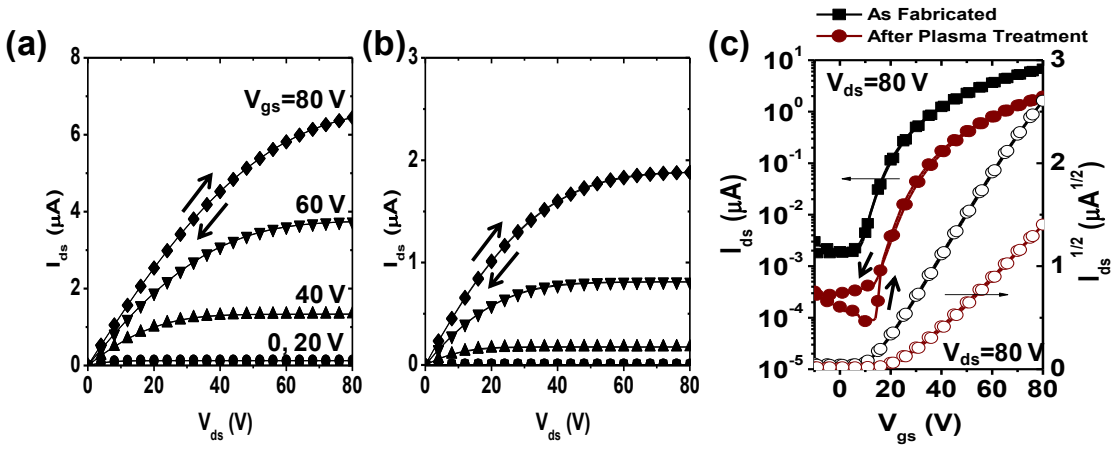

Figure 4-9. Electrical characterization of a BBL transistor with PS buffer layer under nitrogen atmosphere (a) before and (b) after exposure to air-plasma for 5 min. (c) Overlays of transfer curves before and after the plasma treatment.

4.4. Conclusions

It is observed that the performance of solution-processed *n*-channel polymer OFETs can be significantly enhanced by applying a low-*k* polymer dielectric buffer layer. The field-effect electron mobility has been increased by two orders of magnitude by applying the polymer buffer layer. A systematic study shows that the electron mobility exponentially decays as the dielectric constant of the buffer layer increases. In the limit of air or vacuum as the dielectric buffer layer (k=1), the room temperature electron mobility of the BBL OFETs is projected to be as high as 1.85 cm^2/Vs. The low-*k* polymer dielectric buffer layer also enhances the stability under multicycling test. The voltage shift during 1000 cycles of gate voltage scans of the BBL OFETs with a PS buffer layer is ~0 V. This finding emphasizes the importance of energetic nature of dielectric/semiconductor interfaces for understanding electron transport in organic semiconductors.

Chapter 5. Charge Transport in Poly(3-butylthiophene) Nanocomposites

This chapter investigates charge transport properties and performance of polymer semiconductor nanocomposite-based FETs. The results in this chapter are reprinted in part with permission from Macromolecules, submitted for publication (Copyright 2012 American Chemical Society).[224]

5.1. Introduction

The charge transport properties of polymer semiconductors and their one-dimensional nanostructures[225-227] are central to the device applications of the semiconductors in electronics and optoelectronics.[17,35,228-232] In the device applications, especially in organic field-effect transistors (OFETs), the conjugated polymer semiconductor can be in the form of single-component thin films with amorphous or polycrystalline morphology or as part of multicomponent thin films with morphology of higher complexity.[34,41,53-55,57,59,65,146,177,233-241] Because of the prospect for greater control of their spatial organization, crystallinity, and overall morphology, one-dimensional nanowires (NWs) and nanobelts of polymer semiconductors are expected to offer approaches to improve the performance of current thin film devices and the design of new nano- and micro-electronic/optoelectronic devices.[225-227,242-247] For example, it has been shown that efficient bulk heterojunction solar cells can be constructed in which conjugated polymer NWs function as the donor component and primary absorber and fullerene as the acceptor, providing a means to rationally control the nanoscale morphology of the devices.[242-245] Conjugated polymer NWs also offer new opportunities for studies and understanding of underlying nanostructure–charge transport relationships in polymer semiconductors.[225-227,246-256]

In this chapter, studies of charge transport in solution-phase self-assembled poly(3-butylthiophene) (P3BT) NWs and their nanocomposites with an insulating polystyrene (PS) matrix are presented (Figure 5-1). It is shown that the self-assembled P3BT NWs, which are nearly monodisperse in width (11.8 nm)

and have high aspect ratios (~10^2–10^3), exhibit field-effect hole mobility as high as 0.2 cm^2/Vs. Thus, high-performance OFETs were realized from the P3BT-NW/PS nanocomposites with as low as 2 wt% of the polymer semiconductor. The rather low percolation threshold (~0.5 wt% P3BT NWs) explains the high field-effect carrier mobility and high dc conductivity observed in the polystyrene dispersions of P3BT NWs. I have also analyzed the experimentally observed trends of charge carrier mobility as a function of composition by using an equivalent circuit model, and revealed the importance of intra-nanowire charge transport.

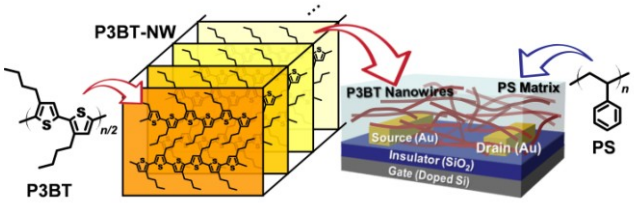

Figure 5-1. Chemical structures of P3BT and PS, molecular packing in P3BT NWs, and schematic of P3BT-NW/PS nanocomposite OFETs. Reproduced in part with permission from Ref.[224] Copyright 2012 American Chemical Society.

5.2. Experimental Methods

P3BT with 97% head-to-tail regioregularity and a molecular weight of 54 kg/mol (Aldrich; specification provided by the supplier) and amorphous PS with a molecular weight of 125–250 kg/mol (Polysciences, Inc.) were used as received. A P3BT solution (2–6 mg/mL) in 1,2-dichlorobenzene (ODCB, Aldrich) was stirred and heated at 100 °C for 24 hours to fully dissolve the polymer, and then cooled down to room temperature for at least 3 days. The clear red-orange solution of fully dissolved P3BT in ODCB at 100 °C became opaque with a dark purplish-brown color and high viscosity after it was cooled to room temperature, indicating the formation of P3BT NWs dispersed in ODCB.[236,242,257-258] The resulting dispersion of P3BT NWs was mixed with a PS solution in ODCB (6–10 mg/mL) to make binary P3BT-NW/PS nanocomposites of 2–80 wt% P3BT NWs.

The OFETs were fabricated using the bottom-contact and bottom-gate geometry (Figure 5-1) on a heavily doped silicon substrate with thermally grown silicon dioxide (100 nm) and interdigitated gold electrodes (3300 μm or 6000 μm channel width, 100 μm or 30 μm channel length) with a thin adhesive layer of Cr or TiW. The SiO_2/Si substrates were treated with octyltriethoxysilane (OTS8) vapor before deposition of the P3BT NWs or P3BT-NW/PS nanocomposite thin films. The polymer nanocomposite films were spin-coated (3000 rpm) onto the substrates and dried overnight under vacuum at room temperature. Average film thickness was in the range of 10–24 nm depending on the composition. The P3BT-NW/PS films were prepared without thermal annealing, which may otherwise induce a morphological change of the films.

Absorption spectra were taken on a Perkin–Elmer Lambda 900 UV/Vis/NIR spectrometer. Samples for solution absorption were prepared by diluting a P3BT solution or a P3BT-NW dispersion to ~5×10^{-6} M in ODCB. Nanocomposite absorption spectra were taken from spin-coated films of P3BT-NW/PS on glass substrates. The morphology of the P3BT-NW/PS nanocomposite thin films was imaged by using transmission electron microscopy (TEM; Philips EM420 at 100 kV) and tapping mode atomic force microscopy (AFM; Veeco Dimension 3100) with force modulation etched silicon probe (FESP) tips. The P3BT-NW/PS nanocomposites were also spin-coated directly onto carbon-coated copper grids without dilution for TEM imaging. A solution was gently dispensed onto the copper grids which were carefully fixed on a glass substrate by adhesive tape, and the substrate was immediately spun at 3000 rpm. Care was taken to prepare and detach the TEM samples as the carbon-coated grids were very delicate. Electrical performance of the transistors was measured using a Keithley 4200 semiconductor analyzer under ambient air and dark conditions. Applied voltage bias was selected ($\leq$ 70 V) in order to prevent dielectric breakdown of the silicon dioxide layer (100 nm thick). Values of electrical parameters were averaged from at least 10 different devices made and characterized in 3 different batches.

5.3. Results and Discussion

5.3.a. Photophysical properties and morphology of P3BT nanocomposites

Figure 5-2 shows the normalized absorption spectra of P3BT solutions, dispersions, and thin films of P3BT-NW/PS nanocomposites. A solution of as-dissolved P3BT in ODCB shows a featureless absorption band with the maximum peak at 462 nm. As P3BT-NW grew in the solution, the maximum peak red-shifted and additional shoulders evolved at 555 nm and 610 nm. Fully grown P3BT NWs had the maximum peak at 515 nm, similar to the reported values in recent literature.[257-258] The small shoulder at 462 nm of the P3BT-NW dispersion likely comes from P3BT molecules isolated by thermal motion in a dilute solution at room temperature. Films of P3BT-NW/PS nanocomposite had similar spectra as a dispersion of pre-assembled P3BT NWs in ODCB solvent, except for the lack of the shoulder at 462 nm and the increase in UV absorption due to PS. Such a similarity of absorption spectra of a P3BT-NW dispersion in ODCB and P3BT-NW/PS nanocomposites proves that the nanowires are indeed assembled in solution and that the assembled structures are quite stable even when diluted in a strong solvent such as ODCB. The absorption spectra of the P3BT-NW/PS nanocomposites showed little or no change as the composition was varied.

The morphology of the P3BT NWs and P3BT-NW/PS nanocomposites was investigated by using TEM (Figure 5-3) and AFM (Figure 5-4). Highly interconnected P3BT NWs are clearly seen in both TEM and AFM images. Unlike thin films prepared from a homogeneous solution of polymer blends,[65,235-237,239,259] there is no evidence of spinodal decomposition or other large-scale phase separation in the thin films (10–24 nm thick) of nanocomposites of pre-assembled P3BT NWs and high molecular-weight PS. The P3BT NWs are on average 11.8 (±1.2) nm wide and several micrometers (4–10 μm) long, resulting in quite large aspect ratios of ~330–850. It should be noted that the length of NWs is shorter than the OFET channel length (30–100 μm), suggesting that multiple NWs are required to make electrical connection

between source and drain electrodes. The height determined from AFM images was in the 3–7 nm range. The variation in height may be a result of folded conformations of the polymer backbone similar to reports for regioregular poly(3-hexylthiophene) (P3HT) thin films.[260] In general, these dimensions of P3BT NWs are similar to observed sizes in previous reports for P3BT NWs[242,251,257] and for P3HT NWs.[248-250] It should be noted that these morphological features of P3BT NWs are the same for the pure polymer as for the P3BT-NW/PS nanocomposites. The concentration (number density) of the P3BT NWs in the P3BT-NW/PS nanocomposites clearly varies with composition, increasing with the amount (wt%) of P3BT. Considering that the P3BT NWs and PS are well-dispersed in ODCB, and the thickness of P3BT-NW/PS nanocomposite films was very thin (10–22 nm), it is likely that the P3BT NWs are uniformly distributed in the PS matrix.

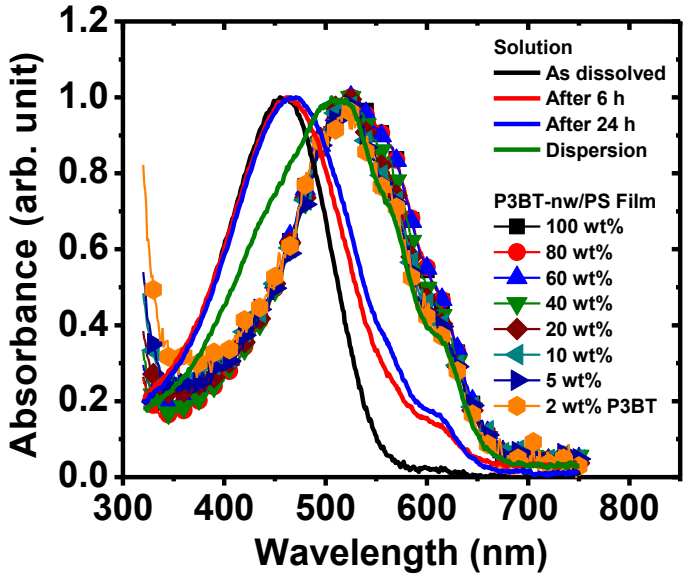

Figure 5-2. Absorption spectra of a P3BT solution in ODCB and films of P3BT-NW/PS nanocomposite. Samples for solution absorption spectra were taken from a P3BT solution after indicated time and then diluted to ~5×10^{-6} M in ODCB. Nanocomposite absorption spectra were taken from spin-coated films of P3BT-NW/PS (2–100 wt% P3BT-NW) on a glass substrate. Reproduced in part with permission from Ref.[224] Copyright 2012 American Chemical Society.

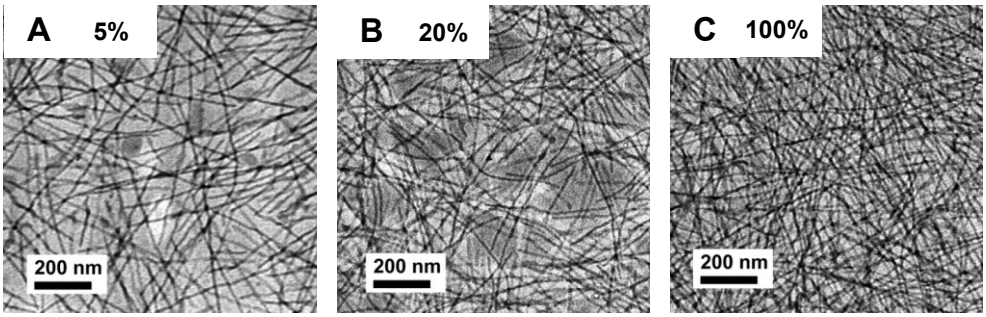

Figure 5-3. Transmission electron microscopy images of P3BT-NW/PS nanocomposites: (A) 5 wt%, (B) 20 wt%, and (C) 100 wt% P3BT NWs. Reproduced in part with permission from Ref.[224] Copyright 2012 American Chemical Society.

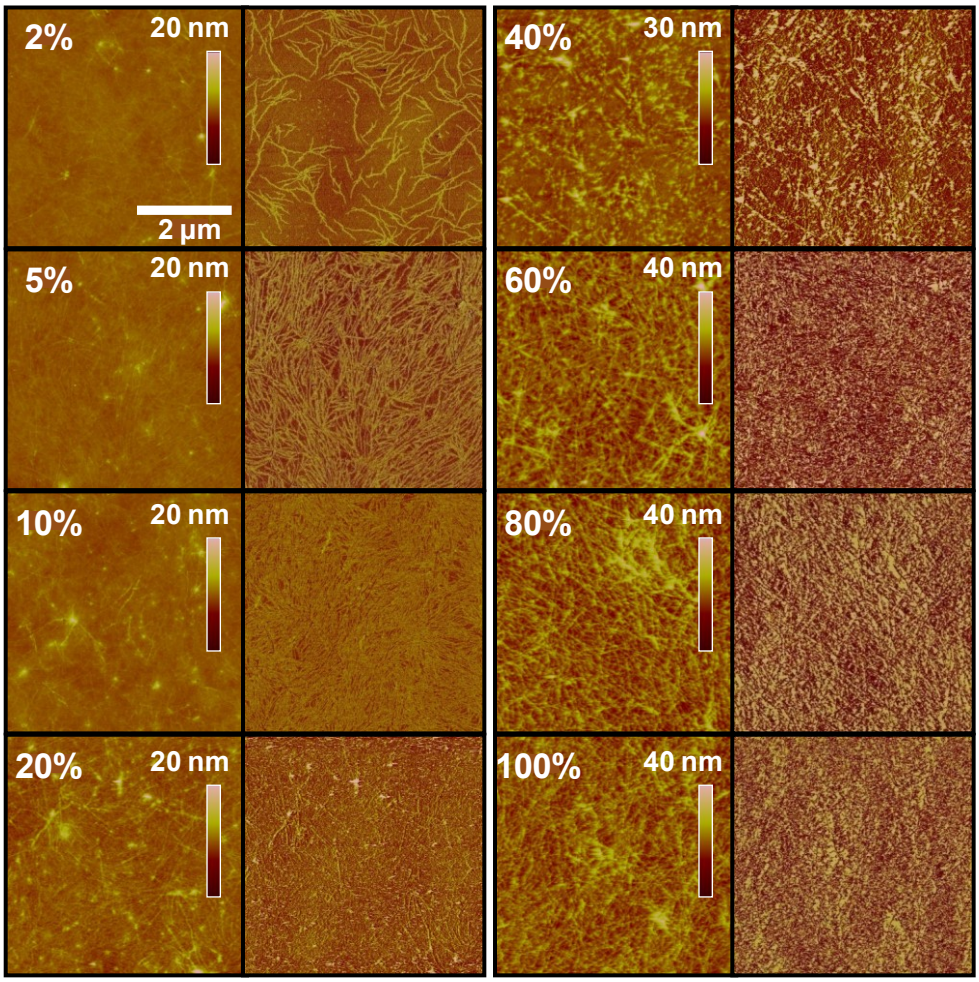

Figure 5-4. Surface morphology of P3BT NWs and P3BT-NW/PS nanocomposite films. At each composition both topographical (left) image and phase image (right) are shown. Reproduced in part with permission from Ref.[224] Copyright 2012 American Chemical Society.

5.3.b. Electrical characteristics of nanocomposite FETs

The OFET output and transfer characteristics, exemplified by those of the P3BT NWs and 20 wt% and 5 wt% P3BT-NW/PS nanocomposites, are shown in Figure 5-5. All the OFETs showed good current modulation and saturation. Interestingly, the nanocomposite OFETs with 20 wt% P3BT NWs showed a larger on-state current at V_{gs} = –50 V and a smaller off-state current at V_{gs} = 20 V than the P3BT NW (100 wt%) transistors, resulting in a larger I_{on}/I_{off}. The on/off current ratio increased from 2×10^2 to 10^4 as the concentration of P3BT NWs decreased from 100 wt% to 2 wt% (Table 5-1; Figure 5-6A). The improvement in on/off current ratio as the number of nanowires across source-drain electrodes decreases is a consequence of the insulating nature of the host polymer and can be a useful means of improving the performance of polymer-based OFETs. The electrical parameters, such as threshold voltage (V_t) and effective field-effect mobility (μ_{eff}), were calculated from I_{ds}–V_{gs} relationship in the saturation region,[35] $I_{ds}=\mu_{eff}WC_i(V_{gs}-V_t)^2/(2L)$, where C_i is the gate dielectric capacitance per unit area (33 nF/cm^2), W is the channel width, and L is the channel length. The threshold voltage (V_t) of these p-channel OFETs was positive (Figure 5-5d,e,f), decreasing from ~30 V in P3BT NWs (100 wt%) to 10 V in the most dilute P3BT-NW/PS nanocomposite (2 wt%) (Table 5-1; Figure 5-6A). The positive V_t value likely arises from unintentional doping of P3BT in air and has similarly been observed in previous reports of P3BT-based transistors.[58,117] The observed decrease of V_t with decreasing concentration of P3BT NWs in the P3BT-NW/PS nanocomposites is consistent with this interpretation; the PS host shields better the P3BT NWs from oxygen doping at low concentrations. The measured high dc conductivity in the P3BT NWs and nanocomposites, to be discussed below, further confirm unintentional doping as the source of the positive threshold voltage in the transistors.

The average effective field-effect mobility (μ_{eff}) of holes in films of pure P3BT NWs was 0.009 cm^2/Vs. This value is comparable to the reported mobility of holes in P3BT thin films, which is in the range of 0.0015–0.010 cm^2/Vs, depending on the device geometry and fabrication process.[58,116-117,251-252]

In contrast, the average effective mobility of holes in the P3BT-NW/PS nanocomposites is in the range of 0.012–0.016 cm^2/Vs throughout the composition (Figure 5-6B). This trend is quite different from the trend seen in blends of poly(3-hexylthiophene) (P3HT) and PS, which showed a monotonic decrease of field-effect mobility with decreasing weight fraction of P3HT.[235,237,239]

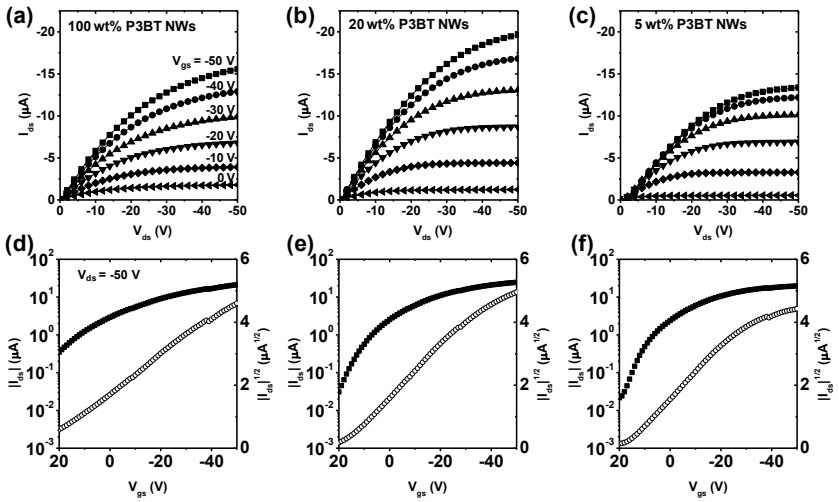

Figure 5-5. Output (a-c) and transfer (d-f) characteristics of P3BT-NW thin film transistor (a,d) and P3BT-NW/PS nanocomposite (b,e: 20 wt% P3BT NWs; c,f: 5 wt% P3BT NWs) thin film transistors. Reproduced in part with permission from Ref.[224] Copyright 2012 American Chemical Society.

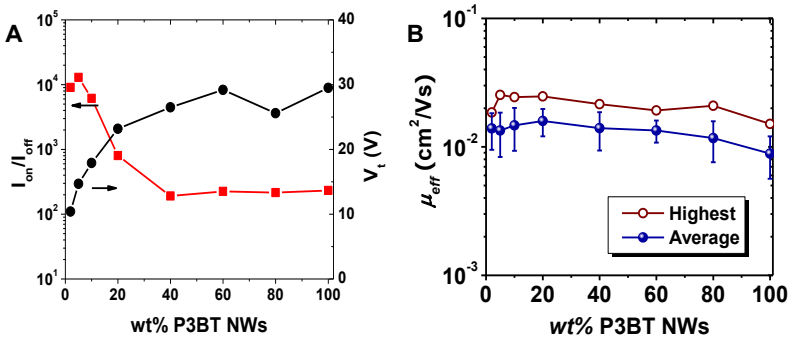

Figure 5-6. (A) On/off current ratio and threshold voltage of nanocomposite transistors as a function of composition. (B) Average and highest field-effect mobility of holes in P3BT-NW/PS nanocomposite thin films as a function of composition. The error bar is one standard deviation based on 10 devices. Reproduced in part with permission from Ref.[224] Copyright 2012 American Chemical Society.

The intra-nanowire carrier mobility (μ_{NW}) in polymer semiconductor NWs can be expected to be substantially higher than the effective field-effect mobility (μ_{eff}) in these P3BT-NW/PS nanocomposites. This expectation is from the high degree of ordered π-stacking, crystallinity, absence or minimum number of crystalline domain boundaries, and optimum direction for charge transport along the NW.[225-226] Because of the many difficulties in reproducible measurement of μ_{NW} in single-NW polymer transistor experiments,[249-250,253] I used the measured carrier transport in P3BT-NW/PS nanocomposites in conjunction with the fractional area of OFET channel occupied by NWs to estimate μ_{NW},[247,250] based on the assumptions that P3BT NWs are uniformly distributed in the PS matrix and that the charge transport is mainly contributed by the nanowires at the gate interface. The average surface coverage of the P3BT NWs in the nanocomposites, determined from AFM phase images, as a function of concentration (wt% P3BT-NW) is shown in Figure 5-7a. The resulting μ_{NW} as a function of concentration is shown in Figure 5-7b. The intra-nanowire carrier mobility increases substantially as the amount of P3BT NWs in the nanocomposite decreases. This enhancement in carrier mobility with decreasing number density of P3BT NWs in the nanocomposite can be understood as a consequence of substantial reduction in barrier to transport at nanowire/nanowire (grain) boundaries, allowing intra-nanowire charge transport to become dominant. At sufficiently dilute concentration of P3BT NWs in the nanocomposite, the domain-boundary-free field-effect mobility in P3BT NWs can be as high as 0.2 cm^2/Vs. This value is comparable or slightly higher than the highest field-effect mobility reported for P3HT thin films (~0.1 cm^2/Vs).[77] It is also higher than carrier mobilities (0.02–0.06 cm^2/Vs) reported for single-NW OFETs made from P3HT[249-250,253] and P3BT.[252]

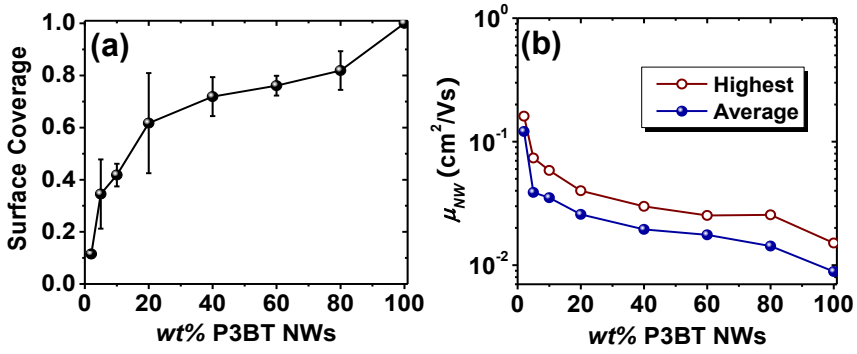

Figure 5-7. (a) Fractional surface coverage of P3BT NWs in spin-coated P3BT-NW/PS nanocomposite films as evaluated from AFM images. (b) Average and highest field-effect mobility of holes in P3BT nanowires. Reproduced in part with permission from Ref.[224] Copyright 2012 American Chemical Society.

The observed high effective carrier mobility (μ_{eff}) in the nanocomposites can be further understood in terms of an equivalent circuit model of charge transport in polycrystalline thin films in the channel of an OFET.[261] Considering a NW of average transport length l_{NW} and mobility μ_{NW} in series with a nanowire/nanowire contact (or grain boundary) of average length l_{inter} and mobility μ_{inter}, the effective mobility of the channel (μ_{eff}) can be estimated from the Eq. 5-1:[261]

$$\mu_{\text{eff}} = \frac{\mu_{\text{NW}}\mu_{\text{inter}}(l_{\text{NW}} + l_{\text{inter}})}{\mu_{\text{NW}}l_{\text{inter}} + \mu_{\text{inter}}l_{\text{NW}}} \quad \text{(Eq. 5-1)}$$

If the concentration of P3BT NWs in the nanocomposite film is high, inter-nanowire hopping frequency is high and a single-event length of intra-nanowire transport is comparable to that of inter-nanowire transport (i.e. $l_{\text{NW}} \sim l_{\text{inter}}$). Given that intra-nanowire transport along the crystalline nanowire is much faster than inter-nanowire transport across a barrier ($\mu_{\text{NW}} >> \mu_{\text{inter}}$),[225-226] Eq. 5-1 is simplified to

$$\mu_{\text{eff}} = \mu_{\text{inter}}\left(1 + \frac{l_{\text{NW}}}{l_{\text{inter}}}\right) \quad \text{(Eq. 5-2)}$$

Eq. 5-2 shows that the effective mobility in the nanocomposites will be dominated by the effects of grain boundaries or nanowire/nanowire contacts.

On the other hand, if the concentration of P3BT NWs in the nanocomposite film is low, the number of inter-nanowire contacts is small and the distance of intra-nanowire transport is much longer than that of inter-nanowire transport ($l_{NW} >> l_{inter}$). In this case, with the fast intra-nanowire transport ($\mu_{NW} >> \mu_{inter}$),[225-226] a product of μ_{inter} and l_{NW} in the denominator of Eq. 5-1 becomes non-negligible compared to the other product ($\mu_{NW} l_{inter}$). Then, Eq. 5-1 becomes

$$\mu_{eff} = \frac{\mu_{NW}}{1 + \frac{\mu_{NW} l_{inter}}{\mu_{inter} l_{NW}}}, \qquad \text{(Eq. 5-3)}$$

and the effective mobility will be dominated by the intra-nanowire mobility. Given that l_{NW} is larger than hundreds of nanometers and l_{inter} is on the order of a nanometer or less, $l_{NW} \geq 100 l_{inter}$, and in the case of nanocomposites with a dilute concentration (*e.g.*, 2 wt% P3BT NWs) where μ_{eff} = 0.014 cm^2/Vs (Figure 5-6), Eq. 5-3 can be used to estimate μ_{inter} as 1.6×10^{-4} cm^2/Vs, which is much smaller than the measured μ_{NW} (0.12 cm^2/Vs). As observed here, a lower μ_{inter} compared to μ_{NW} has also been recently suggested by others in an independent study.[252] Furthermore, from Eq. 5-3 one sees that effective mobility in the nanocomposites is increased by decreasing the number density of P3BT NWs in the nanocomposites. It should be noted that I do not rule out the dipolar effect of the insulating polymer matrix.[235-236,262] However, the contributions of intra-nanowire and inter-nanowire are likely dominant in the observed charge transport properties as a function of the thin film composition in our system.

The dc conductivity (σ_{dc}) of the P3BT NW films and P3BT-NW/PS nanocomposite films as a function of composition of the nanocomposites was measured by using the device structure of the OFETs with interdigitated electrodes. The conductivity was calculated from I_{ds}–V_{ds} relationship at 0 V gate voltage (V_{gs}) and low source–drain voltage (V_{ds}), $\sigma_{dc} = (I_{ds}L)/(tWV_{ds})$, where W is the channel width, L is the channel length, and t is the film thickness. The average dc conductivity, shown in Figure 5-8, is quite high (≥ 0.39 mS/cm) throughout the composition range studied. I attempted to fit the conductivity–volume

fraction data to percolation theory:[263] $\sigma_{dc} = A(f-f_c)^{\alpha}$, where A is a pre-exponential factor, f is volume fraction of the conducting material which can be calculated based on the weight fraction and densities of P3BT (1.24 g/cm^3) and PS (1.05 g/cm^3),[264-265] f_c is the percolation threshold, and the exponent α is 1.5–2.0 and 1–1.3 for three- and two-dimensional systems, respectively.[263] It should be noted that this equation is valid near the percolation threshold ($f \sim f_c$).[263] As expected from the very large aspect ratios of the NWs dispersed in the PS thin films, a low percolation threshold (f_c = 0.0043; 0.5 wt%) is obtained. It should be noted that the value of the exponent α (0.87) in the nanocomposite thin films (10–24 nm) is close to the theoretical value for 2-D system (~1),[263] and smaller than 1.97–3.2 found in the much thicker films (≥ 20 μm) of polyaniline or poly(3-octylthiophene) blended with an insulating polymer,[266-267] likely due to the differences in dimensionality, morphology, and conductivity range of the films.

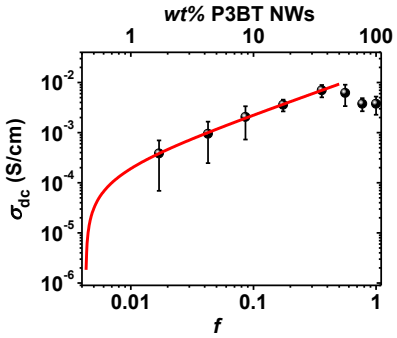

Figure 5-8. Compositional dependence of the dc conductivity of the nanocomposite films. The solid line represents the least-square-fit of the data to percolation theory near the percolation threshold ($f \sim f_c$). Reproduced in part with permission from Ref.[224] Copyright 2012 American Chemical Society.

The charge carrier concentration in the nanocomposite films and P3BT-NW films was estimated from the measured dc conductivity and effective carrier mobility: $n = \sigma_{dc}/(\mu_{eff}\, e)$, where e is the elementary charge. The charge carrier concentration varied from 1.5×10^{17} cm^{-3} in films of the 2 wt% P3BT-NW/PS nanocomposite to 2.6×10^{18} cm^{-3} in films of P3BT NWs. These values of the carrier density are comparable to reported n values of 5×10^{17} cm^{-3} for P3HT.[268] Thus, rather high carrier densities can be injected into these P3BT-NW/PS nanocomposites, facilitating high-mobility charge transport.

Table 5-1. Electrical parameters of nanocomposite devices with different amount of P3BT NWs. Reproduced in part with permission from Ref.[224] Copyright 2012 American Chemical Society.

P3BT-NW fraction (wt% [vol%]) [a]	t (nm)	σ_{dc} (mS/cm)	μ_{eff} [μ_{eff}^{max}] (cm^2/Vs) [b]	I_{on}/I_{off}	V_t (V) [b]	n ($10^{18}cm^{-3}$)	fraction of surface coverage	μ_{NW} [μ_{NW}^{max}] (cm^2/Vs) [b]
2 [1.7]	18	0.39	0.014 [0.019]	9078	10.4	0.15	0.115	0.12 [0.16]
5 [4.3]	22	0.95	0.013 [0.025]	12970	14.7	0.39	0.345	0.039 [0.074]
10 [8.6]	19	2.05	0.015 [0.024]	6137	17.9	0.82	0.418	0.035 [0.058]
20 [17.5]	17	3.60	0.016 [0.025]	803	23.2	1.5	0.617	0.026 [0.040]
40 [36.1]	10	7.00	0.014 [0.022]	191	26.5	3.3	0.719	0.019 [0.030]
60 [56.0]	12	6.22	0.013 [0.019]	225	29.2	2.9	0.761	0.018 [0.025]
80 [77.2]	14	3.77	0.012 [0.021]	216	25.6	2.0	0.819	0.014 [0.026]
100 [100]	14	3.76	0.0089 [0.015]	232	29.5	2.6	1.000	0.0089 [0.015]

[a] Volume fraction is calculated based on the weight fraction and densities of P3BT (1.24 g/cm^3) and PS (1.05 g/cm^3). [b] Average of at least 10 devices except the maximum mobilities (μ_{eff}^{max}, μ_{NW}^{max}). Symbols: t is film thickness, σ_{dc} is dc conductivity, μ_{eff} is effective mobility of nanocomposite, I_{on}/I_{off} is on/off current ratio, V_t is threshold voltage, n is charge-carrier density, and μ_{NW} is intra-nanowire mobility.

5.4. Conclusions

It is shown that the interconnected, self-organized nanowires of a polymer semiconductor can form efficient charge transport pathways with a low percolation threshold in an insulating polymer matrix, facilitating high dc conductivity and high field-effect charge carrier mobility. The results of studies of charge transport in polymer semiconductor/insulating polymer nanocomposites demonstrate that a few weight percent of a polymer semiconductor such as poly(3-butylthiophene) can provide sufficient carrier mobility and on/off current ratio for fabricating high-performance OFETs. I have showed that nanocomposite OFETs can be a useful tool to investigate the charge transport properties of polymer semiconductor nanowires. The carrier mobility in the domain-boundary-free P3BT nanowires can be as high as 0.2 cm^2/Vs. These results also suggest that high-mobility, crystalline nanowires of polymer semiconductors can find applications in bulk heterojunction polymer solar cells.[242-245]

Chapter 6. Conclusions and Outlook

6.1. Conclusions

Throughout this work, I have studied factors that govern the charge transport properties of polymer semiconductors and performance of polymer-based OFETs. Specifically, among many challenges that organic and polymer electronics community is facing, increase in hole and electron mobilities, control of type of majority charge-carriers, enhancement of electrical stability and durability in air, were addressed.

I have investigated the field-effect charge transport properties of various series of polymer semiconductors, including PhBTs, PTTs, PBTs, PNDIs, and BBL, to gain insights into structure–morphology–charge transport property relationships. Effects of donor–acceptor combinations and side chain substitution were studied in detail. The present studies reveal that small changes in the side chains of a conjugated polymer can dramatically affect the solid-state morphology and thus charge transport properties. Charge-carrier mobility is found to increase by enhanced crystallinity with edge-on orientation. Effects of the relative strengths of electron-donating and electron-withdrawing units in the donor–acceptor copolymer architecture were also studied. The bandgap of the donor–acceptor copolymer semiconductors can be effectively tuned by the molecular design. Well-matched electronic energy levels as well as suitable solid-state morphology result in high field-effect mobility in the range of ~10^{-4}–0.1 cm^2/Vs from the polymer semiconductors. Investigations of long-term air-stability of BBL, P3HT, and PBTOT, reveal that thermodynamic and kinetic aspects should be addressed in designing new polymer semiconductors. The advantages of the complementary approach to electronic circuits, such as excellent switching characteristics with a high voltage gain, large noise-tolerance, and very low power consumption, were also discussed by comparing the performance of an organic complementary inverter with that of a *p*-channel OFET-based inverter.

Studies of ambipolar charge transport properties of donor–acceptor copolymer semiconductors, multilayer polymer semiconductor heterojunctions, and polymer bulk heterojunctions were conducted. Charge-carrier mobilities of 0.001–0.04 cm^2/Vs for electrons and 0.001–0.2 cm^2/Vs for holes were achieved in various systems. Single-component ambipolar polymer semiconductors can be easily deposited as a thin film by simple solution-based processing. The charge transport properties of ambipolar polymer semiconductors were related to their molecular structures, energy levels of frontier molecular orbitals, processing conditions, and morphology, similar to unipolar polymer semiconductors, which were also used to fabricate ambipolar OFETs. Depending on the solubility of constituent polymer semiconductors, bilayer structures or polymer blends were used. Stable operation of ambipolar OFETs in air was also demonstrated based on air-stable unipolar *n*-type and *p*-type polymer semiconductors. High-performance complementary circuits were fabricated without spatial patterning of individual *p*- and *n*-channel transistors. Simple logic circuits of NOT, NAND and NOR gates were fabricated from the ambipolar OFETs and shown to exhibit excellent switching characteristics.

I also investigated the effect of a low-*k* polymer dielectric buffer layer on field-effect charge transport properties of *n*-channel polymer FETs. Solvent orthogonality between BBL and various insulating polymer dielectric enabled exploration of the effects of the buffer layer on electrical characteristics of OFETs. A systematic study with eight different insulating polymers as a buffer layer shows that the electron mobility exponentially increased from 5.2×10^{-4} cm^2/Vs to 0.02 cm^2/Vs as the dielectric constant of the buffer layer decreases from 3.4 to 2.35. The polymer dielectric buffer layer was also found to improve the electrical stability of the devices under multicycling test. These findings highlight the importance of engineering of dielectric/semiconductor interfaces for understanding electron transport in polymer semiconductors and for developing high-performance OFETs.

Finally, a study of polymer semiconductor nanocomposites composed of self-assembled poly(3-butylthiophene) nanowires dispersed in polystyrene matrix showed an unusual composition dependence

of the charge transport properties. Well-dispersed polymer semiconductor nanowires with a high aspect ratio in an insulating polymer matrix resulted in high field-effect mobility (0.02 cm^2/Vs) and dc conductivity (7×10^{-3} S/cm) with low a percolation threshold (0.5 wt%). Based on our analysis, the carrier mobility in the domain-boundary-free poly(3-butylthiophene) nanowires can be as high as 0.2 cm^2/Vs. This study has showed that control of intra-nanowire and inter-nanowire charge transport plays a critical role on the performance of FETs based on the self-organized nanowires.

Overall, this work has added some new knowledge to the great progress made in the area of organic electronics by the community. Knowledge obtained from this study provides an additional guideline to the design of better polymer semiconductors and next-generation organic electronic devices. Further investigation should be continued to expand our understanding and to advance the technology, as there are still many challenges to tackle in the area of organic electronics.

6.2. Outlook

One of the major challenges facing organic electronics community is to precisely control solid-state morphology at the macroscale and at the molecular levels, which could provide a powerful tool to enhance device performance. It has been shown that single-crystals of small-molecule organic semiconductors exhibit superior field-effect charge-carrier mobility compared to disordered/polycrystalline organic semiconductors.[94-96,269-270] Toward this end, growth of polymer semiconductor single-crystals will offer extremely valuable information on the structure–morphology–charge transport property relationships. FET based on polymer semiconductor single-crystals may well outperform the other OFETs, as very high mobility is expected along the well-aligned polymer chains.[271] Detailed investigation of charge-carrier dynamics through studies of charge transport properties, anisotropy, and temperature-dependence in the morphology-controlled polymer semiconductors will

provide better understanding of the polymer semiconductors that guides us to design new polymer semiconductors.

One example of studies to be done in the near future would be an application of nanocomposites using self-organized polymer semiconductor nanowires dispersed in another polymer semiconductor matrix for high-mobility ambipolar OFETs. As shown in the Chapter 5, polymer semiconductor nanowire-based nanocomposite FETs are superior than the network of pure nanowires in terms of the transistor performance and charge-carrier mobility. Besides, the nanocomposite has very low percolation threshold, yielding a wide window of the composition for ambipolar charge transport. A new approach of incorporating nanowires of a *p*-type polymer semiconductor, such as poly(3-butylthiophene) or poly(3-hexylthiophene), into a matrix of an *n*-type polymer semiconductor, such as PNDIs, can be expected to be a means of enhancing ambipolar charge-carrier mobilities in polymer-based FETs. Furthermore, as seen in previous studies on solar cells,[242-243,272] the nanowire approach may result in high-efficiency all-polymer-based solar cells.

Development of new electrode and dielectric materials, and engineering of the electrode/semiconductor and dielectric/semiconductor interfaces are also subjects for further studies in organic electronics. Solution-based deposition and patterning of electrodes and dielectric layers are required to achieve truly low-cost electronic devices. Metal nanoparticles, molecularly-doped conducting polymers, carbon nanotubes, and graphenes are the most promising alternatives for electrodes. For the gate dielectric layer, hybrid low-*k*/high-*k* multilayered gate insulators would significantly reduce the operation voltage and power consumption while maintaining low charge-carrier scattering at the interface of semiconductor and dielectric.

Excellent static characteristics of polymer FET-based circuits have been repeatedly demonstrated as shown in the previous chapters. However, in a real world of signal processing, most electronic devices deal with dynamic signals of any frequency range.[14,172,273] Although a high-frequency response may not

be observed due to the low mobility of polymer semiconductors at current stage, dynamic characterization of the polymer circuits is not only important to know their limits, but also essential to improve the performance through device engineering and to find suitable low- to medium-frequency applications, for example circuits for driving displays, implanted biomedical devices, and contact-less identification tags. In order to tackle many challenges, such as stability, reliability, low-power operation, and biocompatibility, in those applications, it is required to pursue interdisciplinary collaborations between chemical engineers, biomedical engineers, materials scientists, and electrical engineers.

Bibliography

(1) Jenekhe, S. A., The Special Issue on Organic Electronics. In *Chem. Mater.*, 2004; Vol. 16, pp. 4381-4846.

(2) Forrest, S. R.; Thompson, M. E., Organic Electronics and Optoelectronics. In *Chem. Rev.*, 2007; Vol. 107, pp. 923-1386.

(3) Bredas, J.-L.; Marder, S. R.; Reichmanis, E., The Special Issue on Π-Functional Materials. In *Chem. Mater.*, 2011; Vol. 23, pp. 309-922.

(4) Kittel, C., *Introduction to Solid State Physics*. 7th ed.; John Wiley & Sons: New York, 1996.

(5) Sze, S. M.; Ng, K. K., *Physics of Semiconductor Devices*. 3rd ed.; John Wiley & Sons: New York, 2007.

(6) Heeger, A. J.; Kivelson, S.; Schrieffer, J. R.; Su, W. P., Solitons in Conducting Polymers. *Rev. Mod. Phys.* **1988,** *60* (3), 781-850.

(7) Heeger, A. J., Semiconducting and Metallic Polymers: The Fourth Generation of Polymeric Materials (Nobel Lecture). *Angew. Chem., Int. Ed.* **2001,** *40* (14), 2591-2611.

(8) Malliaras, G.; Friend, R., An Organic Electronics Primer. *Phys. Today* **2005,** *58* (5), 53-58.

(9) Roncali, J., Synthetic Principles for Bandgap Control in Linear Pi-Conjugated Systems. *Chem. Rev.* **1997,** *97* (1), 173-205.

(10) Chiang, C. K.; Fincher, C. R.; Park, Y. W.; Heeger, A. J.; Shirakawa, H.; Louis, E. J.; Gau, S. C.; MacDiarmid, A. G., Electrical Conductivity in Doped Polyacetylene. *Phys. Rev. Lett.* **1977,** *39* (17), 1098-1101.

(11) McCullough, R. D.; Williams, S. P., Toward Tuning Electrical and Optical Properties in Conjugated Polymers Using Side-Chains: Highly Conductive Head-to-Tail, Heteroatom Functionalized Polythiophenes. *J. Am. Chem. Soc.* **1993,** *115* (24), 11608-11609.

(12) Groenendaal, L.; Jonas, F.; Freitag, D.; Pielartzik, H.; Reynolds, J. R., Poly(3,4-Ethylenedioxythiophene) and Its Derivatives: Past, Present, and Future. *Adv. Mater.* **2000,** *12* (7), 481-494.

(13) Choi, M.-C.; Kim, Y.; Ha, C.-S., Polymers for Flexible Displays: From Material Selection to Device Applications. *Prog. Polym. Sci.* **2008,** *33* (6), 581-630.

(14) Klauk, H.; Halik, M.; Zschieschang, U.; Eder, F.; Rohde, D.; Schmid, G.; Dehm, C., Flexible Organic Complementary Circuits. *IEEE Trans. Electron. Dev.* **2005,** *52* (4), 618-622.

(15) Sekitani, T.; Zschieschang, U.; Klauk, H.; Someya, T., Flexible Organic Transistors and Circuits with Extreme Bending Stability. *Nat. Mater.* **2010,** *9* (12), 1015-1022.

(16) Hwang, D. K.; Fuentes-Hernandez, C.; Kim, J. B.; Potscavage, W. J.; Kippelen, B., Flexible and Stable Solution-Processed Organic Field-Effect Transistors. *Org. Electron.* **2011,** *12* (7), 1108-1113.

(17) Bao, Z., Materials and Fabrication Needs for Low-Cost Organic Transistor Circuits. *Adv. Mater.* **2000,** *12* (3), 227-230.

(18) Bao, Z.; Feng, Y.; Dodabalapur, A.; Raju, V. R.; Lovinger, A. J., High-Performance Plastic Transistors Fabricated by Printing Techniques. *Chem. Mater.* **1997,** *9* (6), 1299-1301.

(19) Sirringhaus, H.; Kawase, T.; Friend, R. H.; Shimoda, T.; Inbasekaran, M.; Wu, W.; Woo, E. P., High-Resolution Inkjet Printing of All-Polymer Transistor Circuits. *Science* **2000,** *290* (5499), 2123-2126.

(20) Kim, C.; Wang, Z.; Choi, H.-J.; Ha, Y.-G.; Facchetti, A.; Marks, T. J., Printable Cross-Linked Polymer Blend Dielectrics. Design Strategies, Synthesis, Microstructures, and Electrical Properties, with Organic Field-Effect Transistors as Testbeds. *J. Am. Chem. Soc.* **2008,** *130* (21), 6867-6878.

(21) Noh, Y.-Y.; Zhao, N.; Caironi, M.; Sirringhaus, H., Downscaling of Self-Aligned, All-Printed Polymer Thin-Film Transistors. *Nat. Nano.* **2007,** *2* (12), 784-789.

(22) Yan, H.; Chen, Z.; Zheng, Y.; Newman, C.; Quinn, J. R.; Dotz, F.; Kastler, M.; Facchetti, A., A High-Mobility Electron-Transporting Polymer for Printed Transistors. *Nature* **2009,** *457* (7230), 679-686.

(23) Singh, M.; Haverinen, H. M.; Dhagat, P.; Jabbour, G. E., Inkjet Printing-Process and Its Applications. *Adv. Mater.* **2010,** *22* (6), 673-685.

(24) Sun, J.; Zhang, B.; Katz, H. E., Materials for Printable, Transparent, and Low-Voltage Transistors. *Adv. Funct. Mater.* **2010,** *21* (1), 29-45.

(25) Cho, J. H.; Lee, J.; Xia, Y.; Kim, B.; He, Y.; Renn, M. J.; Lodge, T. P.; Daniel Frisbie, C., Printable Ion-Gel Gate Dielectrics for Low-Voltage Polymer Thin-Film Transistors on Plastic. *Nat. Mater.* **2008,** *7* (11), 900-906.

(26) Forrest, S. R., The Path to Ubiquitous and Low-Cost Organic Electronic Appliances on Plastic. *Nature* **2004,** *428* (6986), 911-918.

(27) Bredas, J. L.; Street, G. B.; Themans, B.; Andre, J. M., Organic Polymers Based on Aromatic Rings (Polyparaphenylene, Polypyrrole, Polythiophene): Evolution of the Electronic Properties as a Function of the Torsion Angle between Adjacent Rings. *J. Chem. Phys.* **1985,** *83* (3), 1323-1329.

(28) Bredas, J. L., Relationship between Band Gap and Bond Length Alternation in Organic Conjugated Polymers. *J. Chem. Phys.* **1985,** *82* (8), 3808-3811.

(29) Jenekhe, S. A., A Class of Narrow-Band-Gap Semiconducting Polymers. *Nature* **1986,** *322* (6077), 345-347.

(30) Agrawal, A. K.; Jenekhe, S. A., New Conjugated Polyanthrazolines Containing Thiophene Moieties in the Main Chain. *Macromolecules* **1991,** *24* (25), 6806-6808.

(31) Havinga, E. E.; ten Hoeve, W.; Wynberg, H., Alternate Donor-Acceptor Small-Band-Gap Semiconducting Polymers; Polysquaraines and Polycroconaines. *Synth. Met.* **1993,** *55* (1), 299-306.

(32) Jenekhe, S. A.; Lu, L.; Alam, M. M., New Conjugated Polymers with Donor−Acceptor Architectures: Synthesis and Photophysics of Carbazole−Quinoline and Phenothiazine−Quinoline Copolymers and Oligomers Exhibiting Large Intramolecular Charge Transfer. *Macromolecules* **2001,** *34* (21), 7315-7324.

(33) Zhu, Y.; Champion, R. D.; Jenekhe, S. A., Conjugated Donor-Acceptor Copolymer Semiconductors with Large Intramolecular Charge Transfer: Synthesis, Optical Properties, Electrochemistry, and Field Effect Carrier Mobility of Thienopyrazine-Based Copolymers. *Macromolecules* **2006,** *39* (25), 8712-8719.

(34) Guo, X.; Kim, F. S.; Jenekhe, S. A.; Watson, M. D., Phthalimide-Based Polymers for High Performance Organic Thin-Film Transistors. *J. Am. Chem. Soc.* **2009,** *131* (21), 7206-7207.

(35) Zaumseil, J.; Sirringhaus, H., Electron and Ambipolar Transport in Organic Field-Effect Transistors. *Chem. Rev.* **2007,** *107* (4), 1296-1323.

(36) Meijer, E. J.; de Leeuw, D. M.; Setayesh, S.; van Veenendaal, E.; Huisman, B. H.; Blom, P. W. M.; Hummelen, J. C.; Scherf, U.; Klapwijk, T. M., Solution-Processed Ambipolar Organic Field-Effect Transistors and Inverters. *Nat. Mater.* **2003,** *2* (10), 678-682.

(37) Anthopoulos, T. D.; Setayesh, S.; Smits, E.; Colle, M.; Cantatore, E.; de Boer, B.; Blom, P. W. M.; de Leeuw, D. M., Air-Stable Complementary-Like Circuits Based on Organic Ambipolar Transistors. *Adv. Mater.* **2006,** *18* (14), 1900-1904.

(38) Zaumseil, J.; Donley, C. L.; Kim, J.-S.; Friend, R. H.; Sirringhaus, H., Efficient Top-Gate, Ambipolar, Light-Emitting Field-Effect Transistors Based on a Green-Light-Emitting Polyfluorene. *Adv. Mater.* **2006,** *18* (20), 2708-2712.

(39) Bürgi, L.; Turbiez, M.; Pfeiffer, R.; Bienewald, F.; Kirner, H.-J.; Winnewisser, C., High-Mobility Ambipolar near-Infrared Light-Emitting Polymer Field-Effect Transistors. *Adv. Mater.* **2008,** *20* (11), 2217-2224.

(40) Steckler, T. T.; Zhang, X.; Hwang, J.; Honeyager, R.; Ohira, S.; Zhang, X.-H.; Grant, A.; Ellinger, S.; Odom, S. A.; Sweat, D.; Tanner, D. B.; Rinzler, A. G.; Barlow, S.; Bredas, J.-L.; Kippelen, B.; Marder, S. R.; Reynolds, J. R., A Spray-Processable, Low Bandgap, and Ambipolar Donor-Acceptor Conjugated Polymer. *J. Am. Chem. Soc.* **2009,** *131* (8), 2824-2826.

(41) Kim, F. S.; Guo, X.; Watson, M. D.; Jenekhe, S. A., High-Mobility Ambipolar Transistors and High-Gain Inverters from a Donor-Acceptor Copolymer Semiconductor. *Adv. Mater.* **2010,** *22* (4), 478-482.

(42) Sonar, P.; Singh, S. P.; Li, Y.; Soh, M. S.; Dodabalapur, A., A Low-Bandgap Diketopyrrolopyrrole-Benzothiadiazole-Based Copolymer for High-Mobility Ambipolar Organic Thin-Film Transistors. *Adv. Mater.* **2010,** *22*, 5409-5413.

(43) Chua, L.-L.; Zaumseil, J.; Chang, J.-F.; Ou, E. C. W.; Ho, P. K. H.; Sirringhaus, H.; Friend, R. H., General Observation of N-Type Field-Effect Behaviour in Organic Semiconductors. *Nature* **2005,** *434* (7030), 194-199.

(44) Kang, S.-M.; Leblebici, Y., *Cmos Digital Integrated Circuits: Analysis and Design*. McGraw-Hill: New York, 1996.

(45) Horowitz, G., Organic Field-Effect Transistors. *Adv. Mater.* **1998,** *10* (5), 365-377.

(46) Dimitrakopoulos, C. D.; Malenfant, P. R. L., Organic Thin Film Transistors for Large Area Electronics. *Adv. Mater.* **2002,** *14* (2), 99-117.

(47) Street, R. A.; Salleo, A., Contact Effects in Polymer Transistors. *Appl. Phys. Lett.* **2002,** *81* (15), 2887-2889.

(48) Katz, H. E.; Johnson, J.; Lovinger, A. J.; Li, W. J., Naphthalenetetracarboxylic Diimide-Based N-Channel Transistor Semiconductors: Structural Variation and Thiol-Enhanced Gold Contacts. *J. Am. Chem. Soc.* **2000,** *122* (32), 7787-7792.

(49) Park, S. K.; Jackson, T. N.; Anthony, J. E.; Mourey, D. A., High Mobility Solution Processed 6,13-Bis(Triisopropyl-Silylethynyl) Pentacene Organic Thin Film Transistors. *Appl. Phys. Lett.* **2007,** *91* (6), 063514-3.

(50) Yan, H.; Zheng, Y.; Blache, R.; Newman, C.; Lu, S.; Woerle, J.; Facchetti, A., Solution Processed Top-Gate N-Channel Transistors and Complementary Circuits on Plastics Operating in Ambient Conditions. *Adv. Mater.* **2008,** *20* (18), 3393-3398.

(51) Noh, Y.-Y.; Sirringhaus, H., Ultra-Thin Polymer Gate Dielectrics for Top-Gate Polymer Field-Effect Transistors. *Org. Electron.* **2009,** *10* (1), 174-180.

(52) Coropceanu, V.; Cornil, J.; da Silva Filho, D. A.; Olivier, Y.; Silbey, R.; Brédas, J.-L., Charge Transport in Organic Semiconductors. *Chem. Rev.* **2007,** *107* (4), 926-952.

(53) Sirringhaus, H.; Brown, P. J.; Friend, R. H.; Nielsen, M. M.; Bechgaard, K.; Langeveld-Voss, B. M. W.; Spiering, A. J. H.; Janssen, R. A. J.; Meijer, E. W.; Herwig, P.; de Leeuw, D. M., Two-Dimensional Charge Transport in Self-Organized, High-Mobility Conjugated Polymers. *Nature* **1999,** *401* (6754), 685-688.

(54) Kline, R. J.; McGehee, M. D.; Kadnikova, E. N.; Liu, J. S.; Frechet, J. M. J.; Toney, M. F., Dependence of Regioregular Poly(3-Hexylthiophene) Film Morphology and Field-Effect Mobility on Molecular Weight. *Macromolecules* **2005,** *38* (8), 3312-3319.

(55) Zen, A.; Saphiannikova, M.; Neher, D.; Grenzer, J.; Grigorian, S.; Pietsch, U.; Asawapirom, U.; Janietz, S.; Scherf, U.; Lieberwirth, I.; Wegner, G., Effect of Molecular Weight on the Structure and Crystallinity of Poly(3-Hexylthiophene). *Macromolecules* **2006,** *39* (6), 2162-2171.

(56) Babel, A. Ph.D. Thesis. University of Washington, Seattle, 2006.

(57) Babel, A.; Jenekhe, S. A., High Electron Mobility in Ladder Polymer Field-Effect Transistors. *J. Am. Chem. Soc.* **2003,** *125* (45), 13656-13657.

(58) Park, Y. D.; Kim, D. H.; Jang, Y.; Cho, J. H.; Hwang, M.; Lee, H. S.; Lim, J. A.; Cho, K., Effect of Side Chain Length on Molecular Ordering and Field-Effect Mobility in Poly(3-Alkylthiophene) Transistors. *Org. Electron.* **2006,** *7* (6), 514-520.

(59) Yang, H. C.; Shin, T. J.; Yang, L.; Cho, K.; Ryu, C. Y.; Bao, Z., Effect of Mesoscale Crystalline Structure on the Field-Effect Mobility of Regioregular Poly(3-Hexyl Thiophene) in Thin-Film Transistors. *Adv. Funct. Mater.* **2005,** *15* (4), 671-676.

(60) Ho, P. K. H.; Chua, L. L.; Dipankar, M.; Gao, X. Y.; Qi, D. C.; Wee, A. T. S.; Chang, J. F.; Friend, R. H., Solvent Effects on Chain Orientation and Interchain Pi-Interaction in Conjugated Polymer Thin Films: Direct Measurements of the Air and Substrate Interfaces by near-Edge X-Ray Absorption Spectroscopy. *Adv. Mater.* **2007,** *19* (2), 215-221.

(61) Tiwari, S. P.; Zhang, X.-H.; William J. Potscavage, J.; Kippelen, B., Study of Electrical Performance and Stability of Solution-Processed N-Channel Organic Field-Effect Transistors. *J. Appl. Phys.* **2009,** *106* (5), 054504.

(62) Campbell, I. H.; Rubin, S.; Zawodzinski, T. A.; Kress, J. D.; Martin, R. L.; Smith, D. L.; Barashkov, N. N.; Ferraris, J. P., Controlling Schottky Energy Barriers in Organic Electronic Devices Using Self-Assembled Monolayers. *Phys. Rev. B* **1996,** *54* (20), 14321-14324.

(63) de Boer, B.; Hadipour, A.; Mandoc, M. M.; van Woudenbergh, T.; Blom, P. W. M., Tuning of Metal Work Functions with Self-Assembled Monolayers. *Adv. Mater.* **2005,** *17* (5), 621-625.

(64) Zhou, Y.; Fuentes-Hernandez, C.; Shim, J.; Meyer, J.; Giordano, A. J.; Li, H.; Winget, P.; Papadopoulos, T.; Cheun, H.; Kim, J.; Fenoll, M.; Dindar, A.; Haske, W.; Najafabadi, E.; Khan, T. M.; Sojoudi, H.; Barlow, S.; Graham, S.; Brédas, J.-L.; Marder, S. R.; Kahn, A.; Kippelen, B., A Universal Method to Produce Low–Work Function Electrodes for Organic Electronics. *Science* **2012,** *336* (6079), 327-332.

(65) Chua, L.-L.; Ho, P. K. H.; Sirringhaus, H.; Friend, R. H., Observation of Field-Effect Transistor Behavior at Self-Organized Interfaces. *Adv. Mater.* **2004,** *16* (18), 1609-1615.

(66) Lee, J.; Kaake, L. G.; Cho, J. H.; Zhu, X.-Y.; Lodge, T. P.; Frisbie, C. D., Ion Gel-Gated Polymer Thin-Film Transistors: Operating Mechanism and Characterization of Gate Dielectric Capacitance, Switching Speed, and Stability. *J. Phys. Chem. C* **2009,** *113* (20), 8972-8981.

(67) Yoon, M.-H.; Kim, C.; Facchetti, A.; Marks, T. J., Gate Dielectric Chemical Structure-Organic Field-Effect Transistor Performance Correlations for Electron, Hole, and Ambipolar Organic Semiconductors. *J. Am. Chem. Soc.* **2006,** *128* (39), 12851-12869.

(68) Veres, J.; Ogier, S.; Lloyd, G.; de Leeuw, D., Gate Insulators in Organic Field-Effect Transistors. *Chem. Mater.* **2004,** *16* (23), 4543-4555.

(69) Kim, F. S.; Hwang, D.-K.; Kippelen, B.; Jenekhe, S. A., Enhanced Carrier Mobility and Electrical Stability of N-Channel Polymer Thin Film Transistors by Use of Low-K Dielectric Buffer Layer. *Appl. Phys. Lett.* **2011,** *99* (17), 173303.

(70) Salleo, A.; Chabinyc, M. L.; Yang, M. S.; Street, R. A., Polymer Thin-Film Transistors with Chemically Modified Dielectric Interfaces. *Appl. Phys. Lett.* **2002,** *81* (23), 4383-4385.

(71) Kelley, T. W.; Muyres, D. V.; Baude, P. F.; Smith, T. P.; Jones, T. D., High Performance Organic Thin Film Transistors. *MRS Proceedings* **2003,** *771*, L6.5.

(72) Zhang, X.-H.; Tiwari, S. P.; Kippelen, B., Pentacene Organic Field-Effect Transistors with Polymeric Dielectric Interfaces: Performance and Stability. *Org. Electron.* **2009,** *10* (6), 1133-1140.

(73) Gundlach, D. J.; Royer, J. E.; Park, S. K.; Subramanian, S.; Jurchescu, O. D.; Hamadani, B. H.; Moad, A. J.; Kline, R. J.; Teague, L. C.; Kirillov, O.; Richter, C. A.; Kushmerick, J. G.; Richter, L. J.; Parkin, S. R.; Jackson, T. N.; Anthony, J. E., Contact-Induced Crystallinity for High-Performance Soluble Acene-Based Transistors and Circuits. *Nat. Mater.* **2008,** *7* (3), 216-221.

(74) Tsumura, A.; Koezuka, H.; Ando, T., Macromolecular Electronic Device: Field-Effect Transistor with a Polythiophene Thin Film. *Appl. Phys. Lett.* **1986,** *49* (18), 1210-1212.

(75) Burroughes, J. H.; Jones, C. A.; Friend, R. H., New Semiconductor Device Physics in Polymer Diodes and Transistors. *Nature* **1988,** *335* (6186), 137-141.

(76) Bao, Z.; Dodabalapur, A.; Lovinger, A. J., Soluble and Processable Regioregular Poly(3-Hexylthiophene) for Thin Film Field-Effect Transistor Applications with High Mobility. *Appl. Phys. Lett.* **1996,** *69* (26), 4108-4110.

(77) Sirringhaus, H.; Tessler, N.; Friend, R. H., Integrated Optoelectronic Devices Based on Conjugated Polymers. *Science* **1998,** *280* (5370), 1741-1744.

(78) McCulloch, I.; Heeney, M.; Bailey, C.; Genevicius, K.; Macdonald, I.; Shkunov, M.; Sparrowe, D.; Tierney, S.; Wagner, R.; Zhang, W. M.; Chabinyc, M. L.; Kline, R. J.; Mcgehee, M. D.; Toney, M. F., Liquid-Crystalline Semiconducting Polymers with High Charge-Carrier Mobility. *Nat. Mater.* **2006,** *5* (4), 328-333.

(79) Ong, B. S.; Wu, Y. L.; Liu, P.; Gardner, S., High-Performance Semiconducting Polythiophenes for Organic Thin-Film Transistors. *J. Am. Chem. Soc.* **2004,** *126* (11), 3378-3379.

(80) Zhang, W.; Smith, J.; Watkins, S. E.; Gysel, R.; McGehee, M.; Salleo, A.; Kirkpatrick, J.; Ashraf, S.; Anthopoulos, T.; Heeney, M.; McCulloch, I., Indacenodithiophene Semiconducting Polymers for High-Performance, Air-Stable Transistors. *J. Am. Chem. Soc.* **2010,** *132* (33), 11437-11439.

(81) Tsao, H. N.; Cho, D.; Andreasen, J. W.; Rouhanipour, A.; Breiby, D. W.; Pisula, W.; Müllen, K., The Influence of Morphology on High-Performance Polymer Field-Effect Transistors. *Adv. Mater.* **2009,** *21* (2), 209-212.

(82) Tsao, H. N.; Cho, D. M.; Park, I.; Hansen, M. R.; Mavrinskiy, A.; Yoon, D. Y.; Graf, R.; Pisula, W.; Spiess, H. W.; Mullen, K., Ultrahigh Mobility in Polymer Field-Effect Transistors by Design. *J. Am. Chem. Soc.* **2011,** *133* (8), 2605-2612.

(83) Osaka, I.; Zhang, R.; Sauve, G.; Smilgies, D.-M.; Kowalewski, T.; McCullough, R. D., High-Lamellar Ordering and Amorphous-Like Π-Network in Short-Chain Thiazolothiazole-Thiophene Copolymers Lead to High Mobilities. *J. Am. Chem. Soc.* **2009,** *131* (7), 2521-2529.

(84) Nelson, T. L.; Young, T. M.; Liu, J.; Mishra, S. P.; Belot, J. A.; Balliet, C. L.; Javier, A. E.; Kowalewski, T.; McCullough, R. D., Transistor Paint: High Mobilities in Small Bandgap Polymer Semiconductor Based on the Strong Acceptor, Diketopyrrolopyrrole and Strong Donor, Dithienopyrrole. *Adv. Mater.* **2010,** *22* (41), 4617-4621.

(85) Li, Y.; Sonar, P.; Singh, S. P.; Soh, M. S.; van Meurs, M.; Tan, J., Annealing-Free High-Mobility Diketopyrrolopyrrole−Quaterthiophene Copolymer for Solution-Processed Organic Thin Film Transistors. *J. Am. Chem. Soc.* **2011,** *133* (7), 2198-2204.

(86) Subramaniyan, S.; Xin, H.; Kim, F. S.; Shoaee, S.; Durrant, J. R.; Jenekhe, S. A., Effects of Side Chains on Thiazolothiazole-Based Copolymer Semiconductors for High Performance Solar Cells. *Adv. Energy Mater.* **2011,** *1* (5), 854-860.

(87) Chen, Z.; Lemke, H.; Albert-Seifried, S.; Caironi, M.; Nielsen, M. M.; Heeney, M.; Zhang, W.; McCulloch, I.; Sirringhaus, H., High Mobility Ambipolar Charge Transport in Polyselenophene Conjugated Polymers. *Adv. Mater.* **2010,** *22* (21), 2371-2375.

(88) Chen, Z.; Zheng, Y.; Yan, H.; Facchetti, A., Naphthalenedicarboximide- Vs Perylenedicarboximide-Based Copolymers. Synthesis and Semiconducting Properties in Bottom-Gate N-Channel Organic Transistors. *J. Am. Chem. Soc.* **2009,** *131* (1), 8-9.

(89) Letizia, J. A.; Salata, M. R.; Tribout, C. M.; Facchetti, A.; Ratner, M. A.; Marks, T. J., N-Channel Polymers by Design: Optimizing the Interplay of Solubilizing Substituents, Crystal Packing, and Field-Effect Transistor Characteristics in Polymeric Bithiophene-Imide Semiconductors. *J. Am. Chem. Soc.* **2008,** *130* (30), 9679-9694.

(90) Guo, X.; Ortiz, R. P.; Zheng, Y.; Hu, Y.; Noh, Y.-Y.; Baeg, K.-J.; Facchetti, A.; Marks, T. J., Bithiophene-Imide-Based Polymeric Semiconductors for Field-Effect Transistors: Synthesis, Structure−Property Correlations, Charge Carrier Polarity, and Device Stability. *J. Am. Chem. Soc.* **2011,** *133* (5), 1405-1418.

(91) Durban, M. M.; Kazarinoff, P. D.; Luscombe, C. K., Synthesis and Characterization of Thiophene-Containing Naphthalene Diimide N-Type Copolymers for Ofet Applications. *Macromolecules* **2010,** *43* (15), 6348-6352.

(92) Lin, Y. Y.; Gundlach, D. J.; Nelson, S. F.; Jackson, T. N., Stacked Pentacene Layer Organic Thin-Film Transistors with Improved Characteristics. *IEEE Electron Dev. Lett.* **1997,** *18* (12), 606-608.

(93) Jurchescu, O. D.; Popinciuc, M.; Wees, B. J. v.; Palstra, T. T. M., Interface-Controlled, High-Mobility Organic Transistors. *Adv. Mater.* **2007,** *19* (5), 688-692.

(94) Podzorov, V.; Sysoev, S. E.; Loginova, E.; Pudalov, V. M.; Gershenson, M. E., Single-Crystal Organic Field Effect Transistors with the Hole Mobility ~ 8 Cm[Sup 2]/V S. *Appl. Phys. Lett.* **2003,** *83* (17), 3504-3506.

(95) Sundar, V. C.; Zaumseil, J.; Podzorov, V.; Menard, E.; Willett, R. L.; Someya, T.; Gershenson, M. E.; Rogers, J. A., Elastomeric Transistor Stamps: Reversible Probing of Charge Transport in Organic Crystals. *Science* **2004,** *303* (5664), 1644-1646.

(96) Briseno, A. L.; Mannsfeld, S. C. B.; Ling, M. M.; Liu, S.; Tseng, R. J.; Reese, C.; Roberts, M. E.; Yang, Y.; Wudl, F.; Bao, Z., Patterning Organic Single-Crystal Transistor Arrays. *Nature* **2006,** *444* (7121), 913-917.

(97) Ebata, H.; Izawa, T.; Miyazaki, E.; Takimiya, K.; Ikeda, M.; Kuwabara, H.; Yui, T., Highly Soluble [1]Benzothieno[3,2-B]Benzothiophene (Btbt) Derivatives for High-Performance, Solution-Processed Organic Field-Effect Transistors. *J. Am. Chem. Soc.* **2007,** *129* (51), 15732-15733.

(98) Minemawari, H.; Yamada, T.; Matsui, H.; Tsutsumi, J. y.; Haas, S.; Chiba, R.; Kumai, R.; Hasegawa, T., Inkjet Printing of Single-Crystal Films. *Nature* **2011,** *475*, 364-367.

(99) Garnier, F.; Yassar, A.; Hajlaoui, R.; Horowitz, G.; Deloffre, F.; Servet, B.; Ries, S.; Alnot, P., Molecular Engineering of Organic Semiconductors: Design of Self-Assembly Properties in Conjugated Thiophene Oligomers. *J. Am. Chem. Soc.* **1993,** *115* (19), 8716-8721.

(100) Yoon, M.-H.; DiBenedetto, S. A.; Facchetti, A.; Marks, T. J., Organic Thin-Film Transistors Based on Carbonyl-Functionalized Quaterthiophenes: High Mobility N-Channel Semiconductors and Ambipolar Transport. *J. Am. Chem. Soc.* **2005,** *127* (5), 1348-1349.

(101) Bao, Z.; Lovinger, A. J.; Dodabalapur, A., Highly Ordered Vacuum-Deposited Thin Films of Metallophthalocyanines and Their Applications in Field-Effect Transistors. *Adv. Mater.* **1997,** *9* (1), 42-44.

(102) Bao, Z.; Lovinger, A. J.; Brown, J., New Air-Stable N-Channel Organic Thin Film Transistors. *J. Am. Chem. Soc.* **1998,** *120* (1), 207-208.

(103) Katz, H. E.; Lovinger, A. J.; Johnson, J.; Kloc, C.; Siegrist, T.; Li, W.; Lin, Y. Y.; Dodabalapur, A., A Soluble and Air-Stable Organic Semiconductor with High Electron Mobility. *Nature* **2000,** *404* (6777), 478-481.

(104) Molinari, A. S.; Alves, H.; Chen, Z.; Facchetti, A.; Morpurgo, A. F., High Electron Mobility in Vacuum and Ambient for Pdif-Cn2 Single-Crystal Transistors. *J. Am. Chem. Soc.* **2009,** *131* (7), 2462-2463.

(105) Jones, B. A.; Ahrens, M. J.; Yoon, M.-H.; Facchetti, A.; Marks, T. J.; Wasielewski, M. R., High-Mobility Air-Stable N-Type Semiconductors with Processing Versatility: Dicyanoperylene-3,4:9,10-Bis(Dicarboximides). *Angew. Chem., Int. Ed.* **2004,** *43* (46), 6363-6366.

(106) Haddon, R. C.; Perel, A. S.; Morris, R. C.; Palstra, T. T. M.; Hebard, A. F.; Fleming, R. M., C[Sub 60] Thin Film Transistors. *Appl. Phys. Lett.* **1995,** *67* (1), 121-123.

(107) Zhang, X. H.; Domercq, B.; Kippelen, B., High-Performance and Electrically Stable C[Sub 60] Organic Field-Effect Transistors. *Appl. Phys. Lett.* **2007,** *91* (9), 092114.

(108) Chikamatsu, M.; Nagamatsu, S.; Yoshida, Y.; Saito, K.; Yase, K.; Kikuchi, K., Solution-Processed N-Type Organic Thin-Film Transistors with High Field-Effect Mobility. *Appl. Phys. Lett.* **2005,** *87* (20), 203504-3.

(109) Veres, J.; Ogier, S. D.; Leeming, S. W.; Cupertino, D. C.; Khaffaf, S. M., Low-K Insulators as the Choice of Dielectrics in Organic Field-Effect Transistors. *Adv. Funct. Mater.* **2003,** *13* (3), 199-204.

(110) Kline, R. J.; McGehee, M. D.; Kadnikova, E. N.; Liu, J. S.; Frechet, J. M. J., Controlling the Field-Effect Mobility of Regioregular Polythiophene by Changing the Molecular Weight. *Adv. Mater.* **2003,** *15* (18), 1519-1522.

(111) Kline, R. J.; McGehee, M. D.; Toney, M. F., Highly Oriented Crystals at the Buried Interface in Polythiophene Thin-Film Transistors. *Nat. Mater.* **2006,** *5* (3), 222-228.

(112) Chang, J.-F.; Sun, B.; Breiby, D. W.; Nielsen, M. M.; Sölling, T. I.; Giles, M.; McCulloch, I.; Sirringhaus, H., Enhanced Mobility of Poly(3-Hexylthiophene) Transistors by Spin-Coating from High-Boiling-Point Solvents. *Chem. Mater.* **2004,** *16* (23), 4772-4776.

(113) Park, Y. D.; Lee, H. S.; Choi, Y. J.; Kwak, D.; Cho, J. H.; Lee, S.; Cho, K., Solubility-Induced Ordered Polythiophene Precursors for High-Performance Organic Thin-Film Transistors. *Adv. Funct. Mater.* **2009,** *19* (8), 1200-1206.

(114) Choi, D.; Jin, S.; Lee, Y.; Kim, S. H.; Chung, D. S.; Hong, K.; Yang, C.; Jung, J.; Kim, J. K.; Ree, M.; Park, C. E., Direct Observation of Interfacial Morphology in Poly(3-Hexylthiophene) Transistors: Relationship between Grain Boundary and Field-Effect Mobility. *ACS Appl. Mater. Interfaces* **2009**.

(115) Wu, P.-T.; Ren, G.; Kim, F. S.; Li, C.; Mezzenga, R.; Jenekhe, S. A., Poly(3-Hexylthiophene)-B-Poly(3-Cyclohexylthiophene): Synthesis, Microphase Separation, Thin Film Transistors, and Photovoltaic Applications. *J. Polym. Sci. Part A: Polym. Chem.* **2010,** *48* (3), 614-626.

(116) Kaneto, K.; Lim, W. Y.; Takashima, W.; Endo, T.; Rikukawa, M., Alkyl Chain Length Dependence of Field-Effect Mobilities in Regioregular Poly(3-Alkylthiophene) Films. *Jpn. J. Appl. Phys. Part 2* **2000,** *39* (8B), L872-L874.

(117) Babel, A.; Jenekhe, S. A., Alkyl Chain Length Dependence of the Field-Effect Carrier Mobility in Regioregular Poly(3-Alkylthiophene)S. *Synth. Met.* **2005,** *148* (2), 169-173.

(118) Yamamoto, T.; Yasuda, T.; Sakai, Y.; Aramaki, S., Ambipolar Field-Effect Transistor (Fet) and Redox Characteristics of a <I>Pi</I>-Conjugated Thiophene/1,3,4-Thiadiazole Ct-Type Copolymer. *Macromol. Rapid Commun.* **2005,** *26* (15), 1214-1217.

(119) Beaujuge, P. M.; Amb, C. M.; Reynolds, J. R., Spectral Engineering in Π-Conjugated Polymers with Intramolecular Donor-Acceptor Interactions. *Acc. Chem. Res.* **2010,** *43* (11), 1396-1407.

(120) Wu, P. T.; Kim, F. S.; Champion, R. D.; Jenekhe, S. A., Conjugated Donor-Acceptor Copolymer Semiconductors. Synthesis, Optical Properties, Electrochemistry, and Field-Effect Carrier Mobility of Pyridopyrazine-Based Copolymers. *Macromolecules* **2008,** *41* (19), 7021-7028.

(121) Fong, H. H.; Pozdin, V. A.; Amassian, A.; Malliaras, G. G.; Smilgies, D.-M.; He, M.; Gasper, S.; Zhang, F.; Sorensen, M., Tetrathienoacene Copolymers as High Mobility, Soluble Organic Semiconductors. *J. Am. Chem. Soc.* **2008,** *130* (40), 13202-13203.

(122) Osaka, I.; Abe, T.; Shinamura, S.; Miyazaki, E.; Takimiya, K., High-Mobility Semiconducting Naphthodithiophene Copolymers. *J. Am. Chem. Soc.* **2010,** *132* (14), 5000-5001.

(123) Kim, J.; Lim, B.; Baeg, K.-J.; Noh, Y.-Y.; Khim, D.; Jeong, H.-G.; Yun, J.-M.; Kim, D.-Y., Highly Soluble Poly(Thienylenevinylene) Derivatives with Charge-Carrier Mobility Exceeding 1 Cm2v–1s–1. *Chem. Mater.* **2011,** *23* (21), 4663-4665.

(124) Zhang, M.; Tsao, H. N.; Pisula, W.; Yang, C. D.; Mishra, A. K.; Mullen, K., Field-Effect Transistors Based on a Benzothiadiazole-Cyclopentadithiophene Copolymer. *J. Am. Chem. Soc.* **2007,** *129* (12), 3472-3473.

(125) Babel, A.; Jenekhe, S. A., Electron Transport in Thin-Film Transistors from an N-Type Conjugated Polymer. *Adv. Mater.* **2002,** *14* (5), 371-374.

(126) Jenekhe, S. A.; de Paor, L. R.; Chen, X. L.; Tarkka, R. M., Photoinduced Electron Transfer in Binary Blends of Conjugated Polymers. *Chem. Mater.* **1996,** *8* (10), 2401-2404.

(127) Quinto, M.; Jenekhe, S. A.; Bard, A. J., Polymer Films on Electrodes. 30. Electrochemistry and Scanning Electrochemical Microscopy Characterization of Benzimidazolebenzophenanthroline-Type Ladder (Bbl) and Semiladder (Bbb) Polymer Films. *Chem. Mater.* **2001,** *13* (9), 2824-2832.

(128) Wilbourn, K.; Murray, R. W., The D.C. Redox Versus Electronic Conductivity of the Ladder Polymer Poly(Benzimidazobenzophenanthroline). *J. Phys. Chem.* **1988,** *92* (12), 3642-3648.

(129) Briseno, A. L.; Mannsfeld, S. C. B.; Shamberger, P. J.; Ohuchi, F. S.; Bao, Z.; Jenekhe, S. A.; Xia, Y., Self-Assembly, Molecular Packing, and Electron Transport in N-Type Polymer Semiconductor Nanobelts. *Chem. Mater.* **2008,** *20* (14), 4712-4719.

(130) Zhan, X.; Tan, Z.; Domercq, B.; An, Z.; Zhang, X.; Barlow, S.; Li, Y.; Zhu, D.; Kippelen, B.; Marder, S. R., A High-Mobility Electron-Transport Polymer with Broad Absorption and Its Use in Field-Effect Transistors and All-Polymer Solar Cells. *J. Am. Chem. Soc.* **2007,** *129* (23), 7246-7247.

(131) Zhan, X.; Tan, Z. a.; Zhou, E.; Li, Y.; Misra, R.; Grant, A.; Domercq, B.; Zhang, X.-H.; An, Z.; Zhang, X.; Barlow, S.; Kippelen, B.; Marder, S. R., Copolymers of Perylene Diimide with Dithienothiophene and Dithienopyrrole as Electron-Transport Materials for All-Polymer Solar Cells and Field-Effect Transistors. *J. Mater. Chem.* **2009,** *19* (32), 5794-5803.

(132) Guo, X.; Watson, M. D., Conjugated Polymers from Naphthalene Bisimide. *Org. Lett.* **2008,** *10* (23), 5333-5336.

(133) Guo, X.; Kim, F. S.; Seger, M. J.; Jenekhe, S. A.; Watson, M. D., Naphthalene Diimide-Based Polymer Semiconductors: Synthesis, Structure–Property Correlations, and N-Channel and Ambipolar Field-Effect Transistors. *Chem. Mater.* **2012,** *24* (8), 1434-1442.

(134) Usta, H.; Facchetti, A.; Marks, T. J., Air-Stable, Solution-Processable N-Channel and Ambipolar Semiconductors for Thin-Film Transistors Based on the Indenofluorenebis(Dicyanovinylene) Core. *J. Am. Chem. Soc.* **2008,** *130* (27), 8580-8581.

(135) Sakanoue, T.; Yahiro, M.; Adachi, C.; Takimiya, K.; Toshimitsu, A., Electrical Characteristics of Single-Component Ambipolar Organic Field-Effect Transistors and Effects of Air Exposure on Them. *J. Appl. Phys.* **2008,** *103* (9), 094509-6.

(136) Tsai, J.-H.; Lee, W.-Y.; Chen, W.-C.; Yu, C.-Y.; Hwang, G.-W.; Ting, C., New Two-Dimensional Thiophene-Acceptor Conjugated Copolymers for Field Effect Transistor and Photovoltaic Cell Applications. *Chem. Mater.* **2010,** *22* (10), 3290-3299.

(137) Wu, P.-T.; Kim, F. S.; Jenekhe, S. A., New Poly(Arylene Vinylene)S Based on Diketopyrrolopyrrole for Ambipolar Transistors. *Chem. Mater.* **2011,** *23* (20), 4618-4624.

(138) de Leeuw, D. M.; Simenon, M. M. J.; Brown, A. R.; Einerhand, R. E. F., Stability of N-Type Doped Conducting Polymers and Consequences for Polymeric Microelectronic Devices. *Synth. Met.* **1997,** *87* (1), 53-59.

(139) Abdou, M. S. A.; Orfino, F. P.; Son, Y.; Holdcroft, S., Interaction of Oxygen with Conjugated Polymers: Charge Transfer Complex Formation with Poly(3-Alkylthiophenes). *J. Am. Chem. Soc.* **1997,** *119* (19), 4518-4524.

(140) Jones, B. A.; Facchetti, A.; Wasielewski, M. R.; Marks, T. J., Tuning Orbital Energetics in Arylene Diimide Semiconductors. Materials Design for Ambient Stability of N-Type Charge Transport. *J. Am. Chem. Soc.* **2007,** *129* (49), 15259-15278.

(141) Oh, J. H.; Sun, Y.-S.; Schmidt, R.; Toney, M. F.; Nordlund, D.; Konemann, M.; Wurthner, F.; Bao, Z., Interplay between Energetic and Kinetic Factors on the Ambient Stability of N-Channel Organic Transistors Based on Perylene Diimide Derivatives. *Chem. Mater.* **2009,** *21* (22), 5508-5518.

(142) Newman, C. R.; Frisbie, C. D.; da Silva Filho, D. A.; Bredas, J.-L.; Ewbank, P. C.; Mann, K. R., Introduction to Organic Thin Film Transistors and Design of N-Channel Organic Semiconductors. *Chem. Mater.* **2004,** *16* (23), 4436-4451.

(143) Briseno, A. L.; Kim, F. S.; Babel, A.; Xia, Y.; Jenekhe, S. A., N-Channel Polymer Thin Film Transistors with Long-Term Air-Stability and Durability and Their Use in Complementary Inverters. *J. Mater. Chem.* **2011,** *21* (41), 16461-16466.

(144) Chabinyc, M. L.; Street, R. A.; Northrup, J. E., Effects of Molecular Oxygen and Ozone on Polythiophene-Based Thin-Film Transistors. *Appl. Phys. Lett.* **2007,** *90* (12), 123508.

(145) Ahmed, E.; Subramaniyan, S.; Kim, F. S.; Xin, H.; Jenekhe, S. A., Benzobisthiazole-Based Donor-Acceptor Copolymer Semiconductors for Photovoltaic Cells and Highly Stable Field-Effect Transistors. *Macromolecules* **2011,** *44* (18), 7207-7219.

(146) Kim, F. S.; Ahmed, E.; Subramaniyan, S.; Jenekhe, S. A., Air-Stable Ambipolar Field-Effect Transistors and Complementary Logic Circuits from Solution-Processed N/P Polymer Heterojunctions. *ACS Appl. Mater. Interfaces* **2010,** *2* (11), 2974-2977.

(147) Ahmed, E.; Kim, F. S.; Xin, H.; Jenekhe, S. A., Benzobisthiazole−Thiophene Copolymer Semiconductors: Synthesis, Enhanced Stability, Field-Effect Transistors, and Efficient Solar Cells. *Macromolecules* **2009,** *42* (22), 8615-8618.

(148) Arnold, F. E.; Deusen, R. L. V., Preparation and Properties of High Molecular Weight, Soluble Oxobenz[De]Imidazobenzimidazoisoquinoline Ladder Polymer. *Macromolecules* **1969,** *2* (5), 497-502.

(149) Chen, T. A.; Rieke, R. D., The First Regioregular Head-to-Tail Poly(3-Hexylthiophene-2,5-Diyl) and a Regiorandom Isopolymer: Nickel Versus Palladium Catalysis of 2(5)-Bromo-5(2)-(Bromozincio)-3-Hexylthiophene Polymerization. *J. Am. Chem. Soc.* **1992,** *114* (25), 10087-10088.

(150) Chen, T.-A.; Wu, X.; Rieke, R. D., Regiocontrolled Synthesis of Poly(3-Alkylthiophenes) Mediated by Rieke Zinc: Their Characterization and Solid-State Properties. *J. Am. Chem. Soc.* **1995,** *117* (1), 233-244.

(151) Liu, J.; Zhang, R.; Sauve, G.; Kowalewski, T.; McCullough, R. D., Highly Disordered Polymer Field Effect Transistors: N-Alkyl Dithieno[3,2-B:2',3'-D]Pyrrole-Based Copolymers with Surprisingly High Charge Carrier Mobilities. *J. Am. Chem. Soc.* **2008,** *130* (39), 13167-13176.

(152) Subramaniyan, S.; Xin, H.; Kim, F. S.; Jenekhe, S. A., New Thiazolothiazole Copolymer Semiconductors for Highly Efficient Solar Cells. *Macromolecules* **2011,** *44* (16), 6245-6248.

(153) Rivnay, J.; Toney, M. F.; Zheng, Y.; Kauvar, I. V.; Chen, Z.; Wagner, V.; Facchetti, A.; Salleo, A., Unconventional Face-on Texture and Exceptional in-Plane Order of a High Mobility N-Type Polymer. *Adv. Mater.* **2010,** *22* (39), 4359-4363.

(154) Rivnay, J.; Steyrleuthner, R.; Jimison, L. H.; Casadei, A.; Chen, Z.; Toney, M. F.; Facchetti, A.; Neher, D.; Salleo, A., Drastic Control of Texture in a High Performance N-Type Polymeric Semiconductor and Implications for Charge Transport. *Macromolecules* **2011,** *44* (13), 5246-5255.

(155) Ahmed, E.; Ren, G.; Kim, F. S.; Hollenbeck, E. C.; Jenekhe, S. A., Design of New Electron Acceptor Materials for Organic Photovoltaics: Synthesis, Electron Transport, Photophysics, and Photovoltaic Properties of Oligothiophene-Functionalized Naphthalene Diimides. *Chem. Mater.* **2011,** *23* (20), 4563-4577.

(156) Zhang, R.; Li, B.; Iovu, M. C.; Jeffries-El, M.; Sauve, G.; Cooper, J.; Jia, S.; Tristram-Nagle, S.; Smilgies, D. M.; Lambeth, D. N.; McCullough, R. D.; Kowalewski, T., Nanostructure Dependence of Field-Effect Mobility in Regioregular Poly(3-Hexylthiophene) Thin Film Field Effect Transistors. *J. Am. Chem. Soc.* **2006,** *128* (11), 3480-3481.

(157) Wan, A.; Hwang, J.; Amy, F.; Kahn, A., Impact of Electrode Contamination on the [Alpha]-Npd/Au Hole Injection Barrier. *Org. Electron.* **2005,** *6* (1), 47-54.

(158) Usta, H.; Risko, C.; Wang, Z.; Huang, H.; Deliomeroglu, M. K.; Zhukhovitskiy, A.; Facchetti, A.; Marks, T. J., Design, Synthesis, and Characterization of Ladder-Type Molecules and Polymers. Air-Stable, Solution-Processable N-Channel and Ambipolar Semiconductors for Thin-Film Transistors Via Experiment and Theory. *J. Am. Chem. Soc.* **2009,** *131* (15), 5586-5608.

(159) Hwang, D. K.; Fuentes-Hernandez, C.; Kim, J.; Potscavage, W. J.; Kim, S.-J.; Kippelen, B., Top-Gate Organic Field-Effect Transistors with High Environmental and Operational Stability. *Adv. Mater.* **2011,** *23* (10), 1293-1298.

(160) Jones, B. A.; Facchetti, A.; Marks, T. J.; Wasielewski, M. R., Cyanonaphthalene Diimide Semiconductors for Air-Stable, Flexible, and Optically Transparent N-Channel Field-Effect Transistors. *Chem. Mater.* **2007,** *19* (11), 2703-2705.

(161) Briseno, A. L. Ph.D. Thesis. University of Washington, Seattle, 2008.

(162) Song, H. H.; Fratini, A. V.; Chabinyc, M.; Price, G. E.; Agrawal, A. K.; Wang, C. S.; Burkette, J.; Dudis, D. S.; Arnold, F. E., Crystal Structure and Thin Film Morphology of Bbl Ladder Polymer. *Synth. Met.* **1995,** *69* (1-3), 533-535.

(163) Song, H. H.; Kim, D. Y., Unique Morphology of Surface Grown Aggregates of Bbl Ladder Polymer as Probed by the Atomic Force Microscope. *Bull. Korean Chem. Soc.* **1998,** *19* (5), 516-518.

(164) Zimmerman, C. M.; Koros, W. J., Comparison of Gas Transport and Sorption in the Ladder Polymer Bbl and Some Semi-Ladder Polymers. *Polymer* **1999,** *40* (20), 5655-5664.

(165) Breck, D. W., *Zeolite Molecular Sieves: Structure, Chemistry, and Use*. John Wiley & Sons: New York, 1974.

(166) Zhao, Y.; Yuan, G.; Roche, P.; Leclerc, M., A Calorimetric Study of the Phase Transitions in Poly(3-Hexylthiophene). *Polymer* **1995,** *36* (11), 2211-2214.

(167) Zhao, J.; Swinnen, A.; Van Assche, G.; Manca, J.; Vanderzande, D.; Mele, B. V., Phase Diagram of P3ht/Pcbm Blends and Its Implication for the Stability of Morphology. *J. Phys. Chem. B* **2009,** *113* (6), 1587-1591.

(168) Jenekhe, S. A.; Johnson, P. O., Complexation-Mediated Solubilization and Processing of Rigid-Chain and Ladder Polymers in Aprotic Organic Solvents. *Macromolecules* **1990,** *23* (20), 4419-4429.

(169) Chabinyc, M. L.; Endicott, F.; Vogt, B. D.; DeLongchamp, D. M.; Lin, E. K.; Wu, Y.; Liu, P.; Ong, B. S., Effects of Humidity on Unencapsulated Poly(Thiophene) Thin-Film Transistors. *Appl. Phys. Lett.* **2006,** *88*, 113514.

(170) Osaka, I.; Sauve, G.; Zhang, R.; Kowalewski, T.; McCullough, R. D., Novel Thiophene-Thiazolothiazole Copolymers for Organic Field-Effect Transistors. *Adv. Mater.* **2007,** *19* (23), 4160-4165.

(171) Osaka, I.; Takimiya, K.; McCullough, R. D., Benzobisthiazole-Based Semiconducting Copolymers Showing Excellent Environmental Stability in High-Humidity Air. *Adv. Mater.* **2010,** *22* (44), 4993-4997.

(172) Crone, B.; Dodabalapur, A.; Lin, Y. Y.; Filas, R. W.; Bao, Z.; LaDuca, A.; Sarpeshkar, R.; Katz, H. E.; Li, W., Large-Scale Complementary Integrated Circuits Based on Organic Transistors. *Nature* **2000,** *403* (6769), 521-523.

(173) Facchetti, A., Semiconductors for Organic Transistors. *Mater. Today* **2007,** *10* (3), 28-37.

(174) Dodabalapur, A.; Katz, H. E.; Torsi, L.; Haddon, R. C., Organic Heterostructure Field-Effect Transistors. *Science* **1995,** *269* (5230), 1560-1562.

(175) Anthopoulos, T. D.; de Leeuw, D. M.; Cantatore, E.; Setayesh, S.; Meijer, E. J.; Tanase, C.; Hummelen, J. C.; Blom, P. W. M., Organic Complementary-Like Inverters Employing Methanofullerene-Based Ambipolar Field-Effect Transistors. *Appl. Phys. Lett.* **2004,** *85* (18), 4205-4207.

(176) Singh, T. B.; Senkarabacak, P.; Sariciftci, N. S.; Tanda, A.; Lackner, C.; Hagelauer, R.; Horowitz, G., Organic Inverter Circuits Employing Ambipolar Pentacene Field-Effect Transistors. *Appl. Phys. Lett.* **2006,** *89* (3), 033512.

(177) Babel, A.; Wind, J. D.; Jenekhe, S. A., Ambipolar Charge Transport in Air-Stable Polymer Blend Thin-Film Transistors. *Adv. Funct. Mater.* **2004,** *14* (9), 891-898.

(178) Babel, A.; Zhu, Y.; Cheng, K. F.; Chen, W. C.; Jenekhe, S. A., High Electron Mobility and Ambipolar Charge Transport in Binary Blends of Donor and Acceptor Conjugated Polymers. *Adv. Funct. Mater.* **2007,** *17* (14), 2542-2549.

(179) Shkunov, M.; Simms, R.; Heeney, M.; Tierney, S.; McCulloch, I., Ambipolar Field-Effect Transistors Based on Solution-Processable Blends of Thieno[2,3-<I>B</I>]Thiophene Terthiophene Polymer and Methanofullerenes. *Adv. Mater.* **2005,** *17* (21), 2608-2612.

(180) Cho, S.; Yuen, J.; Kim, J. Y.; Lee, K.; Heeger, A. J., Ambipolar Organic Field-Effect Transistors Fabricated Using a Composite of Semiconducting Polymer and Soluble Fullerene. *Appl. Phys. Lett.* **2006,** *89* (15), 153505.

(181) Cho, S.; Yuen, J.; Kim, J. Y.; Lee, K.; Heeger, A. J.; Lee, S., Multilayer Bipolar Field-Effect Transistors. *Appl. Phys. Lett.* **2008,** *92* (6), 063505.

(182) Rost, C.; Gundlach, D. J.; Karg, S.; Riess, W., Ambipolar Organic Field-Effect Transistor Based on an Organic Heterostructure. *J. Appl. Phys.* **2004,** *95* (10), 5782-5787.

(183) Wang, H.; Wang, J.; Yan, X.; Shi, J.; Tian, H.; Geng, Y.; Yan, D., Ambipolar Organic Field-Effect Transistors with Air Stability, High Mobility, and Balanced Transport. *Appl. Phys. Lett.* **2006,** *88* (13), 133508.

(184) Dinelli, F.; Capelli, R.; Loi, M. A.; Murgia, M.; Muccini, M.; Facchetti, A.; Marks, T. J., High-Mobility Ambipolar Transport in Organic Light-Emitting Transistors. *Adv. Mater.* **2006,** *18* (11), 1416-1420.

(185) Wei, Q.; Tajima, K.; Hashimoto, K., Bilayer Ambipolar Organic Thin-Film Transistors and Inverters Prepared by the Contact-Film-Transfer Method. *ACS Appl. Mater. Interfaces* **2009,** *1* (9), 1865-1868.

(186) Liu, C.; Sirringhaus, H., Electron Transport Along Semiconducting Polymer Heterojunctions. *Org. Electron.* **2010,** *11* (4), 558-563.

(187) Chesterfield, R. J.; Newman, C. R.; Pappenfus, T. M.; Ewbank, P. C.; Haukaas, M. H.; Mann, K. R.; Miller, L. L.; Frisbie, C. D., High Electron Mobility and Ambipolar Transport in Organic Thin-Film Transistors Based on a &Pgr;-Stacking Quinoidal Terthiophene. *Adv. Mater.* **2003,** *15* (15), 1278-1282.

(188) Tang, M. L.; Reichardt, A. D.; Miyaki, N.; Stoltenberg, R. M.; Bao, Z., Ambipolar, High Performance, Acene-Based Organic Thin Film Transistors. *J. Am. Chem. Soc.* **2008,** *130* (19), 6064-6065.

(189) Bijleveld, J. C.; Zoombelt, A. P.; Mathijssen, S. G. J.; Wienk, M. M.; Turbiez, M.; de Leeuw, D. M.; Janssen, R. A. J., Poly(Diketopyrrolopyrrole−Terthiophene) for Ambipolar Logic and Photovoltaics. *J. Am. Chem. Soc.* **2009,** *131* (46), 16616-16617.

(190) Cornil, J.; Brédas, J.-L.; Zaumseil, J.; Sirringhaus, H., Ambipolar Transport in Organic Conjugated Materials. *Adv. Mater.* **2007,** *19* (14), 1791-1799.

(191) Rost, C.; Karg, S.; Riess, W.; Loi, M. A.; Murgia, M.; Muccini, M., Ambipolar Light-Emitting Organic Field-Effect Transistor. *Appl. Phys. Lett.* **2004,** *85* (9), 1613-1615.

(192) Zaumseil, J.; Friend, R. H.; Sirringhaus, H., Spatial Control of the Recombination Zone in an Ambipolar Light-Emitting Organic Transistor. *Nat. Mater.* **2006,** *5* (1), 69-74.

(193) Swensen, J. S.; Soci, C.; Heeger, A. J., Light Emission from an Ambipolar Semiconducting Polymer Field-Effect Transistor. *Appl. Phys. Lett.* **2005,** *87* (25), 253511.

(194) Yamane, K.; Yanagi, H.; Sawamoto, A.; Hotta, S., Ambipolar Organic Light Emitting Field Effect Transistors with Modified Asymmetric Electrodes. *Appl. Phys. Lett.* **2007,** *90* (16), 162108.

(195) Sakamoto, Y.; Suzuki, T.; Kobayashi, M.; Gao, Y.; Fukai, Y.; Inoue, Y.; Sato, F.; Tokito, S., Perfluoropentacene: High-Performance P-N Junctions and Complementary Circuits with Pentacene. *J. Am. Chem. Soc.* **2004,** *126* (26), 8138-8140.

(196) Wang, H.; Wang, J.; Yan, X.; Shi, J.; Tian, H.; Geng, Y.; Yan, D., Ambipolar Organic Field-Effect Transistors with Air Stability, High Mobility, and Balanced Transport. *Appl. Phys. Lett.* **2006,** *88* (13), 133508-3.

(197) Chikamatsu, M.; Mikami, T.; Chisaka, J.; Yoshida, Y.; Azumi, R.; Yase, K.; Shimizu, A.; Kubo, T.; Morita, Y.; Nakasuji, K., Ambipolar Organic Field-Effect Transistors Based on a Low Band Gap Semiconductor with Balanced Hole and Electron Mobilities. *Appl. Phys. Lett.* **2007,** *91* (4), 043506-3.

(198) Tsao, H. N.; Pisula, W.; Liu, Z.; Osikowicz, W.; Salaneck, W. R.; Müllen, K., From Ambi- to Unipolar Behavior in Discotic Dye Field-Effect Transistors. *Adv. Mater.* **2008,** *20* (14), 2715-2719.

(199) Dhar, B. M.; Kini, G. S.; Xia, G.; Jung, B. J.; Markovic, N.; Katz, H. E., Field-Effect-Tuned Lateral Organic Diodes. *Proc. Natl. Acad. Sci.* **2010,** *107* (9), 3972-3976.

(200) Alam, M. M.; Jenekhe, S. A., Efficient Solar Cells from Layered Nanostructures of Donor and Acceptor Conjugated Polymers. *Chem. Mater.* **2004,** *16* (23), 4647-4656.

(201) Zhang, X.; Jenekhe, S. A., Electroluminescence of Multicomponent Conjugated Polymers. 1. Roles of Polymer/Polymer Interfaces in Emission Enhancement and Voltage-Tunable Multicolor Emission in Semiconducting Polymer/Polymer Heterojunctions. *Macromolecules* **2000,** *33* (6), 2069-2082.

(202) Halls, J. J. M.; Walsh, C. A.; Greenham, N. C.; Marseglia, E. A.; Friend, R. H.; Moratti, S. C.; Holmes, A. B., Efficient Photodiodes from Interpenetrating Polymer Networks. *Nature* **1995,** *376* (6540), 498-500.

(203) Yu, G.; Gao, J.; Hummelen, J. C.; Wudl, F.; Heeger, A. J., Polymer Photovoltaic Cells: Enhanced Efficiencies Via a Network of Internal Donor-Acceptor Heterojunctions. *Science* **1995,** *270* (5243), 1789-1791.

(204) Wu, P.-T. Ph.D. Thesis. University of Washington, Seattle, 2010.

(205) Smits, E. C. P.; Anthopoulos, T. D.; Setayesh, S.; van Veenendaal, E.; Coehoorn, R.; Blom, P. W. M.; de Boer, B.; de Leeuw, D. M., Ambipolar Charge Transport in Organic Field-Effect Transistors. *Phys. Rev. B* **2006,** *73* (20), 205316.

(206) Szendrei, K.; Jarzab, D.; Chen, Z.; Facchetti, A.; Loi, M. A., Ambipolar All-Polymer Bulk Heterojunction Field-Effect Transistors. *J. Mater. Chem.* **2010,** *20* (7), 1317-1321.

(207) Sirringhaus, H., Device Physics of Solution-Processed Organic Field-Effect Transistors. *Adv. Mater.* **2005,** *17* (20), 2411-2425.

(208) Gelinck, G.; Heremans, P.; Nomoto, K.; Anthopoulos, T. D., Organic Transistors in Optical Displays and Microelectronic Applications. *Adv. Mater.* **2010,** *22* (34), 3778-3798.

(209) Fritz, S. E.; Kelley, T. W.; Frisbie, C. D., Effect of Dielectric Roughness on Performance of Pentacene Tfts and Restoration of Performance with a Polymeric Smoothing Layer. *J. Phys. Chem. B* **2005,** *109* (21), 10574-10577.

(210) Kim, C.; Facchetti, A.; Marks, T. J., Gate Dielectric Microstructural Control of Pentacene Film Growth Mode and Field-Effect Transistor Performance. *Adv. Mater.* **2007,** *19* (18), 2561-2566.

(211) Yang, H.; Kim, S. H.; Yang, L.; Yang, S. Y.; Park, C. E., Pentacene Nanostructures on Surface-Hydrophobicity-Controlled Polymer/Sio2 Bilayer Gate-Dielectrics. *Adv. Mater.* **2007,** *19* (19), 2868-2872.

(212) Zhao, N.; Noh, Y. Y.; Chang, J. F.; Heeney, M.; McCulloch, I.; Sirringhaus, H., Polaron Localization at Interfaces in High-Mobility Microcrystalline Conjugated Polymers. *Adv. Mater.* **2009,** *21* (37), 3759-3763.

(213) Jang, Y.; Kim, D. H.; Park, Y. D.; Cho, J. H.; Hwang, M.; Cho, K., Influence of the Dielectric Constant of a Polyvinyl Phenol Insulator on the Field-Effect Mobility of a Pentacene-Based Thin-Film Transistor. *Appl. Phys. Lett.* **2005,** *87* (15), 152105.

(214) Nunes, G.; Zane, S. G.; Meth, J. S., Styrenic Polymers as Gate Dielectrics for Pentacene Field-Effect Transistors. *J. Appl. Phys.* **2005,** *98* (10), 104503.

(215) Wang, Y.; Acton, O.; Ting, G.; Weidner, T.; Ma, H.; Castner, D. G.; Jen, A. K.-Y., Low-Voltage High-Performance Organic Thin Film Transistors with a Thermally Annealed Polystyrene/Hafnium Oxide Dielectric. *Appl. Phys. Lett.* **2009,** *95* (24), 243302.

(216) Jang, J.; Nam, S.; Chung, D. S.; Kim, S. H.; Yun, W. M.; Park, C. E., High Tg Cyclic Olefin Copolymer Gate Dielectrics for N,N´-Ditridecyl Perylene Diimide Based Field-Effect Transistors: Improving Performance and Stability with Thermal Treatment. *Adv. Funct. Mater.* **2010,** *20* (16), 2611-2618.

(217) Mark, J. E., *Polymer Data Handbook*. Oxford University Press: New York, 1999.

(218) Abbotto, A.; Beverina, L.; Bradamante, S.; Facchetti, A.; Klein, C.; Pagani, G. A.; Redi-Abshiro, M.; Wortmann, R., A Distinctive Example of the Cooperative Interplay of Structure and Environment in Tuning of Intramolecular Charge Transfer in Second-Order Nonlinear Optical Chromophores. *Chem. Eur. J.* **2003,** *9* (9), 1991-2007.

(219) Yang, T. C. K.; Tsai, S. H. Y.; Wang, S.-F.; Juan, C.-C., Dielectric and Thermal Studies of Inorganic Microfillers on Polymer Microwave Substrates—Metallocene Cyclic Olefin Copolymers (Coc). *Compos. Sci. Tech.* **2002,** *62* (5), 655-661.

(220) Mills, M. E.; Townsend, P.; Castillo, D.; Martin, S.; Achen, A., Benzocyclobutene (Dvs-Bcb) Polymer as an Interlayer Dielectric (Ild) Material. *Microelectron. Eng.* **1997,** *33* (1-4), 327-334.

(221) Stassen, A. F.; Boer, R. W. I. d.; Iosad, N. N.; Morpurgo, A. F., Influence of the Gate Dielectric on the Mobility of Rubrene Single-Crystal Field-Effect Transistors. *Appl. Phys. Lett.* **2004,** *85* (17), 3899-3901.

(222) Richards, T.; Bird, M.; Sirringhaus, H., A Quantitative Analytical Model for Static Dipolar Disorder Broadening of the Density of States at Organic Heterointerfaces. *J. Chem. Phys.* **2008,** *128* (23), 234905.

(223) Hwang, D. K.; Kim, C. S.; Choi, J. M.; Lee, K.; Park, J. H.; Kim, E.; Baik, H. K.; Kim, J. H.; Im, S., Polymer/Yox Hybrid-Sandwich Gate Dielectrics for Semitransparent Pentacene Thin-Film Transistors Operating under 5 V. *Adv. Mater.* **2006,** *18* (17), 2299-2303.

(224) Kim, F. S.; Jenekhe, S. A., Charge Transport in Poly(3-Butylthiophene) Nanowires and Their Nanocomposites with an Insulating Polymer. *Macromolecules* **2012**, Submitted.

(225) Kim, F. S.; Ren, G.; Jenekhe, S. A., One-Dimensional Nanostructures of Π-Conjugated Molecular Systems: Assembly, Properties, and Applications from Photovoltaics, Sensors, and Nanophotonics to Nanoelectronics. *Chem. Mater.* **2011,** *23* (3), 682-732.

(226) Briseno, A. L.; Mannsfeld, S. C. B.; Jenekhe, S. A.; Bao, Z.; Xia, Y., Introducing Organic Nanowire Transistors. *Mater. Today* **2008,** *11* (4), 38-47.

(227) Hoeben, F. J. M.; Jonkheijm, P.; Meijer, E. W.; Schenning, A. P. H. J., About Supramolecular Assemblies of Π-Conjugated Systems. *Chem. Rev.* **2005,** *105* (4), 1491-1546.

(228) Facchetti, A., Π-Conjugated Polymers for Organic Electronics and Photovoltaic Cell Applications. *Chem. Mater.* **2011,** *23* (3), 733-758.

(229) Grimsdale, A. C.; Leok Chan, K.; Martin, R. E.; Jokisz, P. G.; Holmes, A. B., Synthesis of Light-Emitting Conjugated Polymers for Applications in Electroluminescent Devices. *Chem. Rev.* **2009,** *109* (3), 897-1091.

(230) Kulkarni, A. P.; Tonzola, C. J.; Babel, A.; Jenekhe, S. A., Electron Transport Materials for Organic Light-Emitting Diodes. *Chem. Mater.* **2004,** *16* (23), 4556-4573.

(231) Kippelen, B.; Bredas, J. L., Organic Photovoltaics. *Energy Environ. Sci.* **2009,** *2* (3), 251-261.

(232) Thompson, B. C.; Frechet, J. M. J., Organic Photovoltaics - Polymer-Fullerene Composite Solar Cells. *Angew. Chem. Int. Ed.* **2008,** *47* (1), 58-77.

(233) Babel, A.; Jenekhe, S. A., Field-Effect Mobility of Charge Carriers in Blends of Regioregular Poly(3-Alkylthiophene)S. *J. Phys. Chem. B* **2003,** *107* (8), 1749-1754.

(234) Babel, A.; Li, D.; Xia, Y. N.; Jenekhe, S. A., Electrospun Nanofibers of Blends of Conjugated Polymers: Morphology, Optical Properties, and Field-Effect Transistors. *Macromolecules* **2005,** *38* (11), 4705-4711.

(235) Babel, A.; Jenekhe, S. A., Morphology and Field-Effect Mobility of Charge Carriers in Binary Blends of Poly(3-Hexylthiophene) with Poly [2-Methoxy-5-(2-Ethylhexoxy)-1,4-Phenylenevinylene] and Polystyrene. *Macromolecules* **2004,** *37* (26), 9835-9840.

(236) Lu, G.; Tang, H.; Qu, Y.; Li, L.; Yang, X., Enhanced Electrical Conductivity of Highly Crystalline Polythiophene/Insulating-Polymer Composite. *Macromolecules* **2007,** *40* (18), 6579-6584.

(237) Qiu, L.; Lee, W. H.; Wang, X.; Kim, J. S.; Lim, J. A.; Kwak, D.; Lee, S.; Cho, K., Organic Thin-Film Transistors Based on Polythiophene Nanowires Embedded in Insulating Polymer. *Adv. Mater.* **2009,** *21* (13), 1349-1353.

(238) Sun, J.; Jung, B.-J.; Lee, T.; Berger, L.; Huang, J.; Liu, Y.; Reich, D. H.; Katz, H. E., Tunability of Mobility and Conductivity over Large Ranges in Poly(3,3'''-Didodecylquaterthiophene)/Insulating Polymer Composites. *ACS Appl. Mater. Interfaces* **2009,** *1* (2), 412-419.

(239) Goffri, S.; Muller, C.; Stingelin-Stutzmann, N.; Breiby, D. W.; Radano, C. P.; Andreasen, J. W.; Thompson, R.; Janssen, R. A. J.; Nielsen, M. M.; Smith, P.; Sirringhaus, H., Multicomponent Semiconducting Polymer Systems with Low Crystallization-Induced Percolation Threshold. *Nat. Mater.* **2006,** *5* (12), 950-956.

(240) Arias, A. C.; Endicott, F.; Street, R. A., Surface-Induced Self-Encapsulation of Polymer Thin-Film Transistors. *Adv. Mater.* **2006,** *18* (21), 2900-2904.

(241) Qiu, L.; Lim, J. A.; Wang, X.; Lee, W. H.; Hwang, M.; Cho, K., Versatile Use of Vertical-Phase-Separation-Induced Bilayer Structures in Organic Thin-Film Transistors. *Adv. Mater.* **2008,** *20* (6), 1141-1145.

(242) Xin, H.; Kim, F. S.; Jenekhe, S. A., Highly Efficient Solar Cells Based on Poly(3-Butylthiophene) Nanowires. *J. Am. Chem. Soc.* **2008,** *130* (16), 5424-5425.

(243) Xin, H.; Ren, G. Q.; Kim, F. S.; Jenekhe, S. A., Bulk Heterojunction Solar Cells from Poly(3-Butylthiophene)/Fullerene Blends: In Situ Self-Assembly of Nanowires, Morphology, Charge Transport, and Photovoltaic Properties. *Chem. Mater.* **2008,** *20* (19), 6199-6207.

(244) Xin, H.; Reid, O. G.; Ren, G.; Kim, F. S.; Ginger, D. S.; Jenekhe, S. A., Polymer Nanowire/Fullerene Bulk Heterojunction Solar Cells: How Nanostructure Determines Photovoltaic Properties. *ACS Nano* **2010,** *4* (4), 1861-1872.

(245) Reid, O. G.; Xin, H.; Jenekhe, S. A.; Ginger, D. S., Nanostructure Determines the Intensity-Dependence of Open-Circuit Voltage in Plastic Solar Cells. *J. Appl. Phys.* **2010,** *108* (8), 084320.

(246) Briseno, A. L.; Mannsfeld, S. C. B.; Lu, X.; Xiong, Y.; Jenekhe, S. A.; Bao, Z.; Xia, Y., Fabrication of Field-Effect Transistors from Hexathiapentacene Single-Crystal Nanowires. *Nano Lett.* **2007,** *7* (3), 668-675.

(247) Briseno, A. L.; Mannsfeld, S. C. B.; Reese, C.; Hancock, J. M.; Xiong, Y.; Jenekhe, S. A.; Bao, Z.; Xia, Y., Perylenediimide Nanowires and Their Use in Fabricating Field-Effect Transistors and Complementary Inverters. *Nano Lett.* **2007,** *7* (9), 2847-2853.

(248) Ihn, K. J.; Moulton, J.; Smith, P., Whiskers of Poly(3-Alkylthiophene)S. *J. Polym. Sci. Part B: Polym. Phys.* **1993,** *31* (6), 735-742.

(249) Merlo, J. A.; Frisbie, C. D., Field Effect Conductance of Conducting Polymer Nanofibers. *J. Polym. Sci. Part B: Polym. Phys.* **2003,** *41* (21), 2674-2680.

(250) Merlo, J. A.; Frisbie, C. D., Field Effect Transport and Trapping in Regioregular Polythiophene Nanofibers. *J. Phys. Chem. B* **2004,** *108* (50), 19169-19179.

(251) Oosterbaan, W. D.; Bolsee, J.-C.; Gadisa, A.; Vrindts, V.; Bertho, S.; D'Haen, J.; Cleij, T. J.; Lutsen, L.; McNeill, C. R.; Thomsen, L.; Manca, J. V.; Vanderzande, D., Alkyl-Chain-Length-Independent Hole Mobility Via Morphological Control with Poly(3-Alkylthiophene) Nanofibers. *Adv. Funct. Mater.* **2010,** *20* (5), 792-802.

(252) Samitsu, S.; Shimomura, T.; Heike, S.; Hashizume, T.; Ito, K., Field-Effect Carrier Transport in Poly(3-Alkylthiophene) Nanofiber Networks and Isolated Nanofibers. *Macromolecules* **2010,** *43* (19), 7891-7894.

(253) Liu, H.; Reccius, C. H.; Craighead, H. G., Single Electrospun Regioregular Poly(3-Hexylthiophene) Nanofiber Field-Effect Transistor. *Appl. Phys. Lett.* **2005,** *87* (25), 253106.

(254) Sauve, G.; McCullough, R. D., High Field-Effect Mobilities for Diblock Copolymers of Poly(3-Hexylthiophene) and Poly(Methyl Acrylate). *Adv. Mater.* **2007,** *19* (14), 1822-1825.

(255) Mas-Torrent, M.; Boer, D. d.; Durkut, M.; Hadley, P.; Schenning, A. P. H. J., Field Effect Transistors Based on Poly(3-Hexylthiophene) at Different Length Scales. *Nanotechnology* **2004,** *15* (4), S265-S269.

(256) Newbloom, G. M.; Kim, F. S.; Jenekhe, S. A.; Pozzo, D. C., Mesoscale Morphology and Charge Transport in Colloidal Networks of Poly(3-Hexylthiophene). *Macromolecules* **2011,** *44* (10), 3801-3809.

(257) Samitsu, S.; Shimomura, T.; Heike, S.; Hashizume, T.; Ito, K., Effective Production of Poly(3-Alkylthiophene) Nanofibers by Means of Whisker Method Using Anisole Solvent: Structural, Optical, and Electrical Properties. *Macromolecules* **2008,** *41* (21), 8000-8010.

(258) Oosterbaan, W. D.; Vrindts, V.; Berson, S.; Guillerez, S.; Douheret, O.; Ruttens, B.; D'Haen, J.; Adriaensens, P.; Manca, J.; Lutsen, L.; Vanderzande, D., Efficient Formation, Isolation and Characterization of Poly(3-Alkylthiophene) Nanofibres: Probing Order as a Function of Side-Chain Length. *J. Mater. Chem.* **2009,** *19*, 5424-5435.

(259) Jaczewska, J.; Budkowski, A.; Bernasik, A.; Moons, E.; Rysz, J., Polymer Vs Solvent Diagram of Film Structures Formed in Spin-Cast Poly(3-Alkylthiophene) Blends. *Macromolecules* **2008,** *41* (13), 4802-4810.

(260) Mena-Osteritz, E.; Meyer, A.; Langeveld-Voss, B. M. W.; Janssen, R. A. J.; Meijer, E. W.; Bäuerle, P., Two-Dimensional Crystals of Poly(3-Alkyl- Thiophene)S: Direct Visualization of Polymer Folds in Submolecular Resolution. *Angew. Chem., Int. Ed.* **2000,** *39* (15), 2679-2684.

(261) Horowitz, G., Tunneling Current in Polycrystalline Organic Thin-Film Transistors. *Adv. Funct. Mater.* **2003,** *13* (1), 53-60.

(262) Borsenberger, P. M.; Gruenbaum, W. T.; Magin, E. H.; Sorriero, L. J., Hole Transport in Tri-P-Tolylamine Doped Polymers: The Role of the Polymer Dipole Moment. *Chem. Phys.* **1995,** *195* (1-3), 435-442.

(263) Kirkpatrick, S., Percolation and Conduction. *Rev. Mod. Phys.* **1973,** *45* (4), 574-588.

(264) Arosio, P.; Moreno, M.; Famulari, A.; Raos, G.; Catellani, M.; Meille, S. V., Ordered Stacking of Regioregular Head-to-Tail Polyalkylthiophenes: Insights from the Crystal Structure of Form I' Poly(3-N-Butylthiophene). *Chem. Mater.* **2008,** *21* (1), 78-87.

(265) Brandrup, J.; Immergut, E. H., *Polymer Handbook*. Wiley: New York, 1989.

(266) Reghu, M.; Yoon, C. O.; Yang, C. Y.; Moses, D.; Heeger, A. J.; Cao, Y., Superlocalization of the Electronic Wave Functions in Conductive Polymer Blends at Concentrations near the Percolation Threshold. *Macromolecules* **1993,** *26* (26), 7245-7249.

(267) Wang, Y.; Rubner, M. F., Electrically Conductive Semiinterpenetrating Polymer Networks of Poly(3-Octylthiophene). *Macromolecules* **1992,** *25* (12), 3284-3290.

(268) Dicker, G.; de Haas, M. P.; Warman, J. M.; de Leeuw, D. M.; Siebbeles, L. D. A., The Disperse Charge-Carrier Kinetics in Regioregular Poly(3-Hexylthiophene). *J. Phys. Chem. B* **2004,** *108* (46), 17818-17824.

(269) Takeya, J.; Yamagishi, M.; Tominari, Y.; Hirahara, R.; Nakazawa, Y.; Nishikawa, T.; Kawase, T.; Shimoda, T.; Ogawa, S., Very High-Mobility Organic Single-Crystal Transistors with in-Crystal Conduction Channels. *Appl. Phys. Lett.* **2007,** *90* (10), 102120.

(270) Ahmed, E.; Briseno, A. L.; Xia, Y.; Jenekhe, S. A., High Mobility Single-Crystal Field-Effect Transistors from Bisindoloquinoline Semiconductors. *J. Am. Chem. Soc.* **2008,** *130* (4), 1118-1119.

(271) Donovan, K. J.; Wilson, E. G., Demonstration of an Ultra-High Mobility Organic Polymer. *Philosophical Magazine Part B* **1981,** *44* (1), 9-29.

(272) Fabiano, S.; Chen, Z.; Vahedi, S.; Facchetti, A.; Pignataro, B.; Loi, M. A., Role of Photoactive Layer Morphology in High Fill Factor All-Polymer Bulk Heterojunction Solar Cells. *J. Mater. Chem.* **2011,** *21* (16), 5891-5896.

(273) Anthopoulos, T. D.; Singh, B.; Marjanovic, N.; Sariciftci, N. S.; Ramil, A. M.; Sitter, H.; Colle, M.; de Leeuw, D. M., High Performance N-Channel Organic Field-Effect Transistors and Ring Oscillators Based on C[Sub 60] Fullerene Films. *Appl. Phys. Lett.* **2006,** *89* (21), 213504.

VITA

Felix Sunjoo Kim was born in Austin, Texas, on January 11, 1981. He moved to Seoul, Korea, along with his family in his age of two.. He has lived in Seattle, Washington, since 2006. He earned a Bachelor of Science in Chemical Engineering from the Seoul National University, Seoul, Korea, in 2003, and a Master of Science in Chemical Engineering from the University of Washington, Seattle, Washington, in 2008. He pursued his Ph.D. degree and performed his research on polymer field-effect transistors under the guidance of Professor Samson A. Jenekhe. During his graduate studies, he received the Ford Motor Company Fellowship in 2008 from the College of Engineering, and the Jane and Joseph McCarthy Outstanding Teaching Award in 2010 from the Department of Chemical Engineering. He was one of the finalists for the 2012 Frank J. Padden Jr. Award for Excellence in Polymer Research by the American Physical Society, and was recognized by the American Chemical Society Polymer Division for Excellence in Graduate Polymer Research in 2012. He is a member of the Materials Research Society, the American Chemical Society, the American Physical Society, the American Institute of Chemical Engineers, and the Korean-American Scientists and Engineers Association.

The following is the list of the author's publications:

1. Xin, H.; **Kim, F. S.**; Jenekhe, S. A. "Highly Efficient Solar Cells Based on Poly(3-butylthiophene) Nanowires," *J. Am. Chem. Soc.* **2008**, *130* (16), 5424-5425.
2. Xin, H.; Ren, G.; **Kim, F. S.**; Jenekhe, S. A. "Bulk Heterojunction Solar Cells from Poly(3-butylthiophene)/Fullerene Blends: In Situ Self-Assembly of Nanowires, Morphology, Charge Transport, and Photovoltaic Properties," *Chem. Mater.* **2008**, *20* (19), 6199-6207.
3. Wu, P.-T.; **Kim, F. S.**; Champion, R. D.; Jenekhe, S. A. "Conjugated Donor-Acceptor Copolymer Semiconductors. 2. Synthesis, Optical Properties, Electrochemistry, and Field-Effect Carrier Mobility of Pyridopyrazine Based Copolymers," *Macromolecules* **2008**, *41* (19), 7021-7028.
4. Wu, P.-T.; Bull, T.; **Kim, F. S.**; Luscombe, C. K.; Jenekhe, S. A. "Organometallic Donor-Acceptor Conjugated Polymer Semiconductors: Tunable Optical, Electrochemical, Charge Transport, and

Photovoltaic Properties with Varying Electron-Accepting Strength," *Macromolecules* **2009**, *42* (3), 671-681.

5. Guo, X.; **Kim, F. S.**; Jenekhe, S. A.; Watson, M. D. "Phthalimide-Based Polymers for High Performance Organic Thin-Film Transistors," *J. Am. Chem. Soc.* **2009**, *131* (21), 7206-7207.

6. Xin, H.; Guo, X.; **Kim, F. S.**; Ren, G.; Watson, M. D.; Jenekhe, S. A. "Efficient solar cells based on a new donor-acceptor copolymer semiconductor: morphology, charge-transport, and photovoltaic properties of poly(*N*-(dodecyl)-3,6-bis(4-dodecyloxythiophen-2-yl))phthalimide," *J. Mater. Chem.* **2009**, *19*, 5303-5310; One of top ten most-accessed J. Mater. Chem. articles in July 2009.

7. **Kim, F. S.**; Guo, X.; Watson, M. D.; Jenekhe, S. A. "High-Mobility Ambipolar Transistors and High-Gain Inverters from a Donor-Acceptor Copolymer Semiconductor," *Adv. Mater.* **2010**, *22* (4), 478-482; Featured as a cover page of the issue; Highlighted in UW News, Technology Review, and Softpedia in August 2009; One of top five most-accessed Adv. Mater. articles in August 2009.

8. Ahmed, E.; **Kim, F. S.**; Xin, H.; Jenekhe, S. A. "Benzobisthiazole-Thiophene Copolymer Semiconductors: Synthesis, Enhanced Stability, Field-Effect Transistors, and Efficient Solar Cells," *Macromolecules* **2009**, *42* (22), 8615-8618.

9. Wu, P.-T.; Xin, H.; **Kim, F. S.**; Ren, G.; Jenekhe, S. A. "Regioregular poly(3-pentylthiophene): Self-assembly of nanowires, thin film transistors, and efficient photovoltaic cells," *Macromolecules* **2009**, *42* (22), 8817-8826.

10. Wu, P.-T.; Ren, G.; **Kim, F. S.**; Li, C.; Mezzenga, R.; Jenekhe, S. A. "Poly(3-hexylthiophene)-b-poly(3-cyclohexylthiophene): Synthesis, Microphase Separation, Thin Film Transistors, and Photovoltaic Applications," *J. Polym. Sci. Part A: Polym. Chem.* **2010**, *48* (3), 614-626.

11. Xin, H.; Reid, O. G.; Ren, G.; **Kim, F. S.**; Ginger, D. S.; Jenekhe, S. A. "Polymer Nanowire/Fullerene Bulk Heterojunction Solar Cells: How Nanostructure Determines Photovoltaic Properties," *ACS Nano* **2010**, *4* (4), 1861-1872.

12. Wang, C.; **Kim, F. S.**; Ren, G.; Xu, Y.; Pang, Y.; Jenekhe, S. A.; Jia, L. "Regioregular Poly(3-alkanoythiophene): Synthesis and Electrochemical, Photophysical, Charge Transport, and Photovoltaic Properties," *J. Polym. Sci. Part A: Polym. Chem.* **2010**, *48* (21), 4681-4690.

13. **Kim, F. S.**; Ahmed, E.; Subramaniyan, S.; Jenekhe, S. A. "Air-Stable Ambipolar Field-Effect Transistors and Complementary Logic Circuits from Solution-Processed n/p Polymer Heterojunctions," *ACS Appl. Mater. & Interfaces* **2010**, *2* (11), 2974-2977.

14. Guo, X.; Xin, H.; **Kim, F. S.**; Jenekhe, S. A.; Watson, M. D. "Thieno[3,4-c]pyrrole-4,6-dione-Based Donor-Acceptor Conjugated Polymers for Solar Cells," *Macromolecules* **2011**, *44* (2), 269-277.

15. **Kim, F. S.**; Ren, G.; Jenekhe, S. A. "One-Dimensional Nanostructures of π-Conjugated Molecular Systems: Assembly, Properties, and Applications from Photovoltaics, Sensors, and Nanophotonics to Nanoelectronics," *Chem. Mater.* **2011**, *23* (3), 682-732 (Invited Review in the Special Issue on π-Functional Materials).

16. Subramanyan, S.; Xin, H.; **Kim, F. S.**; Shoaee, S.; Durrant, J. R.; Jenekhe, S. A. "Effect of Side Chains on Thiazolothiazole-Based Copolymer Semiconductors for High Performance Solar Cells," *Adv. Energy Mater.* **2011**, *1* (5), 854-860.

17. Newbloom, G. M.; **Kim, F. S.**; Jenekhe, S. A.; Pozzo, D. C. "Impact of Mesoscale Morphology on Charge Transport in Colloidal Networks of Poly(3-hexylthiophene)," *Macromolecules* **2011**, *44* (10), 3801-3809.

18. Subramaniyan, S.; Xin, H.; **Kim, F. S.**; Jenekhe, S. A. "New Thiazolothiazole Copolymer Semiconductors for Highly Efficient Solar Cells," *Macromolecules* **2011**, *44* (16), 6245-6248.

19. Ahmed, E.; Subramaniyan, S.; **Kim, F. S.**; Xin, H.; Jenekhe, S. A. "Benzobisthiazole-Based Donor-Acceptor Copolymer Semiconductors for Photovoltaic Cells and Highly Stable Field-Effect Transistors," *Macromolecules* **2011**, *44* (18), 7207-7219.

20. Briseno, A. L.; **Kim, F. S.**; Babel, A.; Xia, Y.; Jenekhe, S. A. "n-Channel Polymer Thin Film Transistors with Long-Term Air-Stability and Durability and their Use in Complementary Inverters," *J. Mater. Chem.* **2011**, *21* (41), 16461-16466.

21. Ahmed, E.; Ren, G.; **Kim, F. S.**; Hollenbeck, E. C.; Jenekhe, S. A. "Design of New Electron Acceptor Materials for Organic Photovoltaics: Synthesis, Electron Transport, Photophysics, and Photovoltaic Properties of Oligothiophene-Functionalized Naphthalene Diimides," *Chem. Mater.* **2011**, *23* (20), 4563-4577.

22. Wu, P.-T.; **Kim, F. S.**; Jenekhe, S. A. "New poly(arylene vinylene)s based on diketopyrrolopyrrole for ambipolar transistors," *Chem. Mater.* **2011**, *23* (20), 4618-4624.

23. **Kim, F. S.**; Hwang, D.-K.; Kippelen, B.; Jenekhe, S. A. "Enhanced carrier mobility and electrical stability of n-channel polymer thin film transistors by use of low-k dielectric buffer layer," *Appl. Phys. Lett.* **2011**, *99*, 173303.

24. Guo, X.; **Kim, F. S.**; Seger, M. J.; Jenekhe, S. A.; Watson, M. D. "Naphthalene Diimide-Based Polymer Semiconductors: Synthesis, Structure-Property Correlations, and n-Channel and Ambipolar Field-Effect Transistors," *Chem. Mater.* **2012**, *24* (8), 1434-1442.

25. Hwang, Y.-J.; **Kim, F. S.**; Xin, H.; Jenekhe, S. A. "New Thienothiadiazole-Based Conjugated Copolymers for Electronics and Optoelectronics," *Macromolecules* **2012**, *45* (9), 3732-3739.

26. **Kim, F. S.**; Jenekhe, S. A. "Charge Transport in Poly(3-butylthiophene) Nanowires and Their Nanocomposites with an Insulating Polymer," **2012**, submitted.